Suitability of *in vitro*, *in silico* and *in vivo* methods to predict intestinal absorption in drug development

Inaugural-Dissertation
to obtain the academic degree
Doctor rerum naturalium (Dr. rer. nat.)
submitted to the Department of Biology, Chemistry and Pharmacy
of Freie Universität Berlin

by
Jeannine Fleth-James
from Berlin

2017

Freie Universität Berlin,
Department of Biology, Chemistry and Pharmacy
Department of Clinical Pharmacy and Biochemistry
Supervisor: Prof. Dr. Charlotte Kloft
2006-2017

1. Gutachter: Prof. Dr. Charlotte Kloft
2. Gutachter: Prof. Dr. Thorsten Lehr

Disputation am: 04 Juli 2018

Table of Contents

List of Abbreviations and Symbols

Å	Ångström
ACAT	Advanced Compartmental Absorption and Transit Model
Ag/AgCl	Silver/Silver Chloride
AIC	Akaike Information Criterion
ASF	Absorption Scale Factor
ATP	Adenosine Triphosphate
AUC	Area Under the Concentration-Time Curve
BBMV	Brush Border Membrane Vesicles
BCS	Biopharmaceutical Classification System
BIC	Bayesian Information Criterion
BLMV	Basolateral Membrane Vesicles
C_1-C_8	Compound 1 - Compound 8
CAT	Compartmental Absorption and Transit Model
CL	Clearance
cm/cm^2	Centimetre / Square Centimetre
CO_2	Carbon Dioxide
CV	Coefficient of Variation
CYP	Cytochrome P450
Da	Dalton
dP / dPe	Difference of Electrical Potential / Difference of Electrical Potential of Electrodes
dpm	Decays per Minute
F	Bioavailability (Systemically Available Fraction)
f_a	Fraction Absorbed
FaSSIF	Fasted State Simulated Small Intestinal Fluid
FeSSIF	Fed State Simulated Intestinal Fluid
g	Gram
GIT	Gastrointestinal Tract
h	Hour
HTS	High-Throughput-Screening
IgA	Immunoglobulin A
Isc	Short-Circuit Current
i.v.	Intravenous
k_a	Absorption Rate Constant
keV	Kiloelectron Volt
kg	Kilogram
KRB	Krebs-Ringer Hydrogen Carbonate Buffer Solution
L	Litre
log $P_{o/w}$	Partition Coefficient in Octanol/Water
log D_{ph}	Distribution Coefficient at Specific pH
LSC	Liquid Scintillation Counting
m	Meter
m^2	Square Meter
MBq	Megabecquerel
mg	Milligram
min	Minute
mL	Millilitre

mM	Millimole per Litre = Millimolar
mmol	Millimole
mae	Mean Absolute Error
mpe	Mean Prediction Error
m-s	Mucosal-Serosal
mV	Millivolt
MW	Molecular Weight
Na^+	Sodium Ion
nm	Nanometre
NSB	Non-Specific Binding
O_2	Oxygen
PAMPA	Parallel Artificial Membrane Permeability Assay
P_{app}	Apparent Permeability
PBPK	Physiologically Based Pharmacokinetics
P_{eff}	Effective Permeability
PEG4000	Polyethylene Glycol with Molecular Weight 4000
Pgp	P-Glycoprotein
pH	Negative Decimal Logarithm of the Hydrogen Ion Activity in a Solution
PK	Pharmacokinetics
pK_a	Negative Decimal Logarithm of the Acid Dissociation Constant
p.o.	per
PSA	Parameter Sensitivity Analysis
R^2	Coefficient of Determination
R_f	Fluid Resistance
rmse	Root Mean Square Error
R_t	Tissue Resistance
ρ	Rho
s	Seconds
SD	Standard Deviation
SGF	Simulated Gastric Fluid
SGFsp	Simulated Gastric Fluid without Pepsin
SI	Small Intestine
s-m	Serosal-Mucosal
TEER	Transepithelial Electrical Resistance
T_{max}	Time Point of Maximum Plasma Concentration
V	Volume of Distribution
Ω	Electrical Resistance
µmol	Micromole
°C	Degree Celsius
µL	Microliter
^{14}C	Radioactive Isotope of Carbon (Carbon-14)
^{3}H	Radioactive Isotope of Hydrogen (Tritium)

1 Introduction

1.1 Intestinal absorption

From the patient's point of view, the oral administration of a drug is the most convenient route of administration and also shows the highest acceptance and compliance [1-3]. The majority of drugs is absorbed across the small intestine as the presence of villi and microvilli increases the absorptive surface area by manifold [4]. Therefore, the epithelial tissue and the physiological aspects of the gastrointestinal tract are of great significance for the absorption of orally administered drugs. Subsequently, this thesis is going to elucidate the factors influencing intestinal drug absorption and how to predict the fraction of dose absorbed in humans at an early stage of the drug development process.

1.2 Anatomy and physiology of the gastrointestinal tract

In order to grasp the process of drug absorption, it is important to understand the complex anatomy and physiology of the gastrointestinal tract (GIT) and consequently the route of the drug through the body.

1.2.1 Oral cavity

The oral cavity forms the entrance to the gastrointestinal tract. It is lined with a mucous membrane in which numerous glands (minor salivary glands) are embedded. Together with the three pairs of salivary glands (parotid, submandibular and sublingual) – ending in the oral cavity but being located outside–, they produce the saliva that is needed to aid the digestion process. Saliva mostly consists of water; the rest being electrolytes, enzymes and mucin. In addition, antimicrobial components like lysozyme and immunoglobulin A (IgA) are present to protect from bacteria and viruses. The human mouth produces 1.0 - 1.5 litres of saliva per day [5]. The pH of the saliva in the pre-prandial state revolves around 6.0, after stimulation it rises to a pH of about 7.0 - 7.5 [6]. As soon as the saliva reaches the stomach, its enzymes are inactivated due to the acidic gastric fluids (low pH). The advantage of buccally absorbed (through the membrane of the cheek inside the oral cavity) compounds is the avoidance of the intestinal and hepatic first-pass effect and the enzymatic degradation within the gastrointestinal tract. Only a few compounds have the properties to use this route of absorption like the well-known glyceroltrinitrate with its vaso-dilating properties [7]. The major absorption mechanism for buccally absorbed substances is passive diffusion [8, 9] but also carrier-mediated diffusion and active transport have been reported [10]. More the charge of

the molecules rather than the size of the compound seems to be a discrimination factor for buccal absorption [11]. Dosage forms that enable buccal absorption are for example chewable capsules that release their liquid content containing the drug into the oral cavity or wafers being placed buccally or sublingually [12, 13].

1.2.2 Oesphagus

The oesophagus connects the oral cavity with the stomach. The human's oesophagus is a 25 cm long muscular tube lined with the same mucous producing epithelial cells as in the oral cavity. It is designed to form a predominantly flexible and well lubricated route to transport a food bolus to the stomach by contraction of the skeletal and smooth muscle layer (peristaltic). Once the peristaltic wave reaches the end of the oesophagus the lower oesophageal sphincter is opened and the food bolus can enter the stomach. There are no enzymatic processes involved in the passage of the oesophagus and it is not a site of drug absorption [14].

1.2.3 Stomach

The stomach follows distally to the oesophagus. It is an organ with a pronounced organisation of three muscle layers unique in the gastrointestinal tract. This structure allows the stomach to contract in various ways in order to adjust to its filling state and to churn the stomach's content with the gastric acid (chyme). Also it helps to emulsify the incorporated fats in order to facilitate the degradation. Eventually, those muscle layers enable the emptying of the chyme into the duodenum of the small intestine. The stomach can be divided into four areas. The part where the oesophagus joins the stomach is the cardia; it is followed by the fundus and the corpus which form the main part of the stomach. The area leading towards the duodenum is named the pyloric antrum.

The already started digestive process in the oral cavity is continuing in the stomach due to the presence of gastric acid. About 2.0 - 3.0 litres are secreted daily in the stomach from glands in the gastric mucosa. The epithelium of the fundus and corpus area is folded into creases and creates deep pits in which the three types of glands are located that produce the components of the gastric acid. The parietal cells are triggered by food intake or even expected food intake and produce mainly hydrochloric acid (HCl) which can lower the gastric pH down to 1.0. HCl denaturizes the three-dimensional structure of proteins in the chyme and prepares it for the following degradation processes. In addition, HCl acts as a

disinfecting agent for possible microorganisms that were incorporated with the food. Besides that, the parietal cells also produce the intrinsic factor (IF) which allows the absorption of vitamin B12 in the small intestine. The chief cells produce pepsinogen, which is activated by acidic pH into the proteolytic pepsin. The purpose of pepsin is to further break down proteins to smaller polypeptides. The chief cells also secrete a small amount of gastric lipase, a fat degrading enzyme. The third type of gland cells in the stomach are the neck cells, their produced mucous is meant to cover the inner surface of the stomach to create a protective film in order to keep the stomach from digesting itself by the aggressive hydrochloric acid and pepsin. This circumstance requires the secretion of mucin all over the gastric surface; therefore neck cells are also present in the cardia area and the pyloric antrum.
Similar to the oral cavity and the oesophagus, absorption of xenobiotics in the stomach is negligible for most substances compared to the small intestine. However, the gastric emptying time is a physiological factor influencing the delivery of the drug to the major sites of absorption. The gastric transit time of a drug depends on the drug dosage form, prandial state and to some extent on the size and density of the particles administered [15, 16]. For drinking solutions in fasted subjects, a gastric transit half-life (50 % of formulation emptied through the pyloric sphincter) of 0.1 to 0.4 hours is reported [17]. Gastric transit times (100 % of formulation emptied through the pyloric sphincter) for pellets and Tablets are up to 2 hours in fasted subjects and increase in the non-fasted state up to 11 hours depending on the meal [18].

1.2.4 Small intestine

The small intestine (SI) of a healthy human has a total length of about 3.0 – 4.0 m and an average diameter of 2.5 cm. It is divided into three structural sections. The duodenum is the first part and follows the pylorus of the stomach. It is with 25 cm the shortest section of the SI but plays and important role in the digestion process, as the bile duct and the pancreatic duct disembogue into this section. Bile (produced by liver and gallbladder) and secreted juice from the pancreas aid in the digestion and absorption of fats, proteins and carbohydrates. Distally, the SI continues with the jejunum (2/5th of total length) and smoothly goes over into the ileum (3/5th of total length). The unique construction of the luminal mucosa which causes an enormous increase of absorptive surface area enables the SI to achieve an absorption performance multiple times higher than its actual tube length would permit (Fig. 1-1). This increase in surface area is managed in three steps. First the mucosa is clinched into circular folds (*plicae circulares*) along the duodenum and the jejunum (Fig. 1-1 A). In the next step each fold is lined with finger-like projections and deep pits referred to as villi and crypts. The

villi accommodate the mature enterocytes which are the absorptive cells of the gastrointestinal tract. The crypt area on the other hand is responsible for processes including mucous production and generating of new enterocytes (Fig. 1-1 B). Subsequently, each enterocyte is lined with additional projections (microvilli) which create the so called brush border membrane. Altogether the absorptive surface area is increased to approximately 200 m^2. Compounds absorbed at the apical side of the enterocytes and exiting on the basolateral side are directly entering the blood capillary and lymphatic system of the small intestine and are transported through the mesenteric vein and the hepatic portal vein directly into the liver. As regards pH values, as a crucial factor to drug absorption, it gradually changes along the gastrointestinal tract. Whereas the duodenum is still slightly acidic from the stomach with a pH of 6.0 it changes towards neutral further along the gastrointestinal tract to pH 7.0 - 7.5 in the ileum region. The small intestinal transit time is about 3.0 - 4.0 hours and unlike the stomach, not effected by prandial state or size and density of the dosage form [18]. Particles not absorbed in the small intestine are transported onwards into the colon via peristaltic waves.

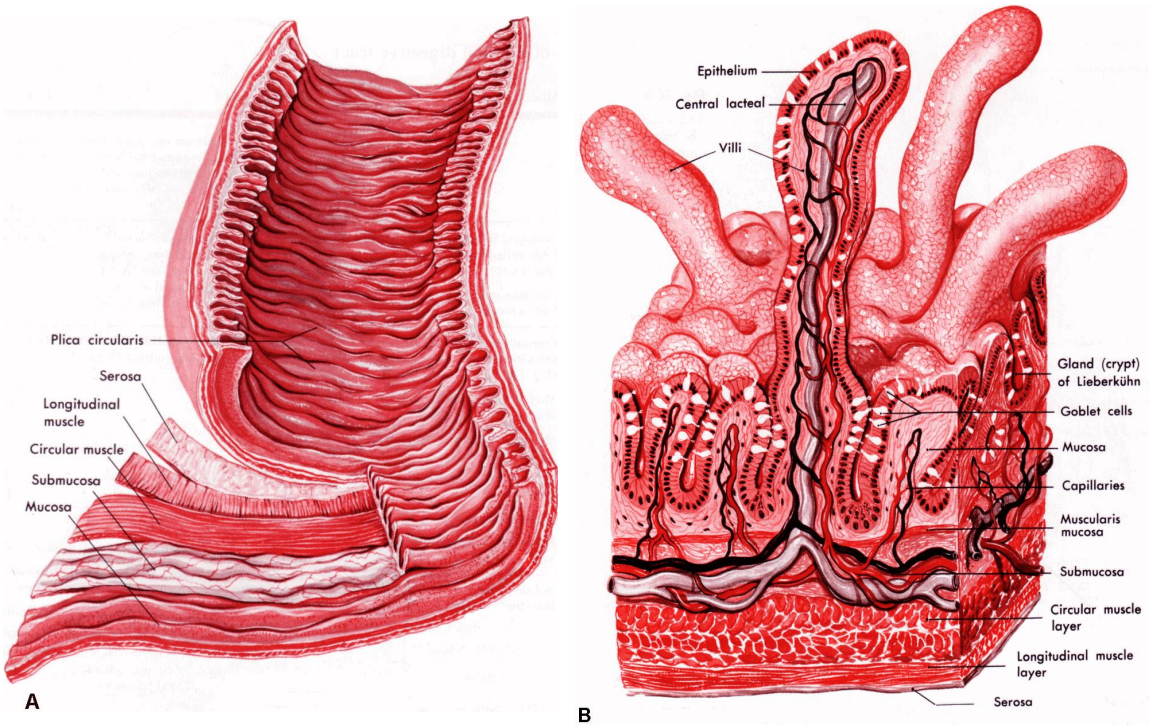

Fig. 1-1: Schematic overview of architecture of the small intestine and the mucosa. (**A)** Section of the small intestine showing the circular folds (*plicae circulares*) and the layers of the intestinal wall. (**B)** Section of the intestinal mucosa showing villi, lacteal vessels and crypts [19, 20].

1.2.5 Large intestine

Colon, rectum and the caecum form the large intestine. In man, the caecum plays a secondary role and is reduced to the appendix of the caecum, whereas in other species (e.g. rodents) it is of higher importance. In this case, the caecum is housing fermenting bacteria, which aid in cellulose digestion in herbivores [21].The main task of the large intestine is the reabsorption of water and electrolytes. The indigestible content of this section is mixed with mucous and condensed along the 1.5 m long large intestine to about 13-18 mL and is excreted by the distal end of the colon (rectum) [22]. From the histological point of view, the epithelium of the large intestine differs from that of the small intestine. *Plicae circulares* in addition to villi are absent. In contrast, the crypts are markedly deeper and mainly intended to produce mucous. The epithelial cells towards the inner lumen have the previously mentioned microvilli structure and aid the reabsorption process. An important physiological difference is the presence of bacteria (e.g. E. coli), forming the so called gut flora or microbiome. Indigestible food particles are degraded further due to fermentation and decomposition processes of the microorganisms. The pH in the large intestine varies between pH 5.5 and pH 7.0. Also, the transit time is highly variable and ranges from 8.0 to 72 hours [23].

1.3 Factors influencing intestinal absorption

A multitude of physiological, physicochemical and drug formulation factors influence the rate and extent of oral drug absorption of xenobiotics. In Chapter 1.2 some of the anatomical and physiological parameters have been discussed; hence this section will focus on physicochemical drug properties (Chapter 1.3.1), formulation factors (Chapter 1.3.2) and the mechanisms of absorption (Chapter 1.3.3).

1.3.1 Physicochemical factors

1.3.1.1 Aqueous solubility

Solubility is one of the key parameters that are mandatory for compounds to interact with the absorptive intestinal membrane. Generally, aqueous solubility is the maximum amount of compound that will dissolve in pure water at a specific temperature and pH [24-26]. As the intestinal pH varies along the GI tract, not only the solubility of a compound at different pH values is of interest, but also the pK_a value of the drug. The effect of gastrointestinal pH on

the absorption process is very complex as it influences the ionization of weak bases and acids as well as the drug dissolution from solid dosage forms. Most drugs are either weak acids or weak bases, and normally only the non-ionized fraction i.e. the most lipophilic form crosses biological membranes, except where transport carriers are involved [27]. Weak basic drugs tend to have a slower dissolution rate at higher pH, whereas weak acidic drugs dissolve faster at higher pH. Therefore meals that elevate gastric pH can decrease the dissolution of a weak base and increase the dissolution of weak acids. As high solubility is beneficial for drug dissolution in aqueous media, the same compounds often exhibit low permeability due to their high polarity and poor lipophilicity [28]. Usually, the solubility is tested by the shake-flask method, using a standard buffer solution of fixed corresponding pH [29].

In order to elucidate the dissolution of a compound a method using dissolution media that mimic the gastrointestinal *in vivo* conditions is applied. There are three commonly used buffer solutions: simulated gastric fluid with and without pepsin (SGF/SGFsp), fasted state simulated intestinal fluids (FaSSIF) and fed state simulated intestinal fluid (FeSSIF) to imitate the intestinal surroundings [30-32]. Dissolution tests in these media are especially valuable to assess dissolution of oral solid dosage forms [31-33].

1.3.1.2 Lipid solubility

The most important physicochemical prerequisite for a solubilised drug that is absorbed by passive transcellular transport is the ability to partition into the highly lipophilic bilayer membrane. The vast majority of orally administered drugs are absorbed via this transport route [34]. The ability to diffuse through lipids has been found to be highly correlated with the capability of a compound to partition between water and the organic solvent octanol. This ability is expressed by the log $P_{o/w}$ (logarithm of the partition coefficient between an octanol and a water phase) value. As a rough guideline, a passively transcellular diffusing compound should have a log $P_{o/w}$ between 0.0 – 5.0 in order to qualify for epithelial permeation [35]. This relationship is also illustrated in Fig. 1-2 in which the influence of the log $P_{o/w}$ on the measured effective jejunal permeability (P_{eff}) in man is displayed for a wide range of compounds (for details see Appendix Tab. 7-1). In order to be well absorbed, a compound needs to exhibit an effective permeability (P_{eff}) value > 1.5E-04 cm/s [36]. Fig. 1-2 demonstrates that passively transcellular well absorbed drugs show a log $P_{o/w}$ greater than zero. Well absorbed substances with a negative log $P_{o/w}$ require a different route of absorption, usually by employing a transmembrane active transporter, to overcome the low lipid solubility of the drug. Chapter 1.3.3 will elucidate the different mechanisms of intestinal

absorption.

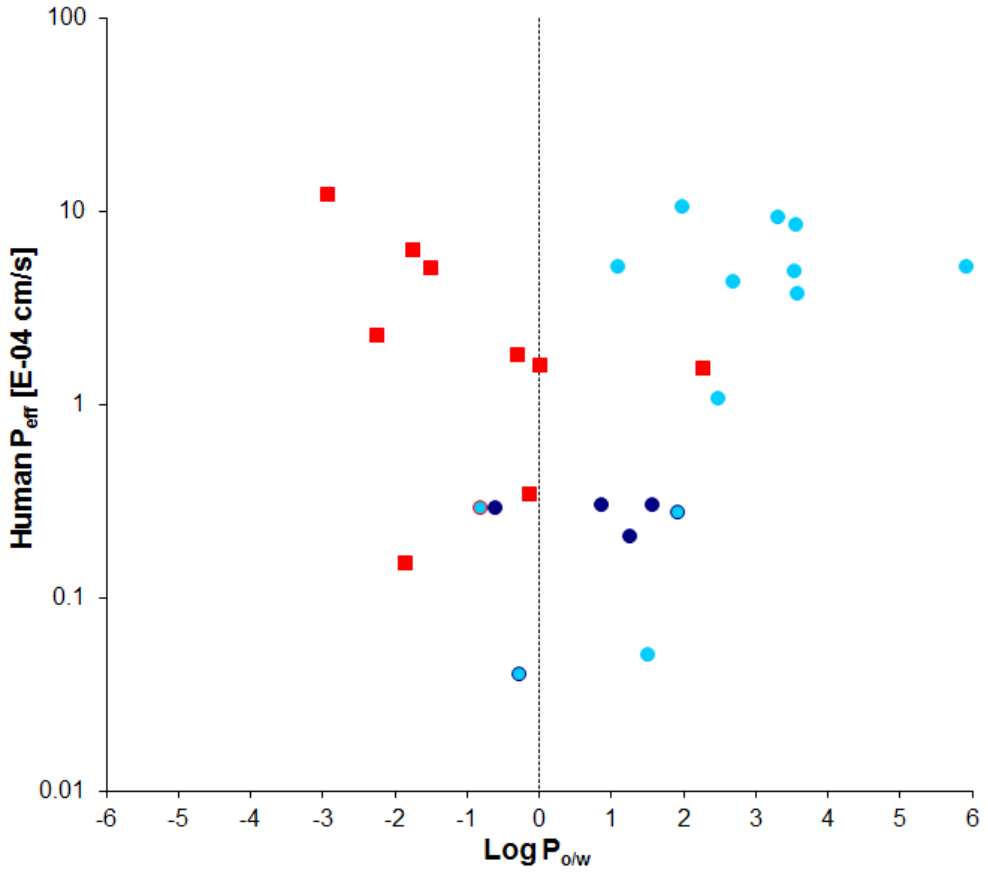

Fig. 1-2: Relationship between logarithm of the partition coefficient between an octanol and a water phase (log $P_{o/w}$) and human *in vivo* permeability expressed as P_{eff} (effective permeability) for a wide range of compounds (data acquired from literature, for details see Tab. 7-1) Transport routes: passive transcellular (●), active (■), passive paracellular through tight junctions (●), other data points combine routes of transport according to colour, whereas the outline symbolises the less dominant pathway.

1.3.2 Drug formulation factors

The role of the drug formulation in the delivery of drug to the site of action should also be mentioned. For solid oral dosage forms, a rapid disintegration is important to have a rapid absorption; therefore a low disintegration time is favourable. Additionally, dissolution time (solubilisation of solid drug substance) is an important factor which can influence the rate and extent of absorption since the drug must be in solution in order to be absorbed from the gastrointestinal tract. Based on these two factors the following order of decreased rate of absorption can be expected: solution > suspension > capsule > tablet > coated tablet. Disintegration and dissolution can also be influence by formulation manufacturing variables like applied granulation method and compression force. Finally, the use of pharmaceutical

excipients (e.g. binder, granulating agents, disintegrates and lubricants) can impact the *in vivo* performance of the dosage form [37].

1.3.3 Permeation of biological membranes

To traverse a cellular barrier like the gastrointestinal mucosa, a molecule has to pass lipid membranes. Mainly, a distinction is made between paracellular and transcellular transport, whereas the latter is divided into passive diffusional transfer and carrier mediated transport.

1.3.3.1 Transcellular transport

1.3.3.1.1 Passive transcellular transport

In order for a molecule to enter the cell it is required to cross the semipermeable biological membrane that separates the intracellular from the extracellular compartment. It consists of a double layer of phospholipids with integral transmembrane proteins. The solute can either passage directly through the lipid bilayer (passive diffusion) or it can diffuse through aqueous pores (aquaporins) formed by the transmembrane transport proteins (facilitated diffusion). For both diffusional transfer mechanisms no energy input is required as the transport is solely triggered by a concentration or electrochemical gradient. Once complete extracellular solubility of the substance is achieved, the main factor that determines the rate of passive diffusion through the biological membrane is the solubility of the molecule in lipids. As described above the partition coefficient (log P) gives a good estimation of the drug's lipid solubility. Usually non-polar molecules (equal sharing of electrons between atoms) permeate effortlessly through biological membranes as they are easily soluble in other non-polar solvents like lipids. However, many drugs are weak acids or bases and their ionization varies with pH. For these compounds, only the uncharged species (the protonated form for a weak acid and the unprotonated form for a weak base) can diffuse across lipid membranes [38]. The marked difference between passive and facilitated diffusion lies in the avoidance of passing directly through the lipid membrane, by diffusing through channel proteins. In order for a molecule to pass through those aqueous channels it has to be hydrophilic, as well as relatively small in size, because the diameter of an aquaporin is only about 0.4 nm (most drug molecules usually exceed 1 nm in diameter) [38]. Although channel proteins play a minor role for drug absorption they are vitally important for the water supply of the cell. Aquaporins are impermeable for charged species, especially protons, to obtain the existing proton gradient which is crucial, as it aids active transport processes across the membrane [39].

1.3.3.1.2 Active transcellular transport

There are three types of ATP-coupled carrier-mediated transporters involved in the transfer of solute across the epithelial membrane (Tab. 1-1). The simplest version is the carrier protein transporting one molecule from one side to the other side of the cell membrane. The molecules, or also ions, are transported against their concentration gradient. This primary active transport is referred to as uniport. The other two active transporters are cotransporters which are only indirectly coupled to ATP. They are classified as secondary active transporters and use the electrochemical potential difference created by ATP-coupled ion-pumps to either transport two molecules into the same direction (symport) or into opposite directions (antiport). For both cases, only one molecule is transported against its concentration gradient, as the other follows from high to low concentration.

Tab. 1-1: List of intestinal transporters that play a role in drug absorption [40].

Transporter	Type	Structure	Known substrates	Comment
PEPT1	symporter	H^+/peptide cotransporter	di- and tripeptides, β-lactam antibiotics, bestatin	target for improving intestinal absorption of poorly absorbed drugs
OATP	antiporter	Na^+-independent organic anion transporter	organic anions e.g. esterone-3-sulfate, dehydroepiandrosterone sulfate, taurocholic acid, pravastatin, fexofenadine	exhibits pH-sensitive transport activity
OCTN2	uni-, sym- and antiporter	organic ion transporter	e.g. carnitine	suggested link to Crohn's disease
MATE	antiporter	H+/organic cation antiporter	e.g. cimetidine, cephalexin	pH-dependent transport properties
Pgp	uniporter	ABC cassette binding transporter	broad substrate specificity, tendencies towards lipophilic cationic compounds, long list of substrates and inhibitors	suggested cooperation with CYP3A4, multidrug resistance
MRP2	uniporter	organic anion transporter	e.g. glutathiones, glucoinides	located at the proximal small intestine
MRP3	uniporter	ABC cassette binding transporter	e.g. glucuronosyls and sulphated conjugates	expressed at basolateral membrane of enterocytes, enterohepatic recirculation,
BCRP	uniporter	half-ABC cassette binding transporter	transporting diverse range of substrates	mediates efflux of the antibiotic nitrofurantoin

1.3.3.1.3 Transcytosis

Despite its minor influence on drug absorption for small molecule entities, the process of transcytosis should be included in the chapter of transcellular transport for sake of completeness. Molecules are transported across the interior of the cell via vesicles. This mechanism can for instance be triggered by binding to a membrane receptor on the surface of the cell, followed by the incorporation of the molecule by forming a vesicle and transport through the interior of the cell. Finally, the vesicle merges with the membrane on the other side of the cell and the unchanged content of the vesicle is released. The route of transcytosis is useful for proteohormones and antibodies including monoclonal antibodies and antibody conjugates [41, 42].

1.3.3.2 Paracellular transport

The absorptive intestinal epithelium is formed by a single layer of enterocytes. The neighbouring cells are bonded laterally via strands of transmembranal proteins (e.g. claudins, occludins), that have a cell-cell connecting extracellular domain. Those intercellular junctions (tight junctions) maintain the polarity of the cells as well as creating a diffusion barrier. Tight junctions are the gate to the paracellular pathway as they form small pores that allow only certain molecules to pass from the apical to the basolateral side and vice versa. The diameter of a tight junction formed space is 3.0-10 Å and therefore limits the passage of most molecules [43]. Only small (molecular weight < 200 Da), polar and hydrophilic substances are able to use the paracellular route (e.g. water, mannitol, creatinine). There is strong evidence that the density of tight junctions and the number of strands between adjacent cells varies along the GI tract [44]. There are also quantitative differences along the epithelia cells themselves between villus and crypt tight junctions. Furthermore, the structure of villus absorptive cell tight junctions is modulated by the prandial state [45]. The primary driving force for the paracellular transport is the presence of a concentration gradient, but hydrostatic pressure can also play a role. In addition to the passage restriction described above, it should also be kept in mind that the surface area of the brush border membrane lined enterocytes is > 1000-fold larger than the paracellular surface area [46].

1.3.3.3 Quantitative permeability measures

Two types of parameters are usually determined to describe permeability of a drug: the apparent permeability (P_{app}) and the effective permeability (P_{eff}). Both are experimentally

determined, whereas the P_{app} is used for *in vitro* experiments and the P_{eff} for *in situ / in vivo* experiments. The P_{app} is expressed as cm/s and calculated by the following equation:

$$P_{app}\ [cm/s] = \frac{1}{(A[cm^2] \times C_0[\mu mol/mL])} \times \left(\frac{dQ}{dt}\right)[\mu mol/s] \qquad \text{Equation 1}$$

where
A = exposed tissue area
C_0 = initial drug concentration at donor side
dQ/dt = amount of drug transported per time

The P_{eff} is also expressed in cm/s and calculated as follows:

$$P_{eff}[cm/s] = \frac{V[mL/s] \times (C_{in} - C_{out})[\mu mol/mL]}{2\pi \times R[cm] \times L[cm] \times C_{out}[\mu mol/mL]} \qquad \text{Equation 2}$$

where
V = volumic flow rate
C_{in} = concentration of drug at the entry of the intestinal segment
C_{out} = concentration of drug at the exit of the intestinal segment
R = radius of the segment
L = length of the intestinal segment

The accuracy of measurements naturally depends upon the precision of dQ/dt (Equation 1) or C_{out} (Equation 2). Moreover, C_0 (Equation 1) and C_{in} (Equation 2) are limited by the solubility of the drug, the analytical sensitivity, and the effects of high drug concentrations on epithelial integrity [47].
A P_{app} value can be converted into a P_{eff} value by means of regression analysis. In order to do so, P_{app} values for known compounds covering low and high permeabilities retrieved from a standard in-house permeability assay or absorption model (e.g. Caco-2 cells, Ussing chamber) can be related with P_{eff} values for these compounds reported in literature [48-53]. Via the calculated regression equation, P_{app} values for unknown research and development compounds can be converted into a P_{eff} value. For P_{app} values from Caco-2 cells, regression

analysis should be done for every assay type and laboratory as they can vary due to differences e.g. in cell culturing [54-56].

1.4 Physiologically based *in silico* simulation of intestinal absorption

The constant increase of high-throughput screening (HTS) techniques to identify new drug candidates leads to a higher demand on assessing pharmacokinetic (PK) properties for those compounds. These properties are usually determined using *in vivo* animal studies. In order to optimise the use of such *in vivo* testing, there has been a growing interest in predicting the PK behaviour of potential drug candidates [57, 58]. The appealing idea of predicting the rate and extent of human intestinal absorption only from physicochemical properties and data from simple *in vitro* tests in combination with anatomical and physiological data led to physiologically based *in silico* absorption models. A variety of commercially available databases and software systems provide promising tools for lead optimisation and compound selection [58]. Examples include Intellipharm® PK (Intellipharm, LCC, Niantic, CT, USA), PK-Sim® (Bayer Technology Services, Leverkusen, Germany), SimCyp® (Certara USA Inc. Princeton, NJ, USA) and Gastroplus™ (Simulations Plus Inc., Lancaster, CA, USA).

1.5 Aims

The main aim of this thesis was to challenge the common approaches used to investigate the extent of intestinal drug absorption in the pharmaceutical drug development. This task was divided into two parts.

Part I:

a) A literature review was performed to compare absorption models that are commonly used to predict *in vivo* oral drug absorption.

b) As an experimental part, the Ussing chamber absorption model using rat jejunum was implemented and evaluated by:

- performing bidirectional permeability studies for reference compounds comprising transcellular, paracellular and active transcellular absorption mechanisms
- investigating the influence of non-specific binding and tissue preparation techniques and
- assessing the quality of the experiments to assess reliability of the produced permeability data.

Part II:

A commercially available physiologically based *in silico* modelling software was challenged in order to assess its predictive performance through simulation of absorption. This was evaluated via a retrospective data analysis by:

- assessing the ability to correctly predict experimentally observed fraction absorbed (f_a) and rate constant of absorption (k_a)
- evaluating the influence of input parameters and
- comparing predictability for common laboratory species and man.

2 Materials and Methods

2.1 Literature review of absorption models

The literature research on models prediction intestinal absorption for xenobiotics was performed electronically by using the MEDLINE database via the search engine PubMed (http://www.ncbi.nlm.nih.gov/pubmed). Suitable keywords (Tab. 2-1) retrieved review articles to get acquainted with the subject which led to an in-depth search through original articles. A great range of commonly used models to estimate intestinal absorption in man were reviewed. Starting from *in vitro* methods with artificial membranes and few biological components to isolated epithelial cells and finally *in vivo* absorption studies in humans were assessed. Their strengths and weaknesses were illustrated from the viewpoint of preclinical drug development.

Tab. 2-1: List of keywords used for literature research on absorption models used to predict intestinal absorption of xenobiotics in humans.

Primary keywords	Secondary keywords	Modifier keywords
Absorption model	Drug	Prediction
Intestinal absorption	Xenobiotics	*In vitro*
Intestinal permeability	Human	*In silico*
	Pharmaceutical development	*In vivo*
	Fraction absorbed	Preclinical

2.2 Ussing chamber experiments

2.2.1 System specifications

The specifications of the equipment and materials used for the Ussing chamber permeability investigations are described in this chapter and listed in Tab. 2-2 to Tab. 2-5.

2.2.1.1 Equipment

The technical devices used for the Ussing chamber experiments are listed in Tab. 2-2.

Tab. 2-2: List of equipment used for Ussing chamber experiments.

Equipment	Supplier
Ussing chamber system	Dipl. Ing. K. Mussler (DE)
Water bath (5 litre volume)	Julabo (DE)
Thermometer (digital)	Hanna (DE)
TriCarb® liquid scintillation analyser 2100 TR / 2910 TR	Perkin Elmer (DE)

2.2.1.2 Chemicals

The chemicals used for the Ussing chamber experiments are listed in Tab. 2-3.

Tab. 2-3: List of chemicals used for Ussing chamber experiments.

Chemicals	Product number	Supplier
Krebs-Ringer hydrogen carbonate buffer, containing 1800 mg/L glucose	K4002	Sigma-Aldrich (DE)
D-(+)-glucose	G7528	Sigma-Aldrich (DE)
D-mannitol	M9546	Sigma-Aldrich (DE)
Potassium chloride	P5405	Sigma-Aldrich (DE)
Magnesium chloride	M4880	Sigma-Aldrich (DE)
Sodium dihydrogen phosphate	S3139	Sigma-Aldrich (DE)
Sodium hydrogen carbonate	S5761	Sigma-Aldrich (DE)
Sodium hydrogen phosphate	71639	Sigma-Aldrich (DE)
Sodium chloride	S5886	Sigma-Aldrich (DE)
[ring-^{3}H]-terbutaline, in ethanol	Lot#135-076-000	ViTrax Co. (USA)
[N-Methyl-^{3}H]-verapamil hydrochloride, in ethanol	Lot#3615952	PerkinElmer (USA)
D-[1-^{14}C]-mannitol, in ethanol	Lot#3570098	PerkinElmer (USA)
L-(-)-[4-^{3}H]-propranolol, in ethanol	Lot#3615695	PerkinElmer (USA)
Soluene® 350	6003038	Perkin Elmer (DE)
Ultima Gold™	6013326	Perkin Elmer (DE)
Forene®	-	Abbot AG (DE)
Ethanol	-	Sigma-Aldrich (DE)
[^{14}C]-fexofenadine	-	kindly granted by Sanofi Aventis (DE)

2.2.1.3 Chamber system

All experiments were performed using the vertical Ussing chamber (Fig. 2-1 A-D), that is characterised by its reduced buffer solution volume (< 5 mL) and compact structure compared to the classic Ussing chamber [59]. Each Ussing chamber consists of two half-cells that contain an open reservoir for buffer solution and inlets for electrodes and gas tubes (Fig. 2-1 C and D). The half-cells were united with its reservoirs only separated by the mounted tissue which exposed a tissue area of K = 0.86 cm^2. Both half-cells were joined together through pins and held steady by a high spring-tension retaining ring (Fig. 2-1 D). A fitted rubber ring sealed the site of connection to insure leak-free operation and to prevent edge damage. The supply of carbogen through the gas tubes fulfilled several purposes: First of all, it provided oxygen to the mucosal tissue and it also stabilised the pH of the buffer solution. Secondly, it works as a gas lift, which guaranteed a constant circulation of the solution in the reservoirs and reduced the forming of an unstirred water layer. An Ussing chamber system consists of six Ussing chambers that are placed in a heating block with is temperature controlled by an external water bath (Fig. 2-1 A and B). The buffer solution on each side of the chamber was kept constant at 37°C (Chapter 2.2.1.4). To assure the maximum use of each sacrificed animal, two Ussing chamber systems were operated simultaneously for every experiment (Fig. 2-1 A).

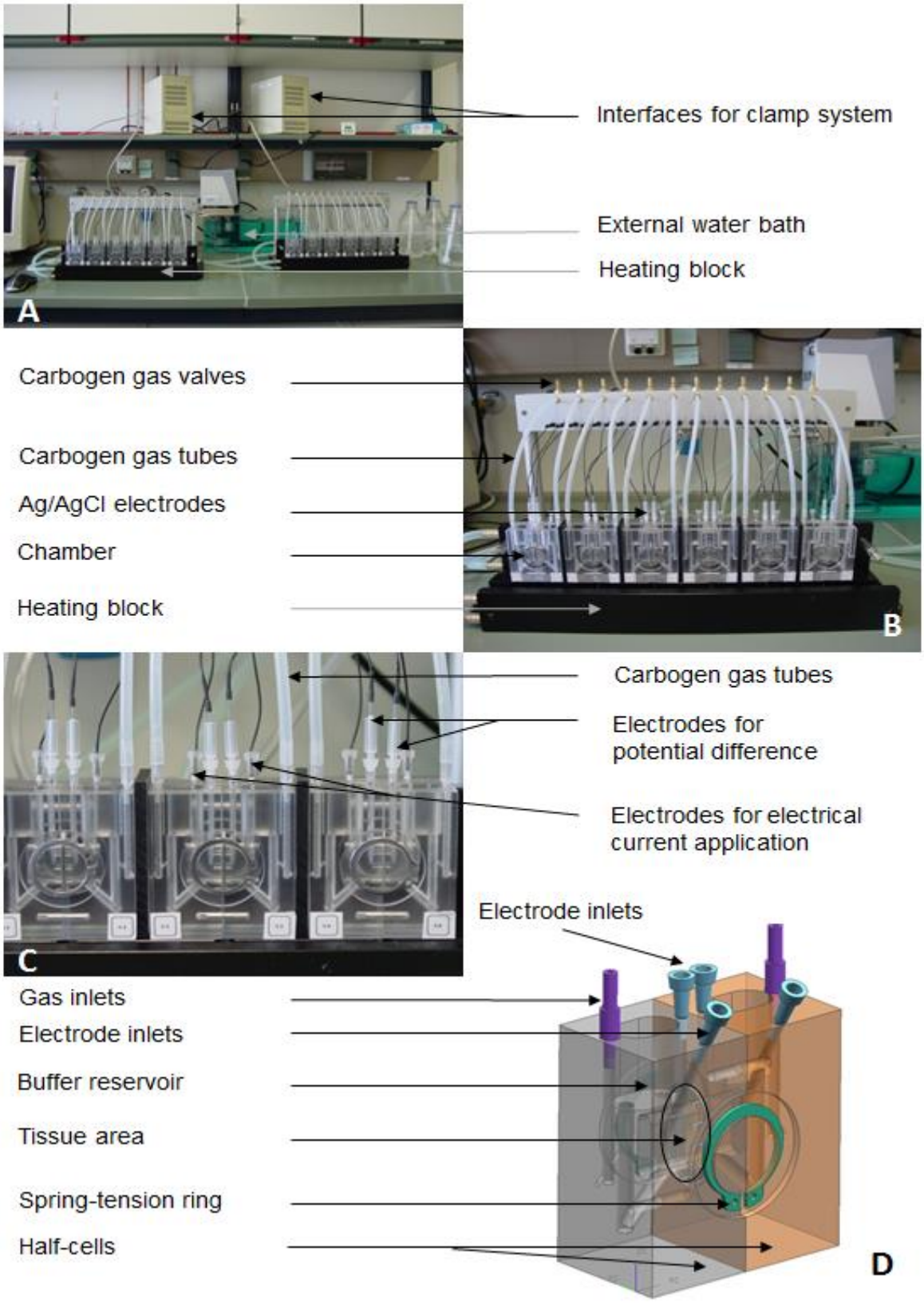

Fig. 2-1: Ussing chamber system. (**A**) Complete set-up with 2x six chambers connected to a water bath, to carbogen gas supply and interfaces for the clamp system. (**B**) Six chambers in heating block with connected electrodes and gas tubes. (**C**) Close-up of the chambers (**D**) Schematic drawing of a single chamber.

2.2.1.4 Buffer solution

Two kinds of Krebs-Ringer hydrogen carbonate buffer solutions (KRB) were used for all experiments. The KRB buffer containing glucose (1 mM) was used on the serosal side to nourish the tissue. As the presence of glucose triggers a Na^+-influx into the cells, and therefore a change of the membrane potential on the mucosal side, which influences the electrical measurements (Chapter 2.2.1.5), mannitol (1 mM) was used as an osmolaric substitute on the mucosal buffer side. The exact composition is shown in Tab. 2-4. The KRB solution was adjusted to a pH of 7.4 using hydrochloric acid or sodium hydrogen carbonate and was continuously gassed with carbogen.

Tab. 2-4: Components of the Krebs-Ringer hydrogen carbonate buffer solution (KRB).

Components	Concentration [g/L]	Concentration [mM]
D-glucose (serosa side) or D-mannitol (mucosa side)	1.80	10.0
Magnesium chloride	0.0468	0.500
Potassium chloride	0.340	4.60
Sodium chloride	7.00	120
Sodium dihydrogen phosphate	0.100	0.700
Sodium hydrogen phosphate	0.180	1.50
Sodium hydrogen carbonate	1.26	15.0

2.2.1.5 Electrical components

Every Ussing chamber contained four connecting tubes for two silver/silver-chloride (Ag/AgCl) electrode pairs. One pair ended in close proximity to the mounted tissue to determine the potential difference (dP) between the mucosal and serosal side (Fig. 2-1 C). The measurements were automatically corrected for fluid resistance (R_f) and the difference of the electrodes potential (dPe), also known as offset. These values were determined prior to tissue mounting. The second pair of Ag/AgCl-electrodes was located furthest away from the epithelial membrane and was used to apply an electric current. Each electrode pair was connected to a multichannel computer-controlled voltage-current clamp system (Fig. 2-1 A). Monitoring the electrophysical parameters of the tissue is a common method to obtain information about the viability and integrity of the tissue in the Ussing chambers [60, 61]. In general, the potential difference (dP) reflects the voltage gradient generated by the intestinal tissue, the transepithelial resistance (R_t) reflects the tissue integrity and the short-circuit

current (Isc) gives information about the ionic fluxes across the epithelium [60]. To avoid the bias of a chemical and hydrostatic gradient, identical volumes and ion concentrations of the KRB solutions were used on both sides of the tissue (Chapter 2.2.1.4). Experiments were performed under open circuit conditions (i.e. no external current was applied).

2.2.1.6 Animals

All animal studies were approved by authorities including the Regional Office for Health and Social Affairs (LAGeSo) for the state and city of Berlin and were performed in accordance with the ethical guidelines of Bayer Pharma AG. For all experiments, excised jejunum from adult male Wistar rats (HsdCpb:WU; Harlan, Netherlands) was used. The body weight of the animals ranged from 200–320 g on day of sacrifice. The rats were kept under 12:12 hour light-dark-cycle conditions and received water and chow ad libitum.

2.2.1.7 Reference compounds

To successfully establish the Ussing chamber technique in the laboratory, a range of well described reference compounds (Tab. 2-5) was chosen from literature and used to evaluate the system [36, 60, 62-69]. In the choice of reference compounds, care was taken to cover all routes of absorption (passive paracellular, active and passive transcellular).

- ^{14}C-mannitol permeates paracellularly through the tight junction located on the apical side of the tissue and therefore does not enter the enterocytes. It was used for all experiments (except for the fexofenadine studies) as a marker to determine the amount of extracellular water in the excised tissue and to monitor the tissue integrity during the permeability experiment (Chapter 2.2.2.4). ^{14}C-mannitol is small (MW 182) and highly hydrophilic molecule with a log P value of - 3.9.
- ^{3}H-terbutaline is a small (MW 225), slightly hydrophilic compound with a log P value of 1.4, which also permeates paracellularly through the tight junctions.
- ^{3}H-propranolol and ^{3}H-verapamil were used as transcellular reference compounds as they are absorbed through the enterocytes. Consequently, both compounds are lipophilic with a log P of 3.0 and 4.7, respectively. Due to their hydrophobicity, these compounds are prone to non-specific binding. In addition, verapamil is also a substrate as well as an inhibitor of the P-glycoprotein [70-72]. This characteristic would allow for mechanistic investigations concerning the involvement of Pgp in the intestinal permeability of development compounds.
- ^{14}C-fexofenadine was included as a reference compound for active transcellular transport. Fexofenadine is substrate to the organic anion-transporting polypeptide

(OATP) which is present in human and rat small intestine [73-75]. Therefore, fexofenadine is a suitable reference compound for active transport in Ussing chamber experiments using rat jejunum. In the fexofenadine studies ^{3}H-terbutaline was used as a substitute for ^{14}C-mannitol, as fexofenadine and mannitol contained the same radiolabel, which restricts distinguishing between reference and tissue integrity marker compound.

Tab. 2-5: Properties of reference compounds used to experimentally establish the Ussing chamber system.

Reference compound	**Mannitol**	**Terbutaline**	**Propranolol**	**Verapamil**	**Fexofenadine**
MW [g/mol]	182.2	225.3	259.3	454.6	501.7
Log $P_{o/w}$	-3.9	1.4	3.0	4.7	5.6
Solubility in water [mg/mL]	216	213	0.07	0.0045	0.0027
Radiolabel	^{14}C	^{3}H	^{3}H	^{3}H	^{14}C
Specific activity [MBq/µmol]	1.89	925	899	2549	1.95
Permeability properties	passive paracellular	passive paracellular	passive transcellular	passive transcellular	active transcellular
Comment	tissue integrity marker	tissue integrity marker	-	substrate and inhibitor of Pgp	substrate of OATP transporter

It should be mentioned that all samples taken during permeability experiments contain two radiolabeled reference compounds: One compound for permeability investigations and one tissue integrity marker compound. In order to distinguish between them, during measurement, it is essential that they have different radiolabels. The compound combinations used for permeability studies are listed in Tab. 2-6. Regardless of their primary function (permeability investigation or tissue integrity marker) they are all also referred to as reference compound.

Tab. 2-6: List of reference compound combinations and their respective functions used during Ussing chamber permeability investigations.

Reference compounds	
Function: permeability investigation	**Function: tissue integrity marker**
^{3}H-propranolol	^{14}C-mannitol
^{3}H-verapamil	^{14}C-mannitol
^{3}H-terbutaline	^{14}C-mannitol
^{14}C-fexofenadine	^{3}H-terbutaline

2.2.2 Experimental settings and procedures

After introducing the components and specifications of the Ussing chamber system (Chapter 2.2.1) this chapter will give details about the experimental settings and procedures used during the permeability investigations.

2.2.2.1 Sampling scheme

During the permeability studies the sampling scheme was the same for all reference compounds and as followed: After the tissue was mounted onto the Ussing chamber and submerged in blank KRB solution, samples of 250 µL were taken from each chamber reservoir prior to the start of an experiment. The samples were measured via liquid scintillation counting (LSC) (Chapter 2.2.2.3) to determine baseline radioactivity in the Ussing chamber equipment. This is mandatory to monitor contamination of the Ussing chamber with radiolabeled compound from previous experiments which can bias subsequent samples from the experiment. Start concentrations of the reference compounds on donor and receiver side were determined prior to the start of the experiment: For the receiver side, a 250 µL sample was drawn from the receiver reservoir as described above (baseline determination). In order to insure homogeneity of the donor side concentration of the radiolabeled reference compounds, a glass vial was prepared for every donor reservoir containing 4 mL KRB and the intended donor start concentration of the reference compounds. Vials were well mixed and a 250 µL sample was taken to determine the donor start concentrations. To start an experiment the blank KRB buffer in the donor reservoir was completely withdrawn with a syringe and immediately replaced by the volume left in the glass vial containing the radiolabeled compounds.

To study the permeability of the reference compounds over time, a sampling scheme was selected that was applied to all studies. Sampling time points were: 5, 10, 20, 40, 60, 90, 120 and 150 minutes (Tab. 2-7). The sampling volume of 250 µL was replaced by blank KRB buffer after each sampling time point. The dilution factor for the reference compounds was considered during evaluation. At the end of each experiment (at 150 min) the tissue was dismounted from each chamber and each tissue sample was prepared as described in Chapter 2.2.2.2.

Tab. 2-7: Sampling scheme for the reference compounds on donor and receiver side of the Ussing chamber including tissue sample for all time points.

Time point [min]	Start	5	10	20	40	60	90	120	150
Donor side	x	-	-	-	-	-	-	-	x
Receiver side	x	x	x	x	x	x	x	x	x
Tissue	-	-	-	-	-	-	-	-	x

2.2.2.2 Sample preparation for measurement of radioactivity

Two kinds of samples were prepared for measurement of radioactivity via liquid scintillation counting (LSC) (Chapter 2.2.2.3). For aqueous samples, the entire sampling volume was thoroughly mixed with 5 mL of the scintillation cocktail Ultima Gold™ (Perkin Elmer, Germany), to obtain a homogeneous measuring sample. For determining radioactivity in tissue, samples were prepared as shown in Fig. 2-2. Briefly, tissue specimens were removed from the Ussing chamber after the permeability experiment and transferred to previously weighed glass vials. Vials were weighed again, to determine the net tissue weight which was used to determine the amount of reference compound in tissue (Chapter 2.2.4.3). Subsequently, the tissue sample was solubilised in 3 mL of a strong organic base (Soluene®350, Perkin Elmer, Germany) for at least 24 hours. Homogenous samples of 1 mL were taken from the dissolved tissue and well mixed with 15 mL of Ultima Gold™. Two aliquots per tissue were prepared and measured as described in the following chapter.

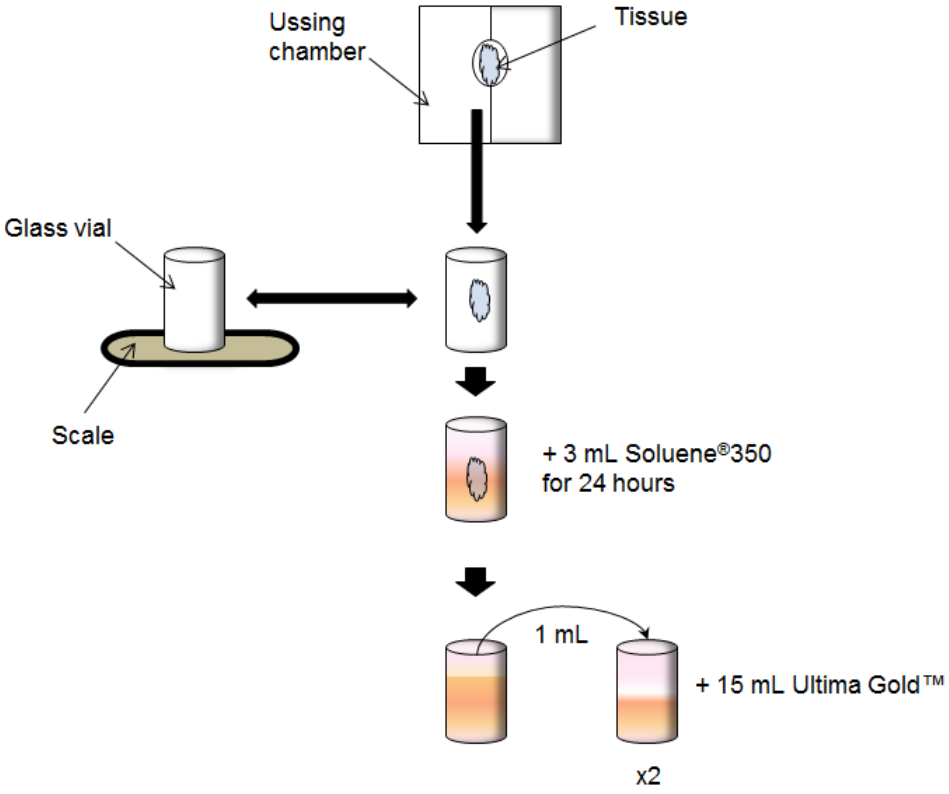

Fig. 2-2: Flow chart of tissue sample preparation for measurement of radioactivity via liquid scintillation counting (LSC).

2.2.2.3 Measurement of radioactivity

Measurements of radioactivity were performed via a previously validated and routinely controlled liquid scintillation counting (LSC) method [76]. The count conditions applied to the radioactivity measurements within this thesis are listed in Tab. 2-8 and were in line with the locally applied validation document and the existing standard operating procedures. LSC is a standard laboratory method to quantify the radioactivity of low energy organic isotopes, mainly used for water soluble β-emitters. The sensitive LSC detection method requires specific cocktails to absorb the emitted energy from the isotopes in order to convert them into detectable light pulses. To accomplish these two actions, absorption and re-emission, the cocktails contain two alkaline components, an aromatic solvent (e.g. toluene) and a scintillator (fluorescing agent). The solvent carries out the energy absorption, and dissolved in the solvent, molecules of the fluorescing agent convert the absorbed energy into light. For

all experiments, the scintillation cocktail Ultima Gold™ was used. The emitted light pulses were registered in the counter. It detected the number of pulses per minute as well as the intensity of each light pulse which corresponded to the emitted energy of the isotope. Counts of pulses were collected into channels with a predefined energy spectrum (Tab. 2-8). This allowed distinguishing between low energy ^{3}H-isotpes and medium energy emitting ^{14}C-isotopes which were used simultaneously in the same measuring sample. This technique is referred to as dual-isotope measuring and was applied to all permeability experiments. To correct the measurement for naturally occurring "background" radiation, a sample of blank KRB or Soluene®350 was freshly prepared and mixed with the appropriated volume of Ultima Gold™ (Chapter 2.2.2.2). Prior to every measuring set, the counts per minute (CPM) measured in the blank sample were determined and automatically subtracted from all following samples in the set. Measuring time was 10 minutes for each blank and 5 minutes for each sample containing radioactivity. Correcting for background radiation and counting efficiency (previously determined chemical and colour quench) allows determining the disintegrations per minute (dpm) in the sample [76]. The by the TriCarb® liquid scintillation analyser automatically calculated dpm values were used for data evaluation (Chapter 2.2.4).

Tab. 2-8: Count conditions for dual-isotope liquid scintillation counting using the TriCarb® liquid scintillation analyser.

Isotope	Region settings	Minimum acceptable efficiency	Quench sets (Indicator tSIE/AEC)	Lower limit of quantitation (LLOQ) [dpm]	Upper limit of detection (ULOD) [dpm]
^{3}H	Region A: Lower limit=0 keV Upper limit=12 keV	60%	Low energy	5	1 000 000
^{14}C	Region B: Lower limit=12 keV Upper limit= 156 keV	95%	Mid energy	10	1 000 000

tSIE/AEC= transformed spectral index of the external standard with automated efficiency control

2.2.2.4 Tissue viability

Tissue viability during the experiments was monitored by measuring the electrical resistance of the mucosal tissue (R_t) (Chapter 2.2.1.5). Also, the appearance of ^{14}C-mannitol on the receiver side was monitored during data evaluation and used to assess tissue integrity (Chapter 2.2.1.7). An over proportional increase of ^{14}C-mannitol on the receiver side was considered as an indicator for tissue damage. In addition, glucose (final concentration

50 mM) was added to the mucosal chamber reservoir at the conclusion of the experiment to test the functional viability of the tissue as it is transported by the SLGT1 transporter. SLGT1 is the intestinal epithelium sodium-glucose symporter that channels Na^+ ions and glucose into the epithelial cells by using the energy from a downhill sodium gradient to transport glucose across the apical membrane against an uphill glucose gradient [77, 78].

2.2.3 Experimental studies

Two types of experiments were performed using the Ussing chamber system: Experimental studies without tissue in order to determine the extent of non-specific binding of the reference compounds to the Ussing chamber material and permeability studies using intestinal tissue from rats.

2.2.3.1 Non-specific binding studies

In order to determine if the reference compounds bind non-specifically to the Ussing chamber, binding studies have been conducted for every used compound. Especially for highly lipophilic compounds, non-specific binding can alter the results to a significant degree, particularly at low concentrations. The setup and conditions for these pre-studies were chosen to be as close as possible to the actual experimental settings of the permeability experiment (Chapter 2.2.3.2.2). For each reference compound, two concentrations have been tested to mimic the expected donor and receiver concentration at t=0 and t=150 minutes, respectively, as the non-specific binding might be time-dependent due to saturation processes. The donor test concentration was about 6.0 nM and the receiver test concentration was approximately 0.1 mM.

Briefly, for non-specific-binding studies, the Ussing chamber system was set up omitting the tissue mounting step (Chapter 2.2.3.2.1) and the chambers (n=3 per compound) were filled with 8 mL of buffer containing radiolabeled reference compound. Samples of 80 µL were taken at the same time points mentioned in the sampling scheme (Tab. 2-7) and prepared and measured as described in Chapters 2.2.2.2 and 2.2.2.3.

In order to determine the total recovery, two washing steps with ethanol were implemented after the non-specific binding experiment. After the last sample was taken (time point 150 min), the remaining buffer solution containing radiolabeled compound was discarded; every chamber was filled with 8 mL of ethanol (a suitable solvent for the compounds, that would not damage the material of the acrylic glass chambers) and was allowed to stand for 10 min. Afterwards, three aliquots of 750 µL were taken from each chamber and prepared

and measured as described before (Chapters 2.2.2.2 and 2.2.2.3). The ethanol washing step was repeated once more. The compound in the taken samples and the compound extracted from the chambers in the washing steps were added up and compared to the initial concentration administered in the non-specific binding experiment and the total recovery for every compound was calculated (Chapter 2.2.4).

2.2.3.2 Permeability studies

In order to perform the permeability studies using the Ussing chamber system, rat jejunum tissue had to be prepared prior to start of the permeability experiment.

2.2.3.2.1 Tissue preparation

Two types of tissue preparations techniques were applied: For each reference compound, full-thickness tissue (mucosa including connected muscle layers and serosa) experiments and stripped tissue (serosal layer removed) experiments were performed. Immediately prior to each experiment, rats were sacrificed by an overdose of isofluran (Forene®) and the abdominal cavity was opened. Blood was withdrawn from the vena cava and the small intestine was removed distally from the pyloric sphincter to proximal of the caecum. Then the lumen was rinsed with ice cold Krebs-Ringer hydrogen carbonate buffer solution (KRB) to remove intestinal debris. Subsequently, the small intestine was transferred into ice-cold KRB containing glucose (1 mM) and was continuously gassed with carbogen (95 % O_2 / 5 % CO_2) for 15 min. After temperature adjustment the first 10 cm of the proximal small intestine was discarded and 12 cm long segments were carefully pushed over a plastic rod (Ø 6 mm). Jejunum sections of approximately 3 cm were separated by circular incision using a scalpel. In case of experiments with stripped tissue the serous membrane of the full-thickness tissue was removed by blunt dissection with forceps prior to sectioning off the segments. All separated segments were opened with a longitudinal cut along the mesenteric border and mounted onto the tissue pins in the half-cells of the Ussing chamber. Immediately afterwards, the chambers were assembled and the reservoirs were filled with the appropriate buffer solutions to quickly submerge the tissue.

2.2.3.2.2 Procedure of the permeability experiment

The microprocessor controlled interface for the clamp system (Chapter 2.2.1.5) and the heating blocks (Chapter 2.2.1.3) were started at least 15 min prior to electrical measurements. At the same time, two types of Krebs-Ringer hydrogen carbonate buffer solutions containing mannitol or glucose, respectively, were tempered and equilibrated with carbogen (Chapter 2.2.1.4). The Ussing chambers were filled with blank mannitol KRB buffer and all electrodes were inserted and connected to the interfaces. Also the gas tubes were connected and the carbogen flow was introduced (Chapter 2.2.1.3). The clamp software (Clamp, Dipl. Ing. K. Mussler, Aachen, Germany) was started and solution resistance (R_f) and inherent potential difference of the electrodes (dPe) were determined and if necessary adjusted for factors influencing dPe determination. This could include removal of air bubbles in contact with the electrode, clearing off possible corrosion or swapping out damaged electrodes for new ones. When the lowest inherent potential difference of each electrode pair was reached (as close as possible to 0 mV), two buffer solutions containing radiolabeled reference compounds were prepared for each permeability experiment, using mannitol KRB and glucose KRB, respectively. Next, the animal was sacrificed and the small intestine removed and handled as described in Chapter 2.2.3.2.1. After taking the chambers apart, the tissue was mounted, the chamber reassembled and the sides were filled with the appropriate blank buffer solution (mannitol KRB on mucosal side and glucose KRB on serosal side). The tissue was immediately exposed to carbogen. Chambers 1-6 were used to investigate mucosal to serosal transport (m-s) and chambers 7-12 were used for serosal to mucosal transport (s-m). To avoid regional differences of absorption the tissue was mounted alternately (mounting sequence: chamber 1, 7, 2, 8, 3, 9, 4, 10, 5, 11, 6, and 12) and the electrical measurements were started (Chapter 2.2.1.5). To start the permeability experiment, the blank buffer was replaced by the appropriate buffer containing radiolabeled reference compounds on the donor side and samples were taken according to the sampling scheme mentioned before (Tab. 2-7). The electrophysiological parameters were recorded for at least 150 min. At the end of the permeability study, the tissue viability test using glucose was performed (Chapter 2.2.2.4). Subsequently, the buffer solution was discarded and the chambers disassembled to remove the tissue. The tissue was transferred into a tared glass vial, weighed and solubilised with Soluene®350 as described in Chapter 2.2.2.2. After preparation, all samples were measured via LSC (Chapter 2.2.2.3).

2.2.4 Data evaluation

2.2.4.1 Calculation of non-specific binding

For every compound, the arithmetic mean was calculated from the 3 samples taken in the non-specific binding (NSB) experiments for every time point (Chapter 2.2.3.1). Then a recovery ratio (Rec_{tx}) was calculated (Equation 3) for each sampling time point which was then used to correct the measured samples from the permeability experiments for the non-specific binding (Equation 4).

$$Rec_{tx} = \frac{C_{tx}[dpm/\mu L]}{C_{t0}[dpm/\mu L]} \qquad \text{Equation 3}$$

C_{tx} = concentration at time point x
C_{t0} = initial concentration
dpm = disintegrations per minute

In order to perform a mass balance of the compound in the NSB experiments, all measured concentrations of the taken samples and the compound recovered in the washing steps (Chapter 2.2.3.1) were extrapolated to the total volume of each chamber (8 mL). The amounts were added up and compared to the initial amount of compound administered to each chamber. The percentage deviation between initial amount of compound and recovered amount of compound was considered the NSB.

2.2.4.2 Calculation of apparent permeability

The apparent permeability (P_{app}) for the permeability studies (Chapter 2.2.3.2) was calculated in the following steps:
Firstly, for every receiver chamber, the concentration of compound in the sample at each time point was corrected for the recovery ratio (Equation 3) of the previously determined respective non-specific binding at the same time point (Equation 4).

$$C_R corrected[dpm/\mu L] = \frac{C_R[dpm/\mu L]}{Rec_{tx}} \qquad \text{Equation 4}$$

$C_R$corrected = concentration in receiver chamber corrected for non-specific binding
C_R = concentration in receiver chamber

Rec_{tx} = recovery ratio of compound at time point x

In a second step, the concentration of compound was corrected to the amount of compound in the receiver chamber volume of 4 mL for each time point. Divided by the specific activity of the radiolabeled compound (Tab. 2-5), the total amount per receiver chamber was calculated (Equation 5).

$$A_R corrected[\mu mol] = \frac{C_R corrected[dpm/\mu L]}{spec.activ.[dpm/\mu mol]} \times 4000 \qquad \text{Equation 5}$$

$A_R$corrected = amount in receiver chamber corrected for non-specific binding
spec. activ. = specific activity of the radiolabeled compound

In the next step, the cumulated corrected amounts of compound in the receiver chamber were plotted against time for each chamber (example Fig. 3-2). The linear slope (m) determined by linear regression represents the increase of permeated drug on the receiver side per time and therefore, the flux rate. Due to a lag time of establishing a flux rate constant across the intestinal membrane, only the slope from the linear part of the curve (i.e. time interval 60-120 min) was evaluated (Tab. 3-6). In combination with the exposed tissue area (Ussing chamber equipment specific constant value), a transport flux in [µmol/cm^2/s] was calculated (Equation 6).

$$Flux[\mu mol/cm^2/s] = \frac{m[\mu mol/min]/K[cm^2]}{60\ [s/min]} \qquad \text{Equation 6}$$

m = linear slope
K = exposed tissue area for each chamber (0.86 cm^2)

In a final step, the P_{app} was calculated as a ratio of flux and reference compound concentration at the end of the experiment on the donor side (Equation 7).

$$P_{app}[cm/s] = \frac{Flux[\mu mol/cm^2/s)]}{C_D end[\mu mol/mL]} \qquad \text{Equation 7}$$

$C_D$end = concentration of compound on donor side at the end of the experiment

2.2.4.3 Calculation of amount of compound in tissue

In order to determine the absorption mechanisms of the reference compounds (transcellular or paracellular), the amount of compound from permeability studies in the enterocytes was calculated with the help of the tissue integrity marker compound as a known paracellularly permeating compound (Tab. 2-5) and therefore also an extracellular marker.

2.2.4.3.1 Calculation of enterocyte mass in tissue

The mass of enterocytes contributing to the overall mounted tissue weight was calculated using the following relationship:

$$M_{\ enterocytes}[g] = M_{wet\ tissue}\ [g] - M_{ECF}[g] \qquad \text{Equation 8}$$

M_{ECF} = mass of extracellular fluid
$M_{enterocytes}$ = mass of enterocytes
$M_{wet\ tissue}$ = mass of wet tissue

In order to calculate the mass of enterocytes in the tissue and subsequently the amount of compound in the enterocytes, the volume or mass of the extracellular fluid had to be determined.

2.2.4.3.2 Calculation of extracellular fluid mass using an extracellular marker

The amount of extracellular fluid adhering to the mounted tissue after the experiment was calculated using the tissue integrity marker compound as an extracellular marker. The following relationship was applied:

$$V_{ECF}[mL] = \frac{M_{ECF+ICF}[dpm]}{C_{ECF}[dpm/mL]} \qquad \text{Equation 9}$$

V_{ECF} = volume of extracellular fluid
$M_{ECF+ICF}$ = mass of extracellular marker compound in extracellular fluid and intracellular fluid
C_{ECF} = concentration of extracellular marker in extracellular fluid

whereas

$$M_{ECF+ICF}[dpm] = M_{wet\ tissue}[dpm] \qquad \text{Equation 10}$$

$M_{wet\ tissue}$ = mass of extracellular marker compound in wet tissue

Further assumptions were made to calculate the volume of extracellular fluid:

$$M_{ICF}[dpm] = 0 \qquad \text{Equation 11}$$

for the extracellular marker ^{14}C-mannitol (or ^{3}H-terbutaline for the fexofenadine experiments) and

$$C_{ECF}[dpm/mL] \triangleq Cdonor_{end}[dpm/mL] \qquad \text{Equation 12}$$

$Cdonor_{end}$ = concentration of extracellular marker compound in the donor side of the chamber by the end of the experiment

The measured concentration of extracellular marker in the extracellular fluid adhering to the tissue should be equivalent to the concentration of extracellular marker in the buffer solution on the donor side of the chamber by the end of the experiment when the tissue was removed.
The calculated V_{ECF} was then converted into mass (M_{ECF}) using the density of water $(\rho = 1g/mL)$.

2.2.4.3.3 Calculation of intracellular concentration of compound

The calculated mass of the extracellular fluid was subtracted from the total wet tissue mass to obtain the mere enterocyte mass as described in Equation 8.
To determine the amount of compound in the enterocytes, the extracellular marker compound adhering to the tissue had to be deducted. It was again assumed, that the concentration of the compound in the extracellular fluid was equal to the concentration on the donor side by end of the experiment.

$$Mcompound_{ECF}\ [dpm] = Cdonor_{end}\ [dpm/mL] \times M_{ECF}[mL] \qquad \text{Equation 13}$$

$Mcompound_{ECF}$ = mass of extracellular marker compound
$Cdonor_{end}$ = concentration of compound on the donor side by the end of the experiment

M_{ECF} = mass of extracellular fluid

By subtracting the extracellular compound from the quantity in the wet tissue, the total amount of compound located in the enterocytes was calculated according to Equation 14.

$$Mcompound_{ICF}[dpm] = M_{wet\ tissue}[dpm] - Mcompound_{ECF}[dpm] \quad \text{Equation 14}$$

Mcompound $_{ICF}$ = mass of intracellular compound
$M_{wet\ tissue}$ = mass of compound in wet tissue

In order to illustrate to what degree the compound was absorbed into the enterocytes, a relationship between the concentration of compound in the cells (compound per gram enterocytes) and concentration of compound on the donor side of the chamber was established.

$$Ccompound_{ICF}[dpm/g] = \frac{Mcompound_{ICF}[dpm\,]}{M_{enterocytes}[g]} \quad \text{Equation 15}$$

$Ccompound_{ICF}$ = concentration of compound in enterocytes

For comparison of different compounds the ratio of intracellular and extracellular compound concentration can be calculated.

$$ratio = \frac{Ccompound_{ICF}\,[dpm/mL]}{Cdonorend_{end}\,[dpm/mL]} \quad \text{Equation 16}$$

2.2.4.4 Calculation of mass balance

All the above calculated values were also used to perform a mass balance, in order to describe the recovery of the compound from in the permeability experiments.

$$Recovery_{tot}[\%] = \frac{\left((Mdonor_{end}[dpm] + Mreceiver_{tot}[dpm] + M_{wet\ tissue}[dpm]) \times 100\right)}{Mdonor_{start}[dpm]} \quad \text{Equation 17}$$

$Recovery_{tot}$ = total recovery of compound

$M_{donor\ end}$ = mass of compound on donor side by end of experiment

$M_{receiver\ tot}$ = total mass of c-ompound on the receiver side by end of experiment

$M_{wet\ tissue}$ = mass of extra- and intracellular compound in wet tissue

$M_{donor\ start}$ = mass of compound on donor side by start of experiment

2.2.4.5 Statistics

For the Ussing chamber experiments, the results are gives as mean ± standard deviation (SD) with the respective coefficients of variation (CV). Calculations were performed in Excel 2007 software (Microsoft Inc., Redmond, WA, USA).

Test statistics were performed using R version 2.13.1 (open source). The Shapiro-Wilk normality test [79] for small data sets was used to test for normal distribution of the calculated P_{app} data. The α-level was set to 0.05 for the null hypothesis (population is normally distributed). Subsequently, the two sample t-test was performed for statistical comparison whether the average difference between two test groups (full-thickness tissue / stripped tissue and mucosal-serosal / serosal-mucosal) was significant for each compound or due to random chance. The α-level for the null hypothesis (groups show difference by random chance) was set to 0.05. With p-value < 0.05 the null hypothesis was rejected and the difference between the two tested groups was considered statistically significant.

2.3 Simulation of intestinal absorption using GastroPlus™

Background information and details on the physiologically based software GastroPlus™ and the process on how the predictive performance regarding intestinal absorption was assessed are given in this chapter.

2.3.1 Advanced compartmental absorption and transit model

GastroPlus™ (Simulations Plus Inc., Lancaster, CA, USA) is a collection of mathematical models and correlations and is primarily used to simulate intestinal absorption of orally administered drugs and to investigate the effect of physiochemical, physiological and formulation factors on gastrointestinal absorption in man and laboratory animal species [80]. This software already contains physiological and anatomical characteristics of the gastrointestinal tract for both human and common laboratory animals. Its mathematical model derives from the compartmental absorption and transit (CAT) model introduced by Yu et al. in 1996 [81]. Their dynamic CAT model was able to predict the fraction of dose absorbed and the absorption rate constant as it considered the temporal variable deriving from the transit flow of the drug. The gastrointestinal tract is divided in various compartments allowing specifications of regional pH, volume of fluids and permeability. For the CAT model a couple of assumptions were made, e.g. that absorption from the stomach and the colon is insignificant compared to the small intestine and that instantaneous dissolution of the drug would occur [82]. These restrictions led to an improvement of the model to the advanced compartmental absorption and transit (ACAT) model that is implemented in the GastroPlus™ software. The ACAT model allows the software to account for low dissolution rates, pH dependent solubility and additionally it can predict the fraction absorbed from controlled release formulations as the colon is considered as an absorptive compartment. Further improved features like implementing carrier-mediated transport or gut wall metabolism are available but require additional *in vitro* input data. Briefly, the ACAT model consists of nine compartments, one for stomach, one for colon and seven compartments for the small intestine. Each is segmented into four subcompartments representing compartments for unreleased, undissolved and dissolved drug and drug in enterocytes (**Fehler! Verweisquelle konnte nicht gefunden werden.**). Precipitation of dissolved compound into undissolved compound can also be accounted for. The ‘unreleased’ compartment refers to drug presented as a solid oral dosage form including capsules, tablets and modified release formulations. Once released, the drug can either dissolve into a solution or stay undissolved as small particles transiting along the gastrointestinal tract until dissolved and able to enter the epithelial cells or leave the gastrointestinal tract and body via excretion. Drug permeating

the intestinal membrane and entering the enterocytes is considered absorbed. If required, gastric absorption can also be accounted for depending on compound properties [83]. Additional stages of the drug fate like different forms of metabolism, entering of the central compartment and clearance following the process of absorption are not further addressed here.

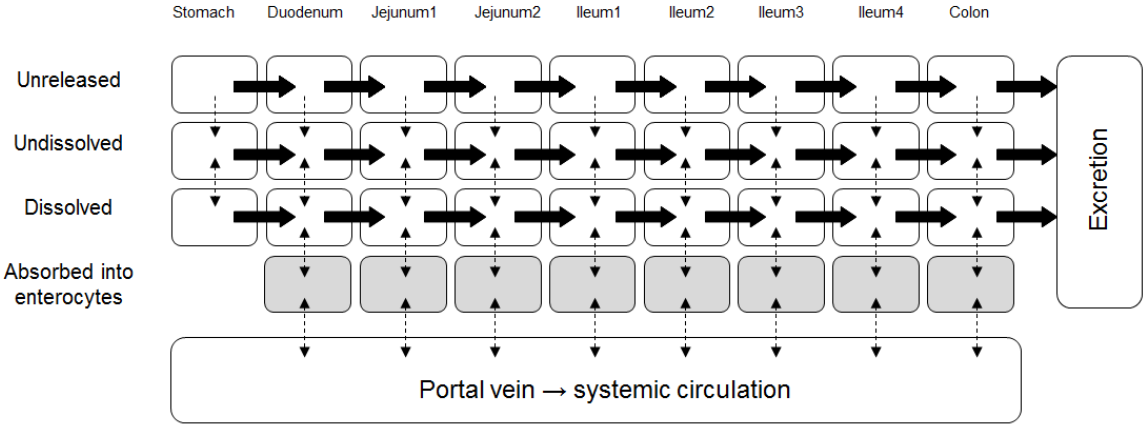

Fig. 2-3: Schematic description of the advanced compartmental absorption and transit (ACAT) model used in GastroPlus™. Bold arrows represent movement of compound along the gastrointestinal tract and dashed arrows represent interchange between subcompartments corresponding to state of compound (unreleased, released, undissolved, dissolved or absorbed) (modified from Agoram 2001 [84]).

2.3.2 Input parameters

For a successful simulation of fraction of dose absorbed and absorption rate constant, some essential input parameters must be provided (Tab. 2-9). For each compound, the log $P_{o/w}$ value, the pH depending solubility and molecular weight was added into the compound tab of the software together with the corresponding formulation, dose and drug specific human effective permeability (P_{eff}) (Chapter 1.3.3.3). In the physiology tab, the respective species (e.g. rat, Beagle dog, human) was selected from the physiology drop-down menu and the appropriate body weight inserted. In addition the appropriate prandial state (fasted or fed) was considered.

The absorption scale factor (ASF) model can be used to scale the effective permeability to account for variations in surface-to-volume ratios of the gastrointestinal tract segments, pH effects, and other absorption-rate-determining effects that differ from one compartment to another [80]. The ASF model was set to “optimized log D model” for all simulations. It

accounts for the change of pH in the gastrointestinal tract and its effect on the charge of the drug molecule and its therefore altered effective permeability [68, 80].

Apart from the P_{eff} value, all physicochemical input properties are standardly available in early drug development. The parameter of human effective permeability is usually determined *in vivo* using an intestinal perfusion technique [85]. The P_{eff} is typically not available for new pharmaceutical compounds; therefore GastroPlus™ contains a permeability converter. It has known human P_{eff} values for a variety of compounds and allows linear regression prediction of P_{eff} values from own in-house Caco-2 cell P_{app} values for these development compounds. Via the slope of the regression line conversion of P_{app} values for new development compounds into P_{eff} values is possible. Therefore, permeability data from routinely performed Caco-2 cell assays was used to obtain the drug specific P_{eff} for the eight selected development compounds (Chapter 2.3.3).

For simulations in different species the obtained human P_{eff} is again transferred to a species specific P_{eff} value. If available for the respective species, this is automatically converted when selecting the species of interest in the physiology selector.

Tab. 2-9: List of input parameters to simulate fraction absorbed in GastroPlus™.

Physicochemical	Physiological	Dosage
Molecular weight	Species	Dosage form
Log $P_{o/w}$ / Log D_{ph}	Body weight	Dose
Solubility / pKa	Prandial state	Dose volume
P_{eff}		

2.3.3 Compounds

Eight compounds (C_1-C_8) were selected for simulations from pharmaceutical research and development at Bayer Pharma AG, Berlin, Germany. The selected compounds covered a broad range of physicochemical properties. The molecular weights ranged between 330 and 690 g/mol and the calculated P_{eff} between 1.3E-04 and 4.2E-04 cm/s. All compounds were lipophilic with a log $P_{o/w}$ ranging from 1.3 to 6.0. The aqueous solubility ranged from 0.001 mg/mL to 0.2 mg/mL. Tab. 2-10 shows the physicochemical properties of the compounds used for the simulations.

Tab. 2-10: Properties of compounds used for simulations in GastroPlus™.

Compound	MW [g/mol]	Log $P_{o/w}$	Solubility [mg/mL]	P_{eff} [cm/s]
C_1	530	3.7	0.014 at pH 6.8	2.7E-04
C_2	370	3.1	0.013 at pH 6.8	3.0E-04
C_3	440	1.3	0.008 at pH 6.8	1.6E-04
C_4	620	4.2	0.002 at pH 6.9	3.0E-04
C_5	470	4.0	0.020 at pH 4.5	3.8E-04
C_6	690	5.9	0.001 at pH 7.0	3.0E-04
C_7	330	2.3	0.200 at pH 7.4	1.3E-04
C_8	350	2.0	0.017 at pH 6.5	4.2E-04

2.3.4 Software

GastroPlus™ version 6.0.0 (Simulations Plus Inc., Lancaster, CA, USA) installed on a terminal server was used for all simulations.

2.3.5 Simulation procedure

A retrospective data evaluation was performed to assess the ability of the applied software to predict intestinal absorption for eight selected compounds (C_1-C_8) with the minimum amount of input data required. The input information derived from standard studies carried out during the pharmaceutical research and development process, such as:

- Physicochemical characterisation
- *In vitro* determination of solubility, dissolution and permeability and
- Preclinical and clinical pharmacokinetic studies.

Two parameters that describe intestinal absorption were focused on; fraction absorbed (f_a) and the absorption rate constant (k_a). Fig. 2-4 gives on overview of the workflow for the simulations of both PK parameters. In order to evaluate the accuracy of the simulations, the predicted results were compared to the results of the experimentally performed preclinical and clinical *in vivo* studies (Tab. 7-16 to Tab. 7-23 in columns ‘obs’). The *in vivo* parameter for fraction absorbed ($(f_a)_{obs}$) was investigated after oral and intravenous administration of radiolabeled compound by measuring concentrations of radioactivity in plasma and calculating the oral-to-intravenous ratio of the dose-normalised area under the concentration-time curve (AUC). The *in vivo* parameter for the absorption rate constant ($(k_a)_{obs}$) derived from compartmental analysis of in vivo pharmacokinetic studies.

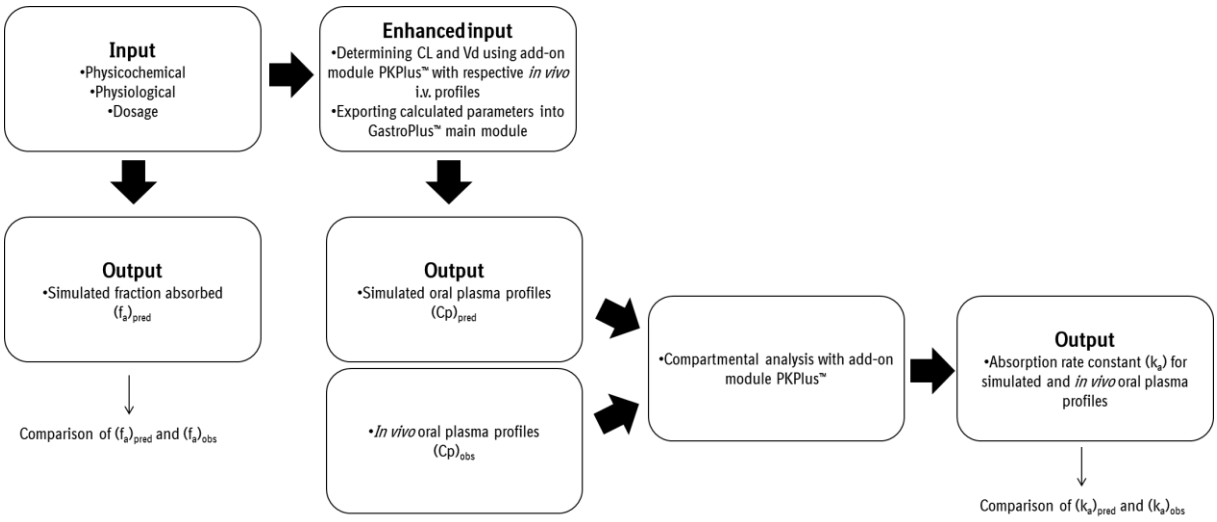

Fig. 2-4: Simulation workflow using GastroPlus™ and PKPlus™ to determine fraction absorbed $(f_a)_{pred}$ and the absorption rate constant $(k_a)_{pred}$ and $(k_a)_{obs}$.

2.3.5.1 Simulation of fraction absorbed

Fraction absorbed portrays the amount of substance absorbed relative to the dose administered. In order to predict f_a, the input parameters shown in Tab. 2-9 were entered into the software corresponding to the *in vivo* data. The values for molecular weight, log $P_{o/w}$ or log D, P_{eff}, dose and dose volume were entered directly into the compound tab. The corresponding dosage formulation was selected in the drop down menu. For the solubility data of the compound, a support file (*.spd) was created, where the solubility measured at several pH values was entered. In the physiology tab the required species was selected and in the pharmacokinetic tab the appropriate body weight was entered. The length of time for each simulation was adjusted to the corresponding experimental *in vivo* data available and the simulation was executed. When dosing a modified or controlled-release formulation, an additional support file was created (*.crd), which contained the *in vitro* dissolution data. The simulation output was the fraction of dose absorbed $(f_a)_{pred}$ in percent (Fig. 2-4).

2.3.5.2 Simulation of absorption rate constant

The absorption rate constant (k_a) describes the transfer rate of drug absorption i.e. the fraction of drug absorbed per unit time. Drug can theoretically be completely absorbed over the entire length of the small and large intestine. That process can be slow, due to a long

transit time, and would exhibit a low absorption rate constant in this case. Alternatively, a highly permeable substance that is completely absorbed in the upper part of the intestine (e.g. duodenum) would be characterised by a high k_a, as it takes markedly less time to transfer from the intestinal lumen to the systemic circulation. As shown in Fig. 2-4, further steps have to be considered when simulating the absorption rate constant (k_a) compared to the simple procedure of predicting f_a. In order to determine k_a, oral plasma concentration-time profiles need to be simulated for every compound, species, dose and formulation. An enhanced input was required to simulate these oral plasma profiles ($(Cp)_{pred}$). In a first step, in addition to the input parameters described in Chapter 2.3.2, species-specific pharmacokinetic parameters of clearance (CL) and volume of distribution (Vd) had to be calculated. They were obtained by performing a compartmental analysis using the corresponding intravenous (i.v.) plasma concentration-time data in the GastroPlus™ add-on module PKPlus™ for each species. A best fitting model was suggested by PKPlus™ referring to the Akaike Information Criterion (AIC) and the Bayesian Information Criterion (BIC) [86, 87]. The suggested model was accepted and the calculated PK parameters were exported into the pharmacokinetic tab of the GastroPlus™ main module. With the help of this additional input information, oral concentration-time profiles were predicted for every compound, species, dosage and formulation, where i.v. plasma profiles were available. Subsequently, the simulated oral plasma profiles and the experimentally observed *in vivo* oral plasma profiles were compared. In a next step, the simulated and the *in vivo* observed p.o. plasma profiles were loaded into PKPlus™ and a compartmental analysis was performed to retrieve values for the parameter $(k_a)_{pred}$ and $(k_a)_{obs}$ (Fig. 2-4). For all analyses, the fitting of the model was done using the default Hooke-Jeeves pattern search method in PKPlus™ [88]. To further characterize the oral plasma profiles, the parameter T_{max} (time point of maximum concentration) was obtained directly from the predicted and observed oral plasma data.

2.3.5.3 Parameter sensitivity analysis

To evaluate the influence of input parameters (e.g. solubility, permeability) and model parameters (e.g. stomach pH, gastrointestinal transit time) on the fraction absorbed, a parameter sensitivity analysis (PSA) was performed. The PSA is an additional simulation mode in GastroPlus™. For all physiochemical, physiological and dosage related parameters (e.g. gastrointestinal pH, dose, solubility, P_{eff}) a value range from the default value can be selected and within this range the fraction absorbed is simulated. This simulation mode gives information about the sensitivity of f_a to the change of certain parameters and therefore an

insight which input and model parameters influence the fraction absorbed for the compound of interest. For the performed PSA simulations, the upper and lower limit of the parameters value range where set as a factor of 10 from the default value in GastroPlus™. Within these limits, the fraction absorbed was simulated for a series of 10 data points. Sensitive parameters were identified and used for interpretation and discussion when comparing predicted and observed f_a (Chapter 3.3.1.3).

2.3.5.4 Evaluation and statistics

Evaluation and descriptive statistics for the PK parameters of the simulations were performed using Excel 2007 software (Microsoft Inc., Redmond, WA, USA). Simulation results of f_a and k_a were evaluated graphically by plotting the observed data from clinical and preclinical reports against the predicted data from the performed simulations. The line of unity was used as a visual tool to evaluate the accuracy of the predictions. In addition, the coefficient of determination (R^2) was calculated as a measure of the goodness of fit for the predictions. To further evaluate the goodness of the predictions of each of the two PK parameters, the route mean square error (rmse) was calculated as followed:

$$rmse = \sqrt{\frac{1}{N}\sum(predicted - observed)^2} \qquad \text{Equation 18}$$

rmse =route means square error
N = number of simulated scenarios (i.e. for each set of compound, formulation, dose, species)
predicted = PK parameter obtained from simulation
observed = PK parameter determined in preclinical or clinical *in vivo* study

The dimensionless rmse value gives a measure of the differences between predicted and observed parameter and allows comparing the goodness of prediction for different groups or categories [89, 90]. In order to give an overall assessment of the predictions for fraction absorbed and absorption rate constant, the percentage within 2-, 2.5- and 3-fold error of the experimental data was calculated for each group. Generally, a deviation factor of 2 (i.e. 2-fold error) from the in vivo data is widely accepted when simulations are assessed [89, 90]. This recommendation is also applied to the simulations results in this thesis.

For a better description of the deviation the mean prediction error (mpe) for each of the two PK parameters was calculated.

$$mpe = \frac{1}{N}\sum(predicted - observed)$$ Equation 19

mpe = mean prediction error
N = number of simulated scenarios (i.e. for each set of compound, formulation, dose, species)
predicted = PK parameter obtained from simulation
observed = PK parameter determined in preclinical or clinical study

The mean prediction error can be artificially small, as individual data points that have very large positive and negative errors can cancel each other out. In order to prevent that, the absolute value of error (mae) was also calculated.

$$mae = \left|\frac{1}{N}\sum(predicted - observed)\right|$$ Equation 20

mae = mean absolute error
N = number of simulated scenarios (i.e. for each set of compound, formulation, dose, species)
predicted = PK parameter obtained from simulation
observed = PK parameter determined in preclinical or clinical study

3 Results

3.1 Literature review of absorption models

In order to estimate the oral absorption of a new compound in drug development, a multitude of absorption models has been established, ranging from methods to simply determine the ability to cross through a lipid bilayer to predicting the extent and rate of intestinal absorption in humans. The key words displayed in Tab. 2-1 guided the literature research and key experiments and models spanning from *in vitro*, *ex vivo*, *in situ*, *in vivo* to *in silico* were reviewed. In the following chapter absorption models applicable to the drug development process and their strengths and limitations are portrayed.

3.1.1 *In vitro* investigations and models

In the first part, *in vitro* absorption models utilizing artificial membranes or biological cell cultures were assessed in their ability to estimation human intestinal absorption.

3.1.1.1 Non-cell based models

There is a variety of *in vitro* non-cell based assays to assess the ability of a molecule to diffuse through a biological membrane. They range from studying the octanol/water distribution, to determining the membrane affinity of a molecule by binding to egg yolk protein coated particles (e.g. Transil™ beads) and to the usage of artificial or isolated membranes [91, 92]. All of these models are used for high-throughput screening. The most frequently applied methods using isolated membrane vesicles or artificial membranes are explained here in more detail.

3.1.1.1.1 Parallel artificial membrane permeability assay

Briefly, the artificial membrane consists of a hydrophobic filter with associated lipids in an organic solvent and is set up in a 96-well plate format [93]. A sandwich plate system is created which separates each well by the filter membrane and physiological pH adjusted aqueous buffer is added. The drug solution is applied to the top well and the rate of appearance in the bottom well gives information about the permeation abilities of the compound. As regards mechanisms of permeation, only passive transcellular diffusion is covered by this method. Optimisation of the system can be achieved with different lipid

compositions and with the use of a hydrophilic filter in order to reduce permeation time [17] [94]. The influence of different pH levels and the effect of cosolvents on the parallel artificial membrane permeability assay (PAMPA) should be closely investigated when using this method, as they can alter the results [17] [95].

3.1.1.1.2 Brush border membrane vesicles and basolateral membrane vesicles

For the study of intestinal absorption, isolated enterocyte membranes easily form into vesicles when manipulated appropriately [96]. Vesicles can either be from the apical side (BBMV) or from the basolateral side of the cell (BLMV), depending on the method employed. The vesicles present the brush border membrane to the outside, in the same manner as enterocytes would *in vivo*, therefore they can be used for permeability studies [97]. Vesicles are suspended in a physiological buffer and shortly incubated with the test compound. This model allows studying the passive transcellular uptake into the vesicles, as intracellular metabolism to provide energy for ATP-dependent active transport is missing. Also the transport along the paracellular pathway is excluded [54].

3.1.1.2 Cell based models

With the intention to predict intestinal drug absorption it would be desirable to have a primary culture of enterocytes as an *in vitro* assay. Unfortunately, attempts have failed due to very poor viability and the fact that cultured enterocytes do not easily differentiate into a polarized monolayer with an apical and a basolateral surface [98]. Varieties of other cell based methods were developed to overcome this deficiency and are discussed here in more detail [99].

3.1.1.2.1 Isolated enterocytes

For this rapid method, intestinal epithelial cells (e.g. from rat) are removed from their connected tissues either by mechanical force or via enzymatic reactions and are subsequently dispensed in a bathing solution which contains the test compound. Due to the preparation process, the cells lose their functional polarity but retain their metabolic and transport capabilities [100] [101]. Therefore, uptake studies consider active as well as passive transcellular processes, but they cannot distinguish between apical or basolateral transport. The uptake of drug in different regions of the mucosa can be studied by applying

the mechanical vibration method for cell isolation [102]. The first fraction will predominantly contain villus cells, whereas the second fraction will consist mainly of crypt cells [103]. The generally short viability of the isolated epithelial cells is compensated by the very short incubation time this method requires [104] [105].

3.1.1.2.2 Caco-2 cells

The most extensively used *in vitro* assay to predict intestinal drug absorption is the human colonic adenocarcinoma derived Caco-2 cell line [106]. When cultured under specific conditions on a semipermeable filter, they differentiate into a polarized (apical and basolateral surface) monolayer and exhibit morphological and biochemical features of intestinal cells (e.g. tight junctions, microvilli, intestinal enzymes, active transporter). The polarized cell layer enables bidirectional transport experiments, from apical to basolateral side and vice versa. Briefly, the test compound is added to the donor side of the monolayer and the appearance on the receiver side is measured. To ensure monolayer integrity (i.e. intact tight junctions), the transepithelial electrical resistance (TEER) is measured. An alternative method is to monitor the permeability of an exclusively paracellular absorbed hydrophilic marker compound (e.g. mannitol). The ability to culture in multiwell format, and the relatively small quantities of compound required, make Caco-2 cells a valuable experimental screening model. Typically, new compounds are compared to high, medium and low permeability markers with known human absorption. The relation of human fraction absorbed and the permeability coefficient determined in the Caco-2 assay for a range of compounds shows a sigmoidal relationship [107, 108]. Generally, compounds that underlie a passive transcellular transport mechanism are adequately predicted, but there are known discrepancies when paracellular diffusion is considered [109]. Permeation of small hydrophilic uncharged compounds is usually underestimated due to “tighter” tight junctions in Caco-2 cells (4.5 Å) than those in the human small intestine (7-15 Å) [110] [111]. Even though Caco-2 cells express important uptake transporters such as peptide transporters (PepT1), organic cation and anion transporters (OCT, OATPs), the level of expression is lower than *in vivo*. The fact that the Caco-2 cell line derives from a colon carcinoma may cause the underestimation of paracellular and active transport, as tight junctions are small in the large intestine (~4 Å) and the expression levels of influx transporters decrease distally from the duodenum along the gastrointestinal tract. The carcinogenic nature of the cell line also accounts for the over-expression of the efflux transporter Pgp, which again can lead to an underestimation of drug permeability. However, the presence of influx and efflux transporters allows studying of drug-drug interactions as transporters can be targeted by

inhibitors or competitive substrates in order to evaluate the sensitivity of the test compound to potential transporter saturation processes.
Despite the many advantages of Caco-2 cells, they comprise some challenges: Inter- and intra-laboratory heterogeneity of the Caco-2 cells is a recognized limitation as well as the sensitivity to culture conditions and culture time [54] [55] [56]. Although this absorption model expresses small intestinal enzymes (e.g. glutathione S-transferase, sulfotransferases) and some cytochrome P450 isoenzymes, it lacks in the drug metabolizing enzyme cytochrome P450 3A4, which plays a major role in the metabolism of xenobiotics [112].
Furthermore, as with most *in vitro* experimental methods, loss of compound can occur due to non-specific binding to plastic or filter material. Performing a mass balance might be useful under these circumstances. Also the addition of serum proteins (e.g. bovine serum albumin) can lead to a reduction of this undesirable effect [113].

3.1.1.2.3 Other cell culture models

There is a range of other commonly used cell lines to predict oral absorption (Tab. 3-1). Some derive from improvement and refining processes of Caco-2 cells, others origin from different species and have slightly different characteristics as regards culture time, enzymatic composition and transport features.

Tab. 3-1: Cell culture permeability assays to predict intestinal permeability [92] [107] [26] [85] [108].

Cell culture	Origin	Comment
Caco-2	Human colon carcinoma	Exhibits active transporters and metabolizing enzymes but not CYP3A4
TC7	Human colon carcinoma	Caco-2 subclone, expresses CYP3A4, grows faster than Caco-2 cells
HT29	Human colon carcinoma	Subclone (HT29-MTX) expresses mucus producing cells
LS180	Human colon carcinoma	Microvilli expressing cells
T84	Human colon carcinoma	Expresses Pgp
MDCK	Dog kidney epithelia	Short culture times, suitable for transfections with complementary DNA to express certain transporters
LLC-PK1	Pig kidney epithelia	Suitable for transfection
2/4/A1	Rat duodenal epithelia	Transepithelial electrical resistance (TEER) is similar to human small intestine

3.1.1.3 Excised tissue models

These *ex vivo* methods use tissue parts removed from laboratory animals or humans, preserving the architectural *in vivo* integrity of the absorptive tissue. The permeability processes are studied under *in vitro* conditions.

3.1.1.3.1 Everted gut sac

The everted gut sac technique is a method that uses excised intestinal segments from rats [114]. After sacrifice of the animal, the segment is quickly removed and rinsed with a physiological buffer solution to remove intestinal debris. The tissue piece is everted, filled with oxygenated buffer and tied into a sac that presents the luminal mucosa on the outside.

The sacs is then submerged into culture medium containing the drug of interest and accumulation in the inner compartment of the sac is measured. This method is fast, inexpensive and enables studying different regions of the small intestine [112]. In addition, the everted gut sac method allows studying potential active influx and efflux processes involved in the intestinal absorption when adding specific transport inhibitors to the culture medium. Disadvantages lie in the short life-time of the model (approx. 2 hours) and that the test compound has to cross additional cell layers (e.g. muscle layers) besides the mucosa that are not involved in the *in vivo* process of absorption [115].

3.1.1.3.2 Ussing chamber

Originally developed by Ussing and Zerahn (1951), the Ussing chamber technique since then has been refined and adapted to different subjects of interest, e.g. by Grass and Sweetana (1988) for the study of gastrointestinal permeability [59, 116]. In principle, a section of excised intestinal tissue is mounted between two buffer filled chambers and the compound of interest is added to the donor side. The disappearance of the drug from the donor side and the appearance on the receiver side is measured as a function of time. Electrodes positioned on both sides of the tissue can measure the potential difference and the current flow across the tissue resulting from the inorganic ion flow across the epithelium [27]. The calculated epithelial resistance is a measure for the tissue integrity. In order to prolong viability of the isolated epithelium, the buffer solution is continuously gassed with an O_2:CO_2 (95:5) mixture. Several advantages make the Ussing chamber technique a valuable method. It allows bidirectional permeability studies, as the test compound can either be added to the mucosal side (apical membrane of the enterocytes) or the serosal side (basolateral membrane of the enterocytes). The route of absorption (paracellular, transcellular passive and active transport) for a drug can be determined by analysing the tissue after the experiment and by measuring flux differences in bidirectional studies. Furthermore, it provides a high degree of freedom in choice of species and region of excised tissue and recent models with small buffer volume require only small amounts of test compound. The limitations this model encounters are mainly due to the nature of removing a section of tissue from an intact organ. Excised pieces of tissue lack the mesenteric blood flow and the permeability measured in the experiment includes mucosa and underlying tissue layers (submucosa, circular muscle layer, longitudinal muscle layer and serosa), that are not involved in the absorption process *in vivo* (Fig. 1-1). Efforts to reduce these artificial layers can be undertaken by removing the serosal layer. This process is referred to as “stripping”. Even after stripping, the additional layers will only be partially removed. In addition, this procedure requires skill and practice. Another issue is

maintaining viability of the tissue. Factors like composition and temperature of the buffer solution play an important role and continuous oxygenation immediately after excising the tissue is mandatory. In order to monitor viability throughout the experiment, paracellular permeating marker substances can be applied. A disproportional increase of the marker in the receiver side can indicate leakage of the tissue and therefore reduced integrity. As this marker only judges the physical viability of the tissue, it is recommended to also check for functional viability. This is achieved by adding e.g. glucose by the end of the experiment, as active transport triggers a change in ion flow across the epithelium and results in a visible change in the potential difference monitored by the electrodes. Despite certain drawbacks, this method allows studying various aspects of the absorption process including the possible involvement of efflux and influx transporters.

3.1.2 *In situ* models

A range of approaches to determined intestinal absorption *in situ* (in the natural position in the body) are comprehensively discussed by Luo et. al (2013) [117]. As the *in situ* intestinal perfusion method in the rat is widely accepted to determine intestinal permeability this chapter focuses on this particular model [118].

3.1.2.1 Rat intestinal perfusion

This *in situ* technique uses isolated intestinal segments in anesthetised rats that are cannulated on both sides (“open loop”). The luminal content is removed and the rinsed segment is exposed to a perfusion solution. Most commonly, the single-pass perfusion method is used, in which the solution has a constant concentration of test compound [119], but there are also experimental set-ups with recirculating perfusion [120]. To determine the permeability, the disappearance of the compound from the perfusion solution is measured. The advantage of this method is that despite surgical manipulation and anaesthesia, the mesenteric blood flow and the innervation of the intestine is still intact, although caution has to be taken which anaesthetic is used [121]. Compared to experiments in whole animals, this *in situ* technique also allows studying the process of absorption independently of enterohepatic recirculation. Studies have shown a good correlation between effective permeability values determined in rat and human jejunum as well as a good predictability of human fraction absorbed from rat intestinal perfusion experiments [119, 122]. However, as only the disappearance of the drug is measured, no information about intestinal efflux and

possible compound accumulation in the enterocytes is provided. Neither does this method elucidate the mechanism of intestinal uptake (passive paracellular and transcellular or active transport). When determining the rate of absorption, it should be kept in mind, that the experimental perfusion flow rate exhibits an influence, as it is effecting the thickness of the unstirred water layer lining the luminal mucosa which can be a rate limiting factor for rapidly absorbed compounds [123-125]. Overall, the rat intestinal perfusion model requires more sophisticated surgical procedures and is therefore more suitable in the late preclinical drug development setting.

3.1.3 *In vivo* models

In this part, *in vivo* models studying intestinal absorption are reviewed. This includes pharmacokinetic studies in conscious animal as well as the “gold standard” method (Loc-I-Gut®) for human absorption [126] .

3.1.3.1 Studies in animals

Drug absorption studies in conscious animals (e.g. rat, dog, minipig and monkey) are commonly used in the preclinical drug development process. Unlike *in vitro* models, these *in vivo* models enable testing of dosage forms (non-rodents) as well as the influence of the prandial state on the degree of intestinal absorption. In addition, intact animals give a complete set of all biological and physiological factors influencing oral drug absorption in the same manner as they are present in man. These factors are similar among mammals, but vary of course across species and, depending on the physicochemical properties of the test compound, have a more or less crucial effect on drug absorption. The use of radiolabeled (e.g. ^{14}C or ^{3}H) compound can enhance the information coming from an *in vivo* animal studies [127]. A good assessment of intestinal absorption can be estimated based on the p.o.- to- i.v. ratio of the values corresponding to the AUC of radioactivity in plasma.
As much as the complex interplay of anatomical and physiological properties gives a holistic picture of drug absorption, it also creates a so called “black box”, where only the input and the output are known, but no information on the absorption mechanism is provided. In addition to the ethical controversy, animal studies are also labour-intensive as they require suitable animal care and experienced experimental skills. Furthermore, larger quantities of compound are needed compared to *in vitro* methods which add to the cost-intensive nature of these studies.

3.1.3.2 Human intestinal perfusion

To evaluate the *in vivo* intestinal permeability (P_{eff}) of the proximal human jejunum the Loc-I-Gut® method was developed [85]. Loc-I-Gut® is an *in vivo* single-pass perfusion technique used in conscious man and has been applied for various compounds [109, 119, 128]. Briefly, a multichannel tube is orally inserted and two balloons attached to the tube are inflated to isolate an approximately 10 cm long segment in the jejunum. The sealed off segment is then exposed to the perfusion solution containing the test compound of interest. The disappearance of the compound from the lumen is measured by sample taking through corresponding channel tubes. To ensure that the isolated segment is not leaking during the experiment, a non-absorbable marker (e.g. PEG4000) is added to the perfusion solution and the recovery is determined. As only the disappearance of the drug is measured in the Loc-I-Gut® experiments, this method cannot distinguish between absorbed and secreted compound. While this technique shows a good correlation between the measured P_{eff} and the extent of fraction absorption in man, it can only be used with known non-toxic compounds when applied to humans [36]. It is therefore not applicable in the development process of new drugs. However, the already collected jejunal P_{eff} data for a variety of compounds provides a good foundation to validate other absorption models (e.g. Caco-2 cells, Ussing chamber).

3.1.4 *In silico* models

Beyond *in vitro*, *ex vivo, in situ*, and *in vivo* absorption models there have been mathematical models developed to predict *in vivo* absorption.

3.1.4.1 Physiologically based *in silico* absorption models

A wide range of software tools using physiologically base PK models to predict intestinal absorption are commercially available by now. The main difference between these absorption models is the underlying mathematical model. Intellipharm® PK is based on a mixing tank model which describes the intestine as one or more tanks that are well mixed and have a uniform concentration of dissolved and solid drug [129, 130]. PK-Sim® (until version 4.2) on the other hand, handles the gastrointestinal tract as a single tube with changing properties along the length of the tube. It should be mentioned that the input parameter of intestinal permeability coefficient (P_{eff}) is not required from *in vitro* tests, as PK-Sim® offers calculating it from the compound's lipophilicity and molecular weight [131]. Another approach is the use

of the compartmental absorption and transit (CAT) model, which divides the gastrointestinal tract into seven compartments which represent the small intestinal absorption best [82]. Later, absorption compartments for stomach and colon where added. This advanced compartmental absorption and transit (ACAT) model is the basis for Gastroplus™. This software allows simulating the rate, extent and location of intestinal absorption in man but also in other common laboratory species. In addition the software is able to simulate absorption of several dosage forms (e.g. solution, suspension and tablet). Gastroplus™ requires, besides physicochemical properties, a P_{eff} value of the compound as an input parameter but offers a converter function for *in vitro* and *in situ* derived permeability data. In order to simulate plasma concentration-time profiles the mentioned absorption models can either be coupled with classic compartmental models (Intellipharm® PK, Gastroplus™) or have underlying detailed physiological and anatomical information about all organs and tissues that are exposed to the absorbed compound (PK-Sim® and Gastroplus™ with add-on module). The ability of these *in silico* models to predict human fraction absorbed (f_a) and the absorption rate constant (k_a) has been evaluated in some studies [131-134]. It should be kept in mind that the accuracy of the prediction is highly dependent upon the quality of the input data from literature or generated in experiments.

3.1.5 Overview of absorption models

After the comprehensive discussion of the most relevant absorption models an overview summarising the strengths and limitations of the discussed model is given in Tab. 3-2.

Tab. 3-2: Overview of reviewed absorption models, their composition and assessment of their strengths and limitations.

Properties / Model	Type	Composition	Transport / Diffusion type	Direction	System requirements	Strengths	Limitations
PAMPA	*in vitro*	Lipophilic artificial membrane	Passive	Unidirectional	Multiwell system + membranes	HTS method Easy and inexpensive	Dependent on lipid composition and pH No physiological components
BBMV / BLMV	*in vitro*	Isolated cell components	Passive transcellular	Bidirectional	Animal / human enterocytes	Fast method Mechanistic uptake studies possible	Only small part of absorption process can be studied Non-specific binding
Isolated intestinal cells	*in vitro*	Isolated enterocytes	Passive transcellular Active transport	Unidirectional	Animal / human enterocytes	Fast method Study of different intestinal regions	Loss of polarity Limited viability of cells
Caco-2 cells	*in vitro*	Cell culture system	Passive transcellular Passive paracellular Active transport	Bidirectional	Multiwell system + cell culture	HTS method Polarized cell culture Expression of transporters	Lack of some CYPs (e.g. 3A4) Unstirred water layer Static model
Everted gut sac	*in vitro (ex vivo)*	Isolated intestinal segment	Passive transcellular Passive paracellular Active transport	Bidirectional	Animal tissue e.g. rat	Easy and inexpensive Study of different intestinal regions Inhibitor for transporter study	Limited tissue viability Presence of additional layers not relevant for absorption process
Ussing chamber	*in vitro (ex vivo)*	Isolated intestinal tissue	Passive transcellular Passive paracellular Active transport	Bidirectional	Animal tissue e.g. rat, human + chambers	Study of different intestinal regions in different species Inhibitor for transporter study	Limited tissue viability Presence of additional layers not relevant for absorption process
Rat intestinal perfusion	*in situ*	Isolated organ in anaesthetised animal	Passive transcellular Passive paracellular Active transport	Unidirectional	Animal + perfusion equipment	Close to *in vivo* situation Only physiological layers involved in absorption process Mesenteric blood flow present	Only disappearance of drug can be measured Sophisticated surgical procedure needed
Animal study	*in vivo*	Conscious animals	Passive transcellular Passive paracellular Active transport	Unidirectional	Animal + radiolabeled compound	Holistic model Influence of formulation and prandial state can be studied	Labour and cost intensive Late stage of drug development "Black box"
Loc-I-Gut®	*in vivo*	Conscious human	Passive transcellular Passive paracellular Active transport	Unidirectional	Clinical study + perfusion equipment	Absorption in target species	Only disappearance of drug can be measured Only for safe compounds with known toxicological profile
Physiologically based *in silico* absorption model	*in silico*	Mathematical model	Passive transcellular Passive paracellular Active transport	Unidirectional	Computer + software	Early assessment of development potential Identification of sensitive parameter influencing absorption	High dependence on extent and quality of input data Difficult to predict complex interplay of processes

3.2 Permeability investigations using the Ussing chamber

3.2.1 Preparatory investigations

Prior to the start of the actual permeability studies, initial experiments to investigate the non-specific binding (NSB) of the reference compounds to the Ussing chamber material were performed. Based on these results, time dependent recovery ratios (Rec_{tx}) were calculated for correction of apparent permeability in the permeability studies.

3.2.1.1 Non-specific binding

The non-specific binding to the acrylic glass of the Ussing chamber was determined for every reference compound as described in Chapter 2.2.3.1. Results are displayed in Tab. 3-3, Tab. 3-4, Tab. 3-5 and in Fig. 3-1 A+B. For the high concentration (expected donor side concentration Tab. 3-5), the non-specific binding for mannitol, terbutaline and fexofenadine was low, ranging up to 3.4 % (Fig. 3-1 A). Propranolol was gradually bound to the Ussing chamber material over time with a maximum of 6.5 % after 120 min. For these compounds the intra-compound variability per time point was low with a CV not exceeding 3.26 % (Tab. 3-3). Verapamil showed the highest non-specific binding of all tested compounds (77.5 %). From the start of the experiment to the first sampling time point after 5 minutes, 70.7 % of verapamil was bound to the material of the chamber. NSB increased to a maximum of 77.5 % by the end of the experiment (Fig. 3-1 A). Intra-compound variability increased over time up to a coefficient of variation of 16 % for the last two time points (Tab. 3-3).
For the low concentration (expected receiver side concentration Tab. 3-5), results for terbutaline, fexofenadine and propranolol suggest low non-specific binding with a maximum binding of 9.1 % (Fig. 3-1 B). Mannitol showed moderate NSB with a higher intra-compound variability of up to 23.6 % (Tab. 3-4). The average binding of mannitol to the acrylic glass was 17.3 %. As seen in the results from the high test concentration, verapamil was extensively bound to the Ussing chamber material. Non-specific binding ranged from 73.6 to 83.3 %, mostly increasing over time of the experiment (Fig. 3-1 B). Variability per time point for verapamil was markedly increased with a coefficient of variation reaching 42.1% for the last time point as shown in Tab. 3-4.

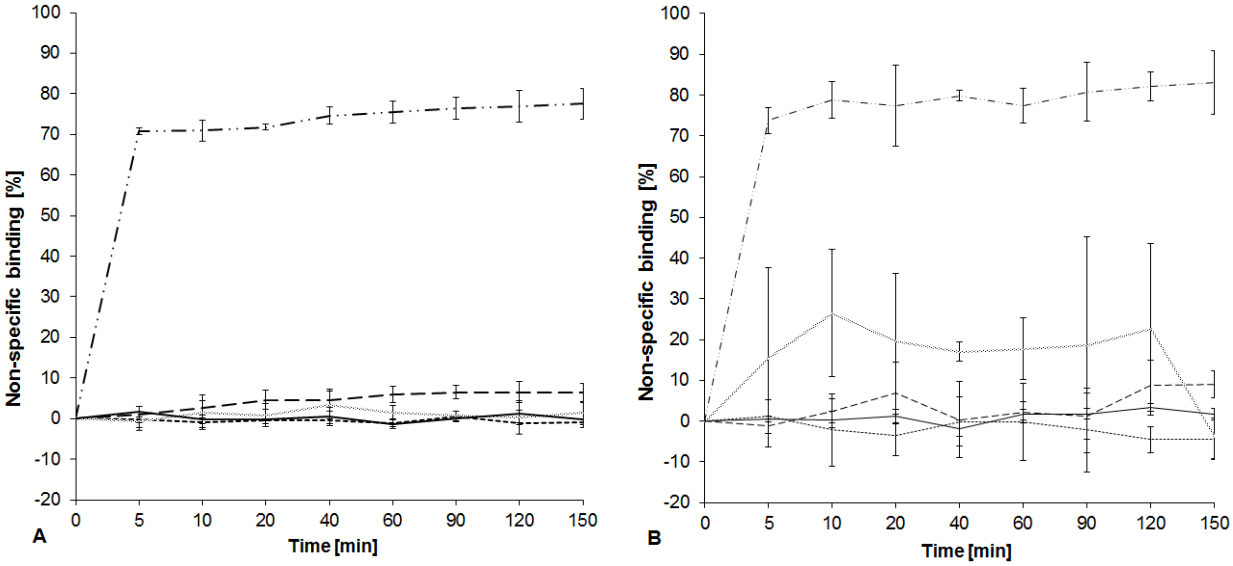

Fig. 3-1: Non-specific binding to Ussing chamber without tissue. Non-specific binding [%] (as (1-Rec_{tx}) with Rec_{tx} being the quotient of the concentration at time point x and the initial compound concentration) over time [min] presented as mean ± standard deviation (n=3). **A:** Non-specific binding in high concentration experiment (expected donor side concentration). **B:** Non-specific binding in low concentration experiment (expected receiver side concentration). Verapamil (— •• — ••), Propranolol (— —), Mannitol (—), Terbutaline (•••••), Fexofenadine (——).

3.2.1.2 Recovery ratio for correction of non-specific binding

In order to correct the permeability results for non-specific binding as described in Chapter 2.2.4.2, a recovery ratio for every time point (Rec_{tx}) was calculated (Tab. 3-3 and Tab. 3-4) according to Equation 3. In the high concentration group, the recovery ratios for fexofenadine, propranolol and mannitol were close to 1.0 (no correction for non-specific binding required) ranging between 0.935 and 1.0 (Tab. 3-3). For terbutaline, the Rec_{tx} was 1.0 for all time points. The recovery ratio was lowest for verapamil, as the compound showed the highest non-specific binding (Fig. 3-1) which ranged between 0.225 and 0.293 (Tab. 3-3).

Tab. 3-3: Non-specific binding to Ussing chamber without tissue for the high concentration (expected donor side concentration). Results of the non-specific binding experiment are presented as the amount of compound per total sample volume for each time point (C_{tx}) in disintegrations per minute [dpm] as mean ± standard deviation for each compound with the respective coefficient of variation [%]. Further, the calculated recovery ratio (Rec_{tx}) for each time point is shown (n= 3).

	Verapamil				**Fexofenadine**			
Time [min]	C_{tx} [dpm]			Rec_{tx}	C_{tx} [dpm]			Rec_{tx}
	mean ± SD		CV [%]	ratio	mean ± SD		CV [%]	ratio
0	4391 ±	21.4	0.49	-	30732 ±	287	0.934	-
5	1287 ±	40.4	3.14	0.293	30240 ±	128	0.422	0.984
10	1276 ±	120	9.42	0.291	30788 ±	578	1.88	1.00
20	1238 ±	33.0	2.67	0.282	30796 ±	46.0	0.148	1.00
40	1116 ±	91.3	8.18	0.254	30593 ±	466	1.52	0.995
60	1074 ±	115	10.7	0.245	31135 ±	290	0.930	1.01
90	1033 ±	116	11.2	0.235	30708 ±	182	0.591	0.999
120	1013 ±	166	16.4	0.231	30372 ±	170	0.559	0.988
150	988 ±	159	16.1	0.225	30813 ±	841	2.73	1.00

	Propranolol				**Mannitol**			
Time [min]	C_{tx} [dpm]			Rec_{tx}	C_{tx} [dpm]			Rec_{tx}
	mean ± SD		CV [%]	ratio	mean ± SD		CV [%]	ratio
0	6918 ±	39.3	0.568	-	752 ±	22.1	2.94	-
5	6849 ±	138	2.02	0.990	756 ±	10.6	1.40	1.01
10	6737 ±	96.3	1.43	0.974	740 ±	18.2	2.46	0.984
20	6600 ±	194	2.94	0.954	745 ±	4.58	0.615	0.991
40	6602 ±	215	3.26	0.954	726 ±	10.3	1.41	0.965
60	6512 ±	173	2.66	0.941	741 ±	11.7	1.58	0.985
90	6472 ±	146	2.26	0.935	747 ±	22.0	2.94	0.993
120	6470 ±	194	3.01	0.935	749 ±	14.0	1.87	0.996
150	6481 ±	130	2.00	0.937	741 ±	1.5	0.206	0.985

	Terbutaline			
Time [min]	C_{tx} [dpm]			Rec_{tx}
	mean	SD	CV [%]	ratio
0	8341 ±	26.4	0.316	-
5	8362 ±	177	2.11	1.00
10	8418 ±	83.0	0.985	1.01
20	8369 ±	40.9	0.488	1.00
40	8374 ±	60.9	0.727	1.00
60	8432 ±	73.9	0.876	1.01
90	8304 ±	23.5	0.282	1.00
120	8442 ±	35.7	0.423	1.01
150	8419 ±	69.8	0.829	1.01

Tab. 3-4: Non-specific binding to Ussing chambers for the low concentration (expected receiver side concentration). Results of the non-specific binding experiment are presented as the amount of compound per total sample volume for each time point (C_{tx}) in disintegrations per minute [dpm] as mean ± standard deviation for each compound with the respective coefficient of variation [%]. Further, the calculated recovery ratio (Rec_{tx}) for each time point is shown (n= 3; Mannitol n= 2).

	Verapamil				**Fexofenadine**		
Time [min]	C_{tx} [dpm] mean ± SD	CV [%]	Rec_{tx} ratio		C_{tx} [dpm] mean ± SD	CV [%]	Rec_{tx} ratio
0	86 ± 4.58	5.33	-		3103 ± 54.2	1.75	-
5	23 ± 3.79	16.7	0.267		3089 ± 30.5	0.988	0.995
10	18 ± 4.93	26.9	0.209		3093 ± 8.19	0.265	1.00
20	19 ± 8.02	41.5	0.221		3066 ± 18.0	0.587	0.988
40	17 ± 0.577	3.33	0.198		3157 ± 13.6	0.430	1.02
60	19 ± 3.21	16.6	0.221		3054 ± 41.3	1.35	0.984
90	16 ± 5.69	34.8	0.186		3047 ± 11.4	0.373	0.982
120	15 ± 2.31	15.1	0.174		2997 ± 65.8	2.20	0.966
150	14 ± 6.03	42.1	0.163		3049 ± 33.1	1.09	0.983

	Propranolol				**Mannitol**		
Time [min]	C_{tx} [dpm] mean ± SD	CV [%]	Rec_{tx} ratio		C_{tx} [dpm] mean ± SD	CV [%]	Rec_{tx} ratio
0	136 ± 4.58	3.37	-		14.5 ± 2.12	14.6	-
5	138 ± 4.73	3.43	1.01		12.0 ± 1.41	11.8	0.828
10	133 ± 3.06	2.30	0.978		10.5 ± 0.707	6.73	0.724
20	126 ± 7.02	5.60	0.926		11.5 ± 0.707	6.15	0.793
40	135 ± 11.1	8.17	0.993		12.0 ± 1.41	11.8	0.828
60	133 ± 1.00	0.80	0.978		12.0 ± 2.83	23.6	0.828
90	134 ± 8.74	6.50	0.985		11.5 ± 2.12	18.4	0.793
120	124 ± 5.29	4.30	0.912		11.0 ± 1.41	12.9	0.759
150	124 ± 3.79	3.10	0.912		15.0 ± 1.41	9.43	1.03

	Terbutaline		
Time [min]	C_{tx} [dpm] mean SD	CV [%]	Rec_{tx} ratio
0	167 ± 4.62	2.76	-
5	165 ± 5.51	3.33	0.988
10	171 ± 9.87	5.78	1.02
20	173 ± 8.89	5.14	1.04
40	167 ± 5.51	3.29	1.00
60	168 ± 14.3	8.53	1.01
90	171 ± 12.6	7.37	1.02
120	175 ± 7.00	4.00	1.05
150	175 ± 6.11	3.50	1.05

Tab. 3-4 shows the results for the low concentration NSB experiments. The compounds fexofenadine, terbutaline and propranolol showed similar Rec_{tx} compared to the high concentration group. Ratios were close to 1.0, ranging between 0.912 and 1.5. For the compound mannitol the Rec_{tx} were between 0.724 (at time point 10 min) and 1.03 (time point 150 min). Recovery ratios were slightly lower than in the high concentrations group. It should be noted that for mannitol in the low concentration group the measurements were close to the lower limit of quantitation (Tab. 2-8). The compound verapamil exhibited the lowest ratios within the low concentration group ranging from 0.163 to 0.267. These recovery ratios were also the lowest for all non-specific binding experiments and 28 % lower than for the high concentration of verapamil.

3.2.1.3 Mass balance of non-specific binding experiments

A mass balance for the NSB studies was performed to evaluate the overall total recovery of each compound in the Ussing chamber experiment. The recovery of compound for the taken samples and the remaining buffer was between 90.4 and 103 % for the compounds propranolol, fexofenadine, terbutaline and mannitol in the high and low test concentration (Tab. 3-5). For verapamil, the recovery of taken samples and remaining buffer was much lower for both concentrations, with 22.5 % for the expected donor side concentration (high) and 16.8 % for the expected receiver side concentration (low). The recovery of compound from both washing steps with the solvent ethanol (Chapter 2.2.3.1) was summed up for every compound. The recovery in the ethanol washing steps for the high concentration ranged between 2.2 and 8.5 % (Tab. 3-5). The variation of recovery in the low concentration was higher with percentages between 0.613 for mannitol and 17.9 for propranolol. The values for total recovery comprise the taken samples and the remaining buffer as well as the recovery from the washing steps. Recovery was complete (≥ 100 %) for the compounds propranolol, fexofenadine, terbutaline and mannitol in both concentration groups with very low fractions (≤ 3.3 %) from the ethanol washing steps for fexofenadine and mannitol (Tab. 3-5). The cumulative recovery of verapamil was substantially smaller compared to the other compounds, with a total recovery of 28.6 % for the high concentration and 30.3 % for the low concentration; hence overall non-specific binding of verapamil was 71.4 and 69.7 % for the high and low concentration group, respectively.

Tab. 3-5: Total recovery of compound from non-specific binding experiments. Results for recovery presented in percent for each compound for the high (n= 3) and low (n= 3; mannitol n= 2) test concentrations.

Reference compound	Test concentration*		Recovery [%]		
			in buffer after 150 min	in both ethanol washing steps	Total
Verapamil	high	6 mM	22.5	6.04	28.6
	low	0.1 mM	16.8	13.4	30.3
Propranolol	high	6 mM	92.9	8.50	101
	low	0.1 mM	90.4	17.9	108
Fexofenadine	high	45 µM	99.2	3.20	102
	low	4.5 µM	97.3	3.31	101
Terbutaline	high	6 mM	99.9	3.21	103
	low	0.1 mM	103	8.80	112
Mannitol	high	1.2 µM	97.7	2.22	100
	low	0.2 nM	101	0.613	101

* Differences in suitable test concentration result from the radioactive label of the compound.

3.2.2 Permeability studies

3.2.2.1 Non-specific binding corrected apparent permeability

All experiments were carried out with rat jejunal tissue mounted onto the Ussing chambers as described in Chapter 2.2.3.2. Fig. 3-2 gives an example on how the amount of compound in the receiver chamber corrected for non-specific binding ($A_R$corrected) over time was used for linear regression and subsequently for determination of the slope (m) used for flux calculation according to Equation 6. The example shows the data from the propranolol experiment using stripped tissue investigating the permeability from the mucosal to the serosal side. Mean regression parameter and their corresponding coefficient of determination (R^2) for this example and all other permeability investigations are given in Tab. 3-6. For all compounds the time interval used for calculation of the slope was 60-120 minutes as they all exhibited a linear flux in this time interval expressed by a high R^2 ($\geq$ 0.846) with a low coefficient of variation.

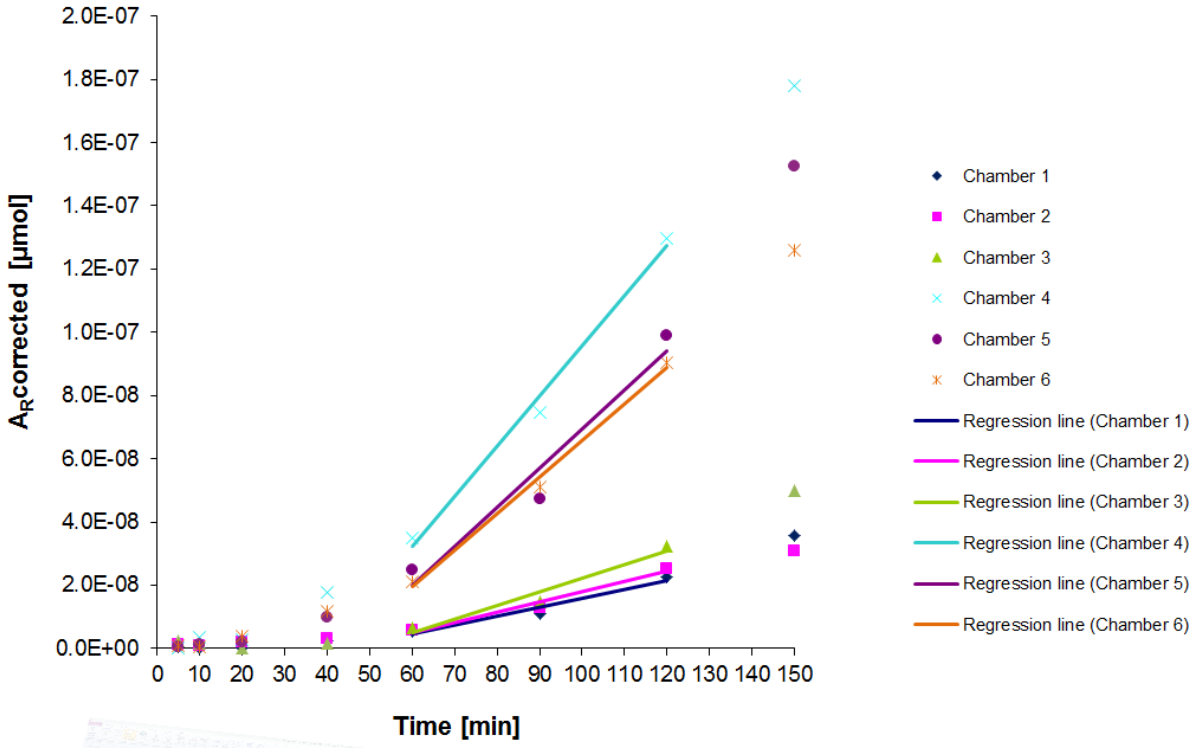

Fig. 3-2: Amount of compound in receiver chamber corrected for non-specific binding ($A_R$corrected) over time [min] for permeability studies from mucosal to serosal side using stripped tissue for the example propranolol (n=6). Data points from 60-120 minutes were used for linear regression and calculation of the slope for all compounds. Mean values of coefficient of determination and of the slope for all experiments are given in Tab. 3-6.

Subsequently, the apparent permeability (P_{app}) was calculated according to Equation 7. All parameters used for P_{app} calculation for all investigations are listed in the Appendix (Tab. 7-2 to Tab. 7-15).

In Tab. 3-7 the overall results of the permeability studies for five compounds, two types of tissue preparation techniques (full-thickness and stripped tissue) and two settings of permeability directions (mucosal to serosal and serosal to mucosal), are displayed.

Verapamil showed the highest permeability with a P_{app} of 6.75E-05 cm/s for stripped tissue for the serosal to mucosal direction (Tab. 3-7). The lowest permeability was exhibited by fexofenadine with a P_{app} of 1.09E-06 cm/s for full-thickness tissue for the mucosal to serosal direction with a CV of 59.0 %.

Tab. 3-6: Linear regression parameters. Slope (m) and coefficient of determination (R^2) of linear part of cumulative corrected amounts of compound in receiver chamber versus time profile for permeability experiments. Parameters are presented as mean ± standard deviation and coefficient of variation for each compound, permeability direction (mucosal-serosal / serosal-mucosal) and tissue preparation (full-thickness / stripped). In addition the number of chambers included into the calculations per experiment (n) is given.

Reference	**Permeability**	**Tissue**	**m* [µmol/min]**			**R^2**			**n**
compound	**direction**	**preparation**	mean ± SD		CV [%]	mean ± SD		CV [%]	
Verapamil	m-s	full-thickness	2.83E-10 ±	7.53E-11	26.6	0.982 ±	0.030	3.08	6
	m-s	stripped	2.83E-10 ±	9.83E-11	34.7	0.963 ±	0.054	5.59	6
	s-m	full-thickness	1.18E-10 ±	5.56E-11	47.3	0.940 ±	0.069	7.37	4
	s-m	stripped	3.00E-10 ±	6.32E-11	21.1	0.963 ±	0.034	3.52	6
Propranolol	m-s	full-thickness	1.42E-10 ±	1.08E-10	75.9	0.875 ±	0.209	23.9	5
	m-s	stripped	8.33E-10 ±	6.59E-10	79.1	0.972 ±	0.018	1.87	6
	s-m	full-thickness	1.12E-10 ±	8.41E-11	75.1	0.846 ±	0.135	15.9	5
	s-m	stripped	6.50E-10 ±	3.56E-10	54.8	0.976 ±	0.031	3.21	6
Fexofenadine	m-s	full-thickness	1.68E-07 ±	9.86E-08	58.7	0.964 ±	0.024	2.47	5
	m-s	stripped	2.20E-07 ±	1.30E-07	59.3	0.989 ±	0.012	1.21	5
	s-m	full-thickness	1.93E-07 ±	1.34E-07	69.1	0.969 ±	0.028	2.93	6
	s-m	stripped	1.75E-07 ±	9.57E-08	54.7	0.965 ±	0.066	6.80	4
Terbutaline	m-s	full-thickness	1.33E-09 ±	5.16E-10	38.7	0.991 ±	0.010	1.01	6
	m-s	stripped	1.00E-09 ±	0.00E+00	0.00	0.993 ±	0.008	0.776	5
	s-m	full-thickness	1.17E-09 ±	4.08E-10	35.0	0.997 ±	0.003	0.257	6
	s-m	stripped	1.17E-09 ±	4.08E-10	35.0	0.989 ±	0.011	1.07	6
Mannitol	m-s	full-thickness	3.41E-04 ±	1.37E-04	40.2	0.920 ±	0.107	11.7	17
	m-s	stripped	4.35E-04 ±	2.18E-04	50.0	0.948 ±	0.084	8.85	17
	s-m	full-thickness	2.99E-08 ±	1.38E-08	46.4	0.885 ±	0.135	15.2	15
	s-m	stripped	4.82E-08 ±	2.51E-08	52.0	0.918 ±	0.094	10.2	17

*Time interval used for linear regression= 60-120 minutes

Tab. 3-7: Calculated apparent permeability (P_{app}) for the performed permeability experiments corrected for non-specific binding. Results are presented as mean ± standard deviation for each compound, permeability direction (mucosal-serosal / serosal-mucosal) and tissue preparation (full-thickness/ stripped). Further, the respective coefficient of variation in percent is shown and the number of chambers included into the calculations per experiment (n).

Reference compound	Permeability direction	Tissue preparation	P_{app} [cm/s] mean ± SD	CV [%]	n
Verapamil	m-s	full-thickness	6.15E-05 ± 2.58E-05	41.9	6
	m-s	stripped	5.92E-05 ± 2.20E-05	37.2	6
	s-m	full-thickness	2.43E-05 ± 1.16E-05	47.6	4
	s-m	stripped	6.75E-05 ± 1.40E-05	20.8	6
Propranolol	m-s	full-thickness	2.85E-06 ± 2.15E-06	75.3	5
	m-s	stripped	1.53E-05 ± 1.22E-05	79.3	6
	s-m	full-thickness	2.14E-06 ± 1.59E-06	74.5	5
	s-m	stripped	1.17E-05 ± 6.55E-06	55.9	6
Fexofenadine	m-s	full-thickness	1.09E-06 ± 6.41E-07	59.0	5
	m-s	stripped	1.47E-06 ± 8.75E-07	59.7	5
	s-m	full-thickness	1.24E-06 ± 8.62E-07	69.7	6
	s-m	stripped	1.16E-06 ± 6.46E-07	55.6	4
Terbutaline	m-s	full-thickness	2.70E-05 ± 1.05E-05	38.8	6
	m-s	stripped	2.03E-05 ± 2.40E-07	1.18	5
	s-m	full-thickness	2.34E-05 ± 7.52E-06	32.1	6
	s-m	stripped	2.37E-05 ± 8.37E-06	35.2	6
Mannitol	m-s	full-thickness	1.42E-05 ± 5.96E-06	42.0	17
	m-s	stripped	1.73E-05 ± 7.19E-06	41.6	17
	s-m	full-thickness	9.20E-06 ± 4.33E-06	47.1	15
	s-m	stripped	1.15E-05 ± 5.33E-06	46.4	17

For verapamil, the non-specific binding correction had a substantial influence on the calculated final P_{app} for the permeability studies (Fig. 3-3 and Tab. 3-8). For example in the study group of stripped intestinal tissue, verapamil exhibited an experimental P_{app} from mucosal to serosal side of 9.73E-06 cm/s, which was increased by a factor of 6.1 up to 5.92E-05 cm/s by including the NSB (Tab. 3-8). Therefore, verapamil exhibited the highest final permeability of all tested compounds in the m-s group with a coefficient of variation of 37.2 %. For the same study group propranolol and mannitol were corrected by a factor of 1.3 and 1.4 to a P_{app} of 1.53E-05 cm/s and 1.73E-05 cm/s, respectively (Tab. 3-8 and Fig. 3-3). For fexofenadine and terbutaline correction was applied but did not show any effect on the apparent permeability as non-specific binding was marginal (Tab. 3-4). Fexofenadine thus

retained the lowest P_{app} value in this study group of 1.47E-06 cm/s with a coefficient of variation of 59.7 % (Tab. 3-7). Permeability of terbutaline remained at 2.03E-05 cm/s with a coefficient of variation of 1.18 %.

Tab. 3-8: Calculated non-specific binding correction factor as a ratio of mean corrected apparent rat jejunal permeability and mean experimental apparent rat jejunal permeability (centimetre per second) from permeability studies using stripped and full-thickness tissue preparation technique in mucosal to serosal permeability direction.

Reference compound	**Tissue preparation**	**P_{app} [cm/s]**		**Correction factor**
		experimental mean	**corrected for NSB** mean	
Verapamil	stripped	9.73E-06	5.92E-05	6.09
	full-thickness	9.39E-06	6.15E-05	6.55
Propranolol	stripped	1.23E-05	1.53E-05	1.25
	full-thickness	2.77E-06	2.85E-06	1.03
Fexofenadine	stripped	1.47E-06	1.47E-06	1.00
	full-thickness	1.07E-06	1.09E-06	1.01
Terbutaline	stripped	2.03E-05	2.03E-05	1.00
	full-thickness	2.70E-05	2.70E-05	1.00
Mannitol	stripped	1.26E-05	1.73E-05	1.37
	full-thickness	1.03E-05	1.42E-05	1.38

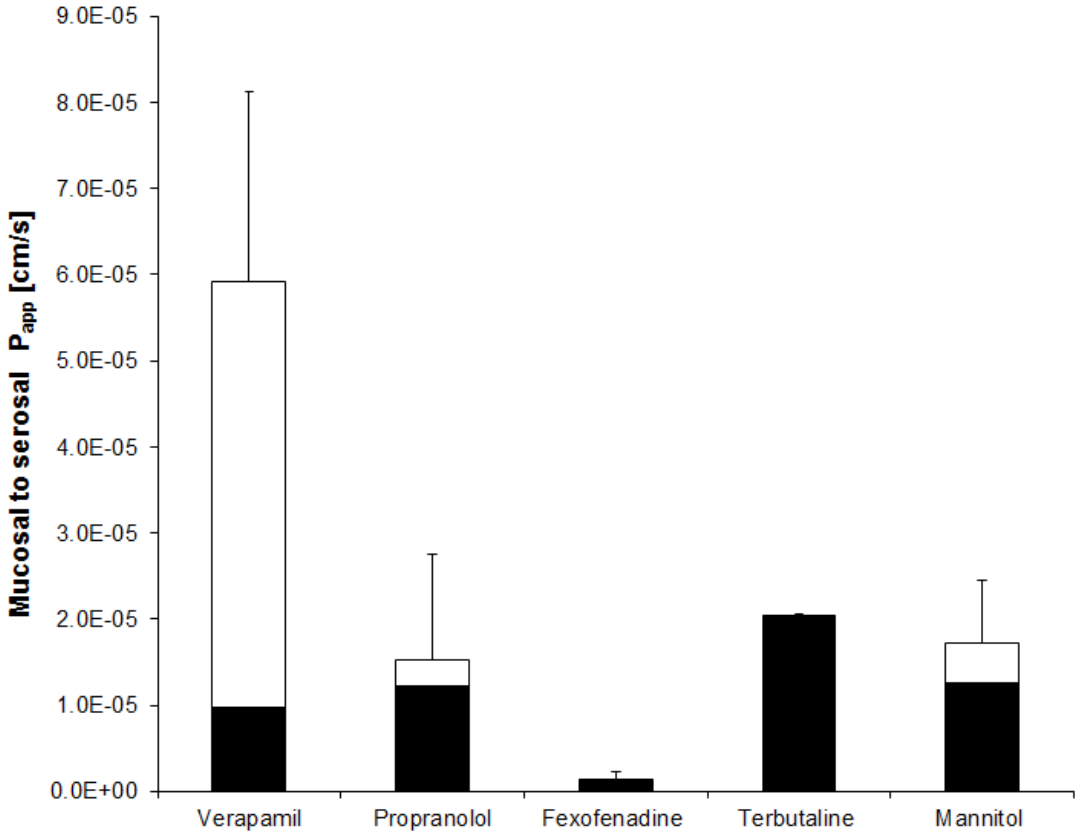

Fig. 3-3: Apparent rat jejunal permeability (P_{app}) from mucosal to serosal side determined in permeability studies using stripped tissue in the Ussing chamber. Total bar represents non-specific binding corrected permeability for each compound presented as mean ± standard deviation. White bar (□) represents the non-specific binding, black bar (■) represents uncorrected experimental permeability. Mannitol (n= 17), verapamil and propranolol (n= 6), terbutaline and fexofenadine (n= 5). Data is given in Tab. 3-8.

Although the influence of the NSB is only displayed for the group of stripped tissue for the mucosal to serosal direction in Fig. 3-3, it was present in all study groups, as correction of the experimental P_{app} was performed using the respective recovery ratios shown in Tab. 3-4.

3.2.2.2 Comparing mucosal to serosal and serosal to mucosal direction

For all reference compounds permeability studies were performed in a bidirectional manner. Therefore, the radiolabeled reference compounds were applied to the mucosal side and permeability to the serosal side was examined or vice versa. By this method, the transport characteristics of the respective compound can be evaluated as compounds undergoing active efflux or influx processes should exhibit different transepithelial fluxes in m-s or s-m direction. Results for the study group of stripped tissue are shown in Fig. 3-4. Here,

verapamil showed tendencies to higher permeability in s-m direction compared to mucosal to serosal direction accounting for known active efflux, but could not be proven statistically significant with a p-value $\leq$ 0.05. In contrast to all other tested compounds, mannitol demonstrated a significantly (p-value = 0.012) higher m-s flux than s-m flux with an apparent permeability of 1.73E-05 cm/s and 1.15E-05 cm/s, respectively (Tab. 3-7). The compound fexofenadine, which is known to undergo active intestinal influx and efflux, showed no significant differences in permeability when comparing both flux directions.

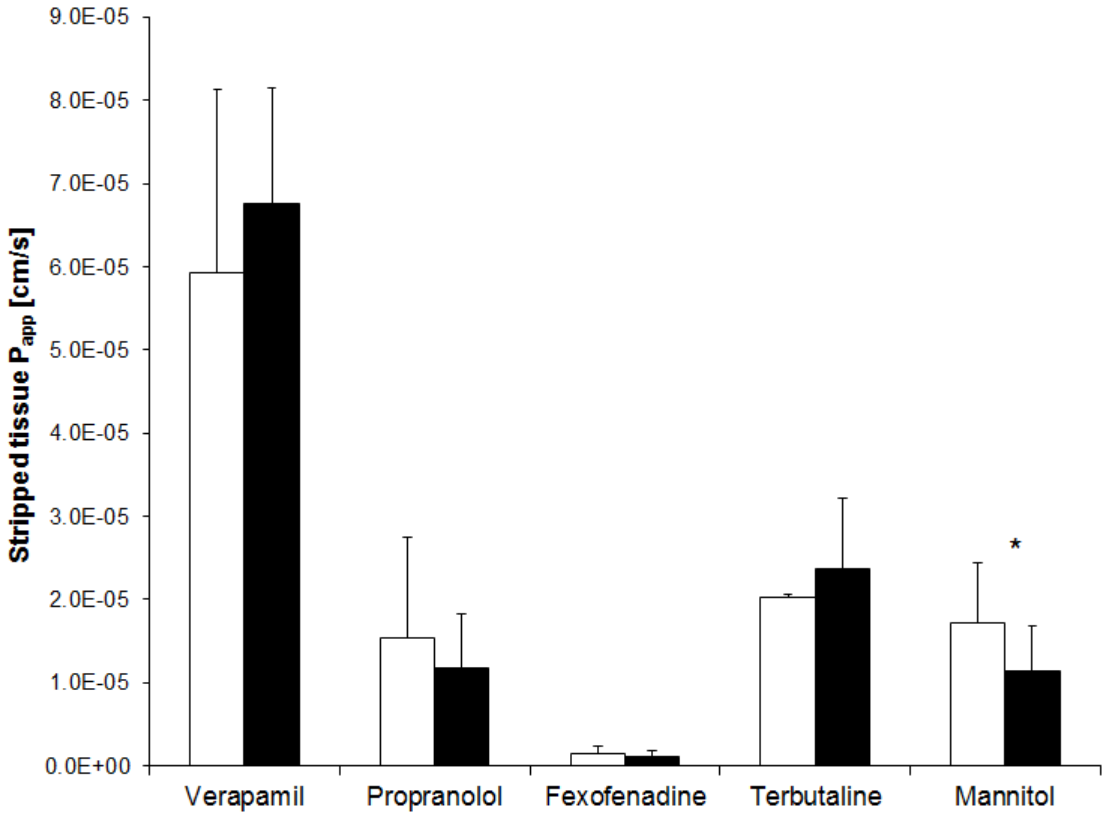

Fig. 3-4: Apparent rat jejunal permeability (P_{app}) corrected for non-specific binding from permeability studies using stripped tissue in the Ussing chamber presented as mean ± standard deviation. White bars (□) represent the permeability from mucosal to serosal side; black bars (■) represent the permeability from serosal to mucosal side for each compound. Mannitol (n= 17); terbutaline, propranolol and verapamil (n= 6), fexofenadine (n= 4), *= statistical significance p ≤ 0.05.

In Fig. 3-5 the bidirectional permeability data is shown for the full-thickness tissue study group. Except for fexofenadine, all tested substances demonstrate a higher mucosal to serosal flux compared to the s-m flux. This difference has been demonstrated statistically significant for verapamil and mannitol. Fexofenadine exhibited hardly any difference between m-s and s-m permeability with a P_{app} of 1.09E-06 cm/s and 1.24E-05 cm/s, respectively. On

the contrary, the permeability for mucosal to serosal direction in verapamil was 2.6 times higher than the s-m flux.

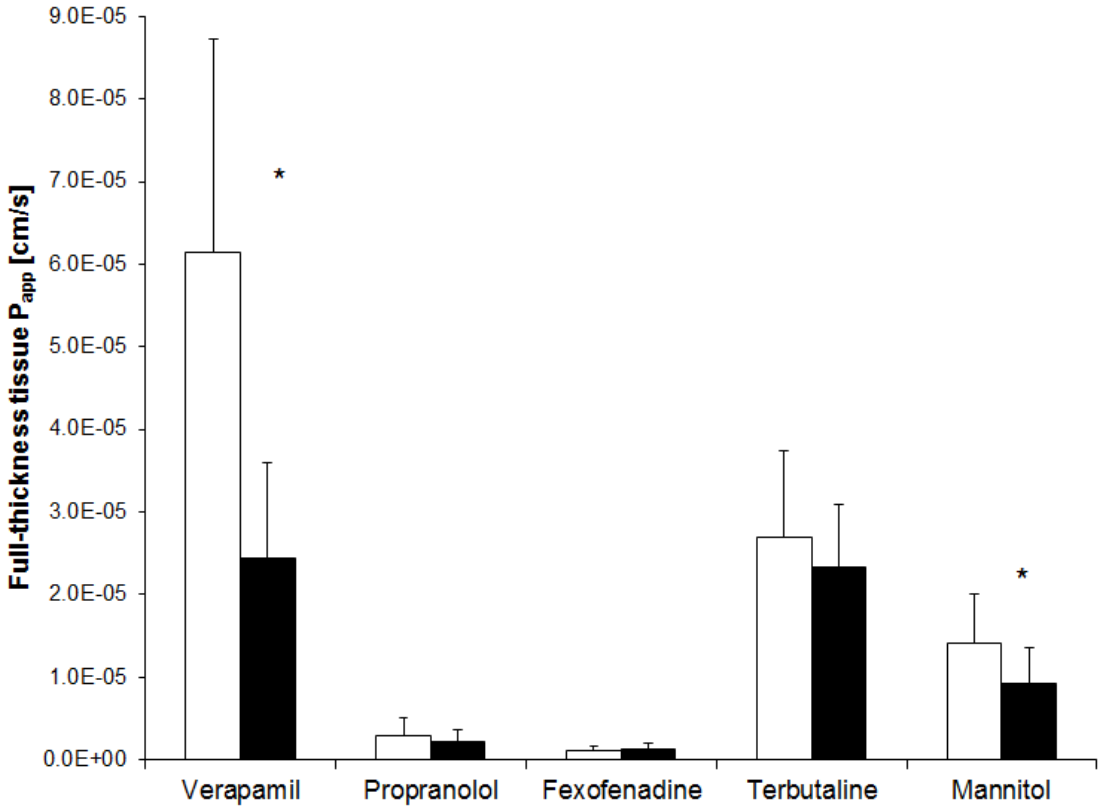

Fig. 3-5: Apparent rat jejunal permeability (P_{app}) corrected for non-specific binding from permeability studies using full-thickness tissue in the Ussing chamber presented as mean ± standard deviation. White bars (□) represent the permeability from mucosal to serosal side; black bars (■) represent the permeability from serosal to mucosal side for each compound. Mannitol (n=15), terbutaline and fexofenadine (n=6), propranolol (n=5), verapamil (n=4), * = statistical significance $p \leq 0.05$.

3.2.2.3 Comparing stripped tissue and full-thickness tissue

The influence of two tissue preparation techniques on the transepithelial permeability was examined. On the one hand, rat jejunum with all its layers (full-thickness tissue) was used; on the other hand the tissue was stripped from its serosal layer (Chapter 2.2.3.2.1). Fig. 3-6 compares the corrected apparent m-s fluxes for stripped and full-thickness tissue. Only for propranolol the removal of the serosal layer enhanced the P_{app} compared to the experiments with full-thickness tissue (p-value ≤ 0.05). The permeability of propranolol for the mucosal to

serosal route was higher in stripped tissue (1.53E-05 cm/s) in contrast to the full-thickness tissue group (2.85E-06 cm/s) by a factor of 5.2.

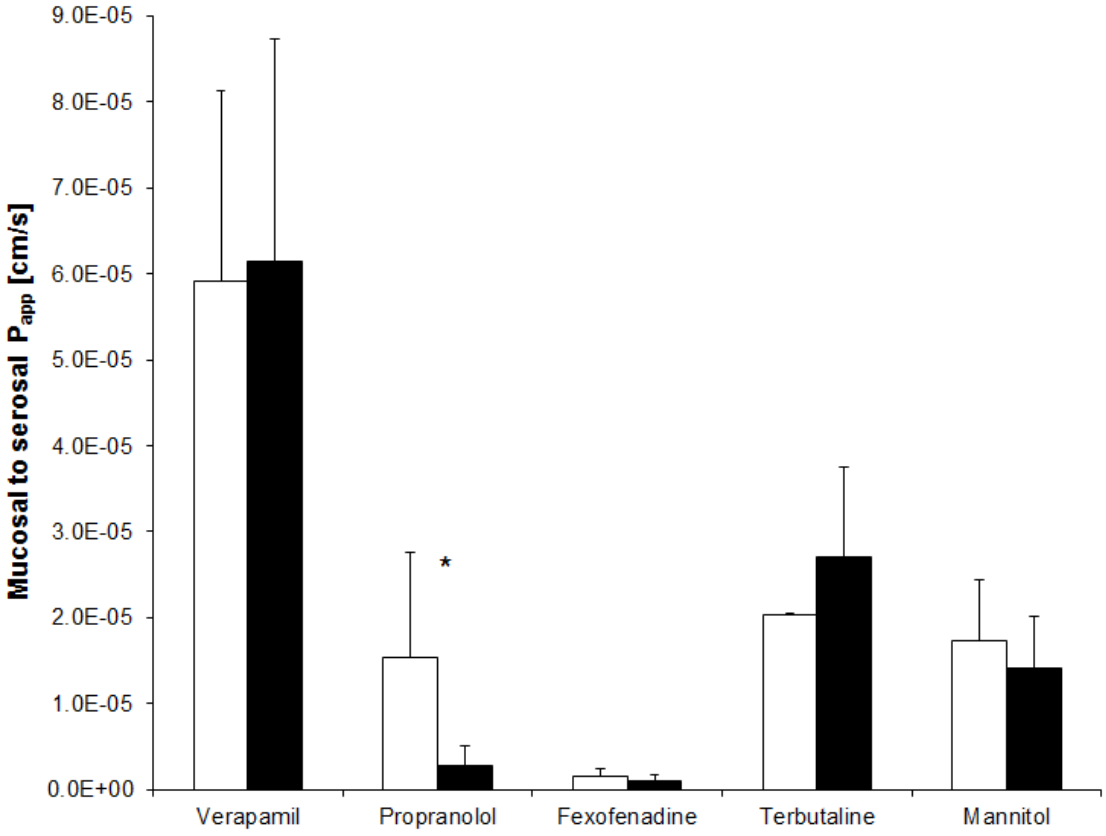

Fig. 3-6: Apparent rat jejunal permeability (P_{app}) corrected for non-specific binding from mucosal to serosal side determined in permeability studies using the Ussing chamber presented as mean ± standard deviation. White bars (□) represent the permeability across stripped tissue; black bars (■) represent the permeability across full-thickness tissue for each compound. Mannitol (n=17), verapamil, propranolol stripped, terbutaline full-thickness (n=6), fexofenadine, terbutaline stripped, propranolol full-thickness (n=5). *= statistical significance $p \leq 0.05$.

As regards the study group serosal to mucosal side (Fig. 3-7), the difference in permeability of the two tissue preparation groups was not significant for the compounds mannitol, terbutaline and fexofenadine ($p \geq 0.05$). For propranolol the apparent permeability in stripped tissue (1.17E-05 cm/s) was demonstrated slightly higher (p-value= 0.011) in comparison to the full-thickness tissue (2.14E-06 cm/s). The serosal to mucosal permeability for verapamil was significantly higher in the stripped tissue study group with a p-value of 0.001. The apparent permeability was 6.75E-05 cm/s and therefore 2.8 times higher than with full-thickness tissue (2.43E-05 cm/s).

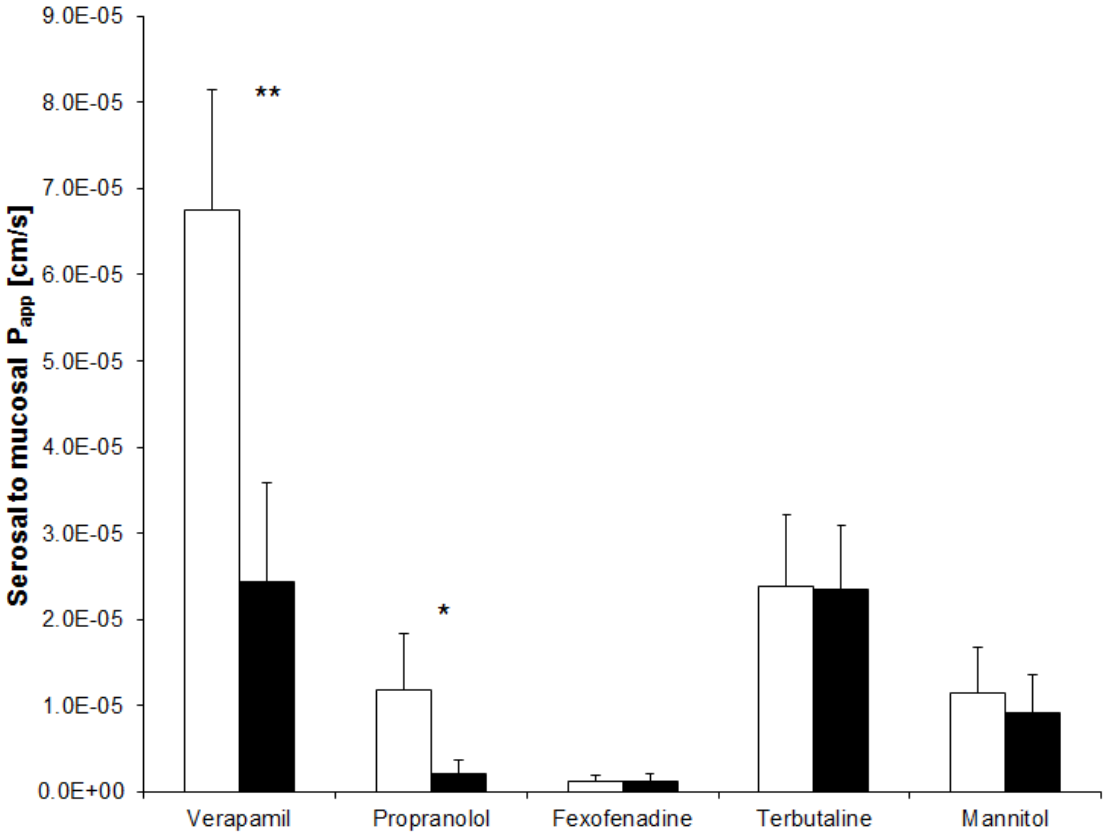

Fig. 3-7: Apparent rat jejunal permeability (P_{app}) corrected for non-specific binding from serosal to mucosal side determined in permeability studies using the Ussing chamber presented as mean ± standard deviation. White bars (□) represent the permeability across stripped tissue; black bars (■) represent the permeability across full-thickness tissue for each compound. Mannitol stripped tissue (n=17), mannitol full-thickness tissue (n=15), terbutaline, fexofenadine full-thickness tissue, propranolol stripped tissue and verapamil stripped tissue (n=6), propranolol full-thickness tissue (n=5), verapamil full-thickness tissue and fexofenadine stripped tissue (n=4), *= statistical significance $p \leq 0.05$, **= statistical significance $p \leq 0.01$.

3.2.2.4 Comparing transcellular and paracellular route

The selection of reference compounds covered the main permeability routes for intestinal absorption (Tab. 2-5). Small hydrophilic molecules like mannitol and terbutaline pass the membrane paracellularly via tight junctions; thus do not enter the epithelial cells. Propranolol, verapamil and fexofenadine cross the mucosal membrane on the transcellular route as they are lipophilic and larger in size. By using mannitol, as a reference substance for not entering the enterocytes (extracellular marker), extra- and intracellular cell space could be differentiated and the amount of compound in the cells was calculated for all remaining substances in this study (Chapter 2.2.4.3).

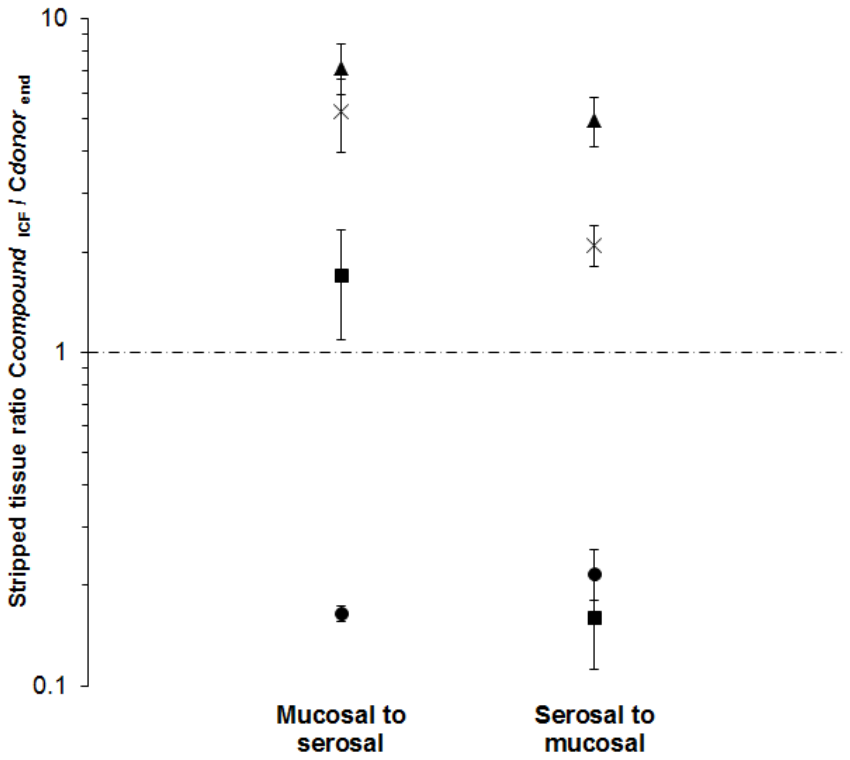

Fig. 3-8: Ratios of intra- and extracellular compound concentration. Compound per gram jejunal cells (C*compound*$_{ICF}$) in relation to compound concentration on donor side of chamber by end of experiment (C*donor*$_{end}$) presented as mean ± standard deviation (n=6). Study group stripped tissue divided into mucosal to serosal and serosal to mucosal permeability experiments. Fexofenadine (■), propranolol (▲), terbutaline (●), verapamil (x). The dashed line (–·–·) represents equal intracellular and extracellular concentration (Ratio=1).

Fig. 3-8 displays the ratio of concentration of compound in the jejunal enterocytes per gram cells (C*compound*$_{ICF}$) and the concentration of compound on the donor side of the chamber by the end of the experiment (C*donor*$_{end}$) in the stripped tissue study group calculated according to Equation 16. Data points located below the dashed line (i.e. ratio < 1) indicate, that more compound was found extracellularly than intracellularly. This was the case for the passively paracellular diffusing terbutaline. On the other hand, the intracellular concentration of verapamil, propranolol and fexofenadine was higher compared to the extracellular concentration on the mucosal side. Fig. 3-8 also distinguishes between fluxes from m-s side and s-m side. Propranolol exhibited the highest intra- to extracellular ratio with 7.15 ± 1.22 for the m-s group and a slightly lower ratio in s-m direction (4.98 ± 0.850). Hence, more compound is located intracellularly than extracellularly as expected for a passively transcellular permeating substance. More verapamil was found intracellularly than extracellularly for all permeability experiments. The ratio for the m-s direction of 5.27 ± 1.32

was significantly higher ($p \leq 0.01$) than the ratio for the serosal to mucosal direction (2.10 ± 0.290). As mentioned above, terbutaline is a paracellularly diffusing substance that does not enter the enterocytes. As anticipated, terbutaline exhibited in all permeability experiments an intra- to extracellular ratio smaller than 1, ranging from 0.155 to 0.278 indicating a 5-fold higher extracellular to intracellular concentration on average. Therefore, more substance was located outside of the intestinal cells compared to inside. Fexofenadine showed significant differences in intra- to extracellular ratios ($p \leq 0.01$) when considering bidirectional experiments. The m-s direction displayed a ratio of 1.71 ± 0.615, where the s-m direction only showed a ratio of 0.161 ± 0.0494. More of the actively transported compound fexofenadine was found inside the cells when considering the mucosal to serosal direction compared to only a tenth of the substance in the serosal to mucosal experiments. It should be noted, that fexofenadine also undergoes active efflux when permeating through the enterocytes.

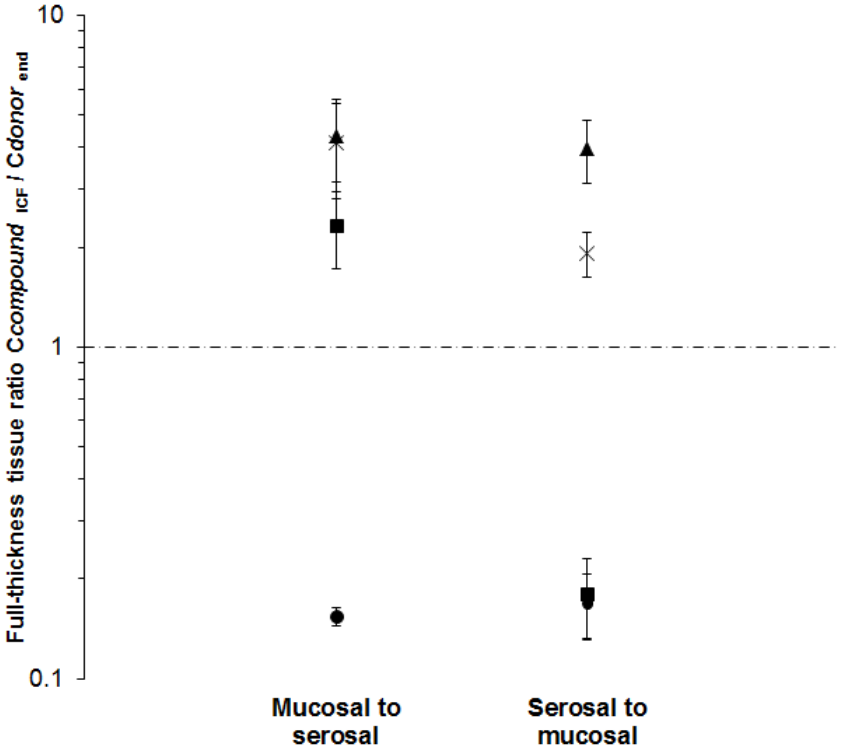

Fig. 3-9: Ratios of intra- and extracellular compound concentration. Compound per gram jejunal cells (C*compound*$_{ICF}$) in relation to compound concentration on donor side of chamber by end of experiment (C*donor*$_{end}$) presented as mean ± standard deviation (n=6). Study group full-thickness tissue divided into mucosal to serosal and serosal to mucosal permeability experiments. Fexofenadine (■), propranolol (▲), terbutaline (●), verapamil (x). The dashed line (–·–·) represents equal intracellular and extracellular concentration (Ratio=1).

Fig. 3-9 displays the same intra- to extracellular ratio as described for Fig. 3-8, but for all experiments conducted with full-thickness tissue. Basically, the intracellular to extracellular distribution of the compounds was the same as mentioned above, with verapamil and fexofenadine showing significantly more compound intracellularly for the m-s experiments compared to the serosal to mucosal studies with a p-value ≤ 0.01. As for the stripped tissue experiments, fexofenadine showed a ratio larger than 1 for the m-s studies and a ratio smaller than 1 for the s-m fluxes. Propranolol exhibited the highest accumulation in the enterocytes, with an intra- to extracellular ratio of 4.36 ± 0.318 for m-s fluxes and a ratio of 3.98 ± 0.279 for the s-m experiments. For all studies, more terbutaline was found extracellularly than intracellularly with ratios below 0.17.

3.2.2.5 Mass balance of experiments

Tab. 3-9 shows the results from the performed mass balance as described in Chapter 2.2.4.4. For the compounds terbutaline and mannitol, the values for non-specific binding (NSB) were negative. This is an artefact resulting from the data in the NSB studies, which displayed a recovery in the taken samples and remaining buffer >100 % (Tab. 3-5). This can be due to variability in measurement. Mannitol, fexofenadine and propranolol each had a total recovery of 88 %, 90 % and 89 %, respectively. Terbutaline followed with a total recovery of 84 %. Total recovery for verapamil was calculated to be 116 %, exceeding a complete recovery. When calculating only the amount of verapamil on the donor side, the receiver side and amount found in the tissue, recovery totals in 35 %. This is an increase of recovery compared to the NSB studies performed without mounted tissue (Tab. 3-5). Bringing in additional material with binding potential, such as tissue, can lower the initial NSB in the experiment, but it should also be kept in mind that non-specific binding was already prone to variability in the NSB studies (Chapter 3.2.1.1). Variability of total recovery within each compound was low for the study group stripped m-s (Tab. 3-9). Coefficient of variation (CV) for total recovery ranged from 1 % to 4 % for terbutaline, verapamil, fexofenadine and propranolol. Whereas for these compounds only one animal was used per experiment, the results for mannitol are averaged from three independent experiments. Due to the additional inter-animal variability, the CV was slightly higher for mannitol (8 %).

Tab. 3-9: Mass balance for permeability experiments from mucosal to serosal side using stripped tissue in the Ussing chamber. Recovery of compound after 150 minutes of experiment from donor side, receiver side and from tissue and the previously determined non-specific binding is shown; the sum is representing the total recovery for each compound. Data is presented in percent as mean ± standard deviation. For total recovery the coefficient of variation [%] is given. (n= 6; mannitol n= 18).

Reference compound	Recovery [%]					
	Donor	Receiver	Tissue	NSB	Total	
	mean ± SD	mean ± SD	mean ± SD	mean ± SD	mean ± SD	CV [%]
Verapamil	29.4 ± 0.852	0.49 ± 0.094	5.48 ± 0.600	80.3 ± 6.26	116 ± 0.97	0.840
Propranolol	66.7 ± 2.34	1.42 ± 0.986	12.9 ± 2.68	7.67 ± 3.00	88.7 ± 3.53	3.98
Terbutaline	80.2 ± 1.30	4.71 ± 0.736	2.10 ± 0.100	-2.70 ± 3.75	84.3 ± 0.8	0.922
Fexofenadine	83.1 ± 2.87	0.32 ± 0.196	5.95 ± 0.46	0.750 ± 1.85	90.1 ± 2.96	3.31
Mannitol	85.0 ± 6.46	1.84 ± 0.636	1.88 ± 0.6	-0.700 ± 4.41	88.0 ± 6.99	7.94

As regards recovery in tissue, the values comprise amount of compound in the intestinal cells, but also compound in the interstitium and adhering to the excised tissue as it is presumably the case for mannitol and terbutaline, as they are known to cross the intestinal membrane through tight junctions without entering the enterocytes. Therefore, the two compounds showed a low recovery in the tissue with only 2 % compared to all other compounds that are known to enter the enterocytes.

3.2.3 Electrical measurements

In order to monitor the viability of the excised tissue, electrical measurements were carried out as described in Chapters 2.2.1.5 and 2.2.2.4.

3.2.3.1 Transepithelial resistance

One important parameter to evaluate the condition of the excised tissue is the transepithelial resistance (R_t) measured with the clamp-system (Chapter 2.2.1.5). It is an indicator for the integrity of the tissue. Disruption or perforation of the tissue during the preparation process influences its integrity and therefore alters R_t and most likely the permeability data collected from the experiments. Tab. 3-10 gives information about the transepithelial resistance of stripped and full-thickness tissue before the start of the permeability experiments. The R_t for full-thickness tissue was 66.1 ± 13.5 Ω/cm^2 and was significantly higher ($p < 0.05$) compared

to the transepithelial resistance of stripped tissue with R_t being 59.6 ± 15.8 Ω/cm^2. As anticipated, the extra layer of the serosa seems to contribute to the overall transepithelial resistance of the excised rat jejunum.

Tab. 3-10: Results for transepithelial resistance (R_t) measurement from the Ussing chamber experiments comparing full-thickness and stripped tissue. Electrical resistance of excised tissue by start of experiment is shown as mean ± standard deviation and coefficient of variation [%]. Full-thickness tissue n= 41, stripped tissue n= 47.

Tissue preparation technique	**R_t [Ω/cm^2]**	
	mean ± SD	CV [%]
Full-thickness tissue	66.1 ± 13.5	20.5
Stripped tissue	59.6 ± 15.8	26.6

3.3 Simulation of intestinal absorption using GastroPlus™

A retrospective data evaluation was performed, to assess the ability of the applied physiology base *in silico* tool, to predict intestinal absorption for eight selected compounds (C_1 - C_8) with the minimum amount of input data required. Two PK parameters that describe intestinal absorption were focused on; fraction absorbed (f_a) and the absorption rate constant (k_a). For the assessment of the success of the simulations, a deviation factor of two (i.e. 2-fold error) from the *in vivo* results was accepted [89, 90].

3.3.1 Fraction absorbed

Fraction absorbed (f_a) was simulated for eight compounds, based on the setting of the performed *in vivo* studies (Appendix 7.2). This included different species, formulations and doses. Evaluation was performed for all simulations and categorised by different properties (e.g. species, physicochemical properties). The data was plotted as a correlation plot comparing predicted versus observed fraction absorbed. It should be noted, that for all graphs, the bold black line is the line of unity and no the regression line. However, the actual coefficient of determination (R^2) for the regression line is presented in the graph. The two dashed lines, forming a 'scissor shape', define the area of accepted deviation. Briefly, data points between the bold and the dashed line are within a deviation factor of two and the simulation results were considered acceptable [89, 90]. This kind of display was chosen to visually facilitate the evaluation. Each data point represents the predicted and observed f_a (determined within the *in vivo* study) for a certain compound, certain species, with a certain formulation and dose. If for example one compound was administered in the same species with the same formulation but in a different dose, two data points will represent those results. For fraction absorbed, 35 simulation scenarios were performed.

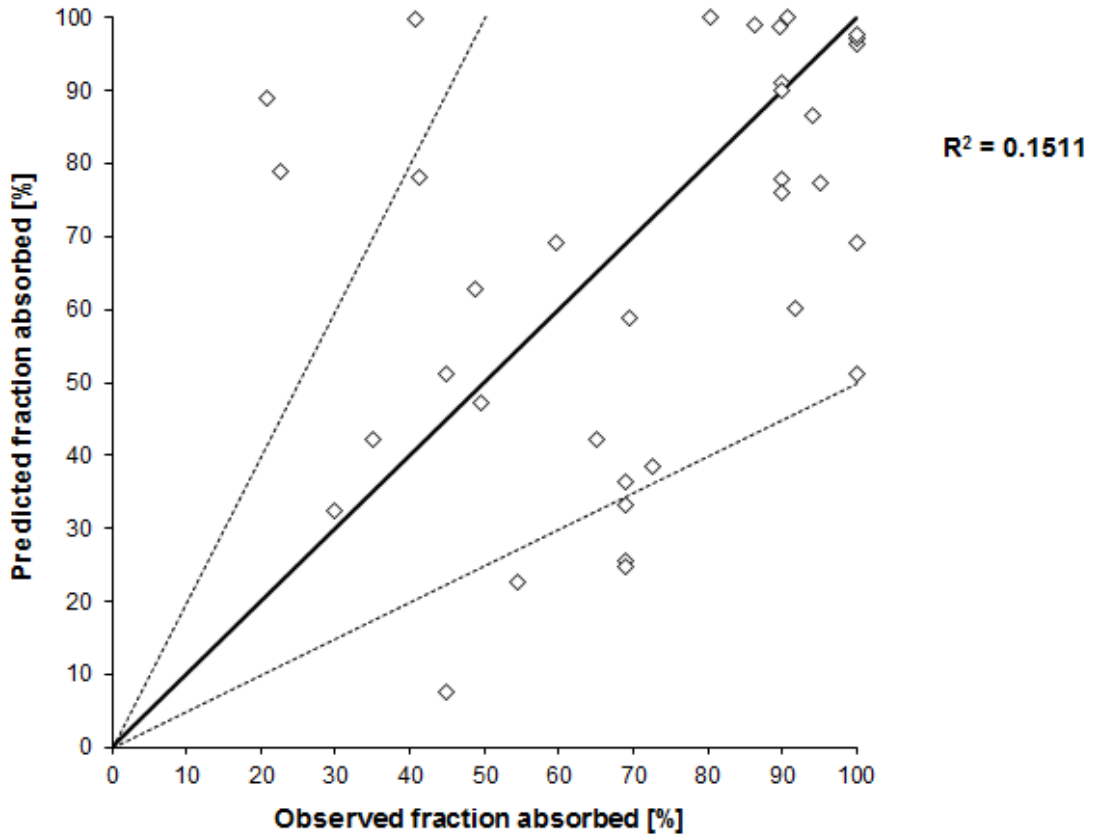

Fig. 3-10: Predicted fraction absorbed using GastroPlus™ versus observed fraction absorbed determined in *in vivo* studies in percent (data points comprise all compounds, species, formulations and doses). Fraction absorbed of compound (◊), line of unity (—) and 2-fold error (- - -), n= 35. In addition the coefficient of determination (R^2) is shown.

Fig. 3-10 shows the overall results for all f_a simulations. For 77.1 % of all simulated scenarios, the prediction was within 2-fold error of the *in vivo* data (Tab. 3-11). Therefore, the majority of data was within the accepted deviation; however the coefficient of determination was low, with 0.151, indicating a very poor correlation between simulated and observed fraction absorbed. Of the 35 simulations, three exhibited a high predicted f_a with 100 %, 89 % and 79 % for *in vivo* experiments with moderate to low f_a of 41 %, 21 % and 23 %, respectively. Five additional predictions were underestimated as they exhibited low to moderate fraction absorbed ranging from 8 % to 33 % in comparison to the *in vivo* determined moderate f_a of 45 % to 69 %. For observed fraction absorbed > 80 % the predicted f_a was variable ranging from 51 % to 100 % but still within the accepted limits.

Tab. 3-11: Quality parameters for *in silico* prediction of *in vivo* fraction absorbed.

Compound category	rmse	% within 2-fold error	% within 2.5-fold error	% within 3-fold error
Low *in vivo* f_a (< 30 %)	62.5	0.00	0.00	0.00
Moderate *in vivo* f_a (≥30 - ≤ 70%)	30.0	62.5	81.3	87.5
High *in vivo* f_a (> 70 %)	20.2	100	N.A.	N.A.
All compounds (n=35)	28.9	77.1	85.7	91.4

N.A. = not applicable
rmse = root mean square error

When categorizing fraction absorbed, < 30 % is considered low, ≥ 30 % to ≤ 70 % is moderate and > 70 % is referred to as high absorption. If Fig. 3-10 is divided into those three categories, the predictions for low *in vivo* f_a could not be matched (0 % within 3-fold error) and were highly overpredicted in the simulations, falsely suggesting high absorption. For moderate observed f_a, *in silico* results varied into both directions, with tendencies to underprediction. Of all three groups, predictions for high observed fraction absorbed were best, as 100 % of the data points were within a 2-fold error (Tab. 3-11). This implies, that the higher the *in vivo* f_a, the better the prediction.

3.3.1.1 Fraction absorbed categorised by species

Fig. 3-11 shows f_a data categorised by all species that were simulated. As rat is a standard species for pharmacokinetic studies, it represent the species with the most simulations (n=12). The coefficient of determination (R^2) for observed versus predicted f_a in the species rat was 0.433. Based on the line of unity, the predictions for rat showed tendencies for an underprediction of f_a compared to *in vivo* with two simulations (16.7 %) outside the 2-fold error. For these two data points, the *in vivo* fraction absorbed was underpredicted by a factor of 2.4 and 5.8, respectively. The opposite observation was made for the species dog, with a tendency to overestimate the absorption *in vivo*. 60 % of the predictions for human f_a were close to the line of unity. One data point was close to the dashed line, but still within the acceptance criteria, and three simulations (30 %) were below the lower dashed line and therefore outside the accepted deviation. It should be mentioned, that those four data points belong to the same compound (Appendix Tab. 7-22). Hence, the poor fit might result from a compound specific feature rather than referring to the actual predictability of the *in silico* tool for this particular species.

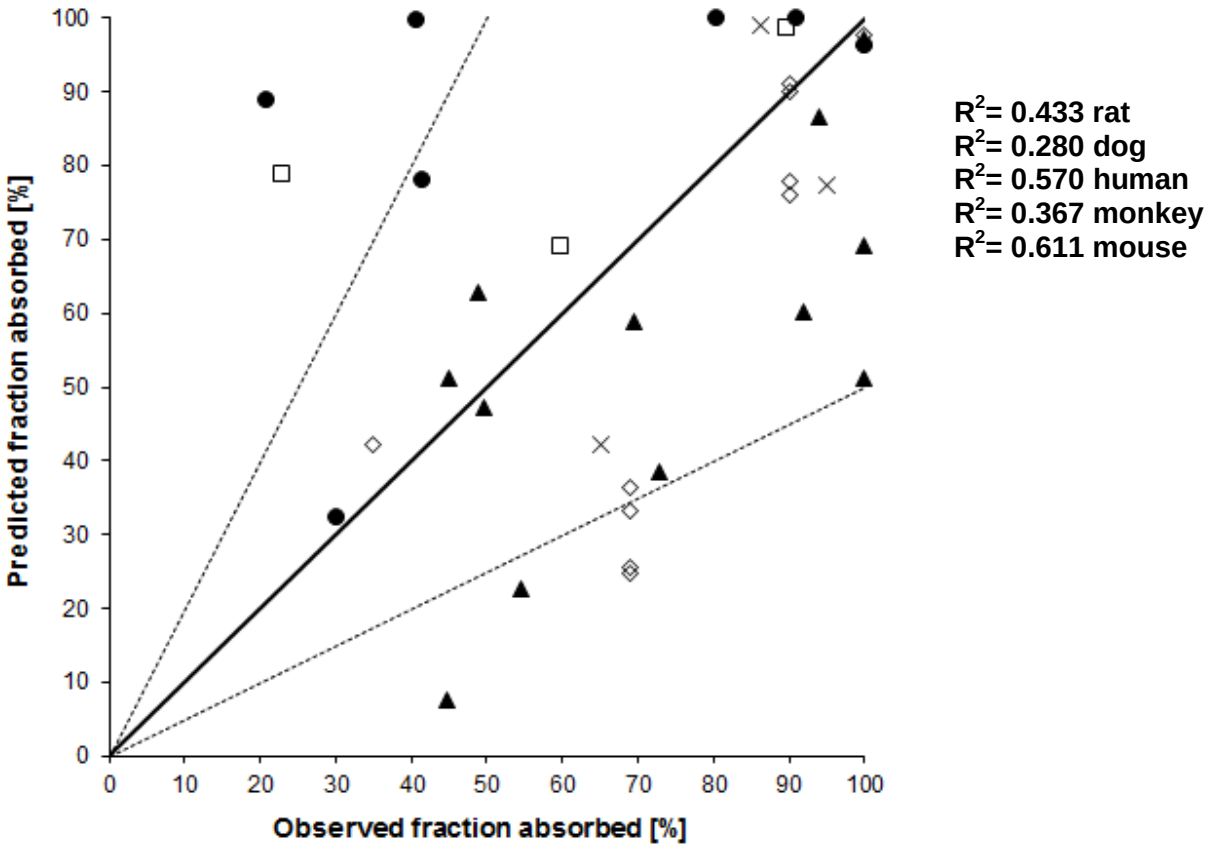

Fig. 3-11: Fraction absorbed categorised by species. Predicted fraction absorbed using GastroPlus™ versus observed fraction absorbed determined in *in vivo* studies in percent (data points comprise all compounds, species, formulations and doses). In addition the coefficient of determination (R^2) is shown per species. Rat n=12 (▲), dog n=7 (●), human n=10 (◊), monkey n=3 (□), mouse n=3 (x), line of unity (—) and 2-fold error (- - -).

Regarding the goodness of the predictions, mouse showed the best accuracy of predictions with a route mean square error of 18.1 followed by human, rat monkey and dog, with 25.7, 26.3, 33.4 and 37.8, respectively (Tab. 3-12). Due to the low number of simulations (n=3) for monkey and mouse, a generalisation of the ability to predict f_a for these species should be avoided.

Tab. 3-12: Quality parameter for *in silico* prediction of *in vivo* fraction absorbed categorised by species.

Species category	rmse	% within 2-fold error	% within 2.5-fold error	% within 3-fold error
f_a in rat (n= 12)	26.3	83.3	91.6	91.6
f_a in dog (n= 7)	37.8	71.4	85.7	85.7
f_a in human (n= 10)	25.7	70.0	80.0	100
f_a in monkey (n= 3)	33.4	66.7	66.7	66.7
f_a in mouse (n= 3)	18.1	100	N.A	N.A
All compounds (n= 35)	28.9	77.1	85.7	91.4

N.A. = not applicable
rmse = root mean square error

3.3.1.2 Fraction absorbed categorised by effective permeability and solubility

Two of the major properties that determine the *in vivo* intestinal drug absorption are the ability to permeate a lipid membrane and the solubility. As described in Chapter 2.3.2 the *in silico* tool requires the input parameter solubility and effective permeability (P_{eff}). The impact of both variables on the overall fraction absorbed is illustrated in Fig. 3-12.

Fig. 3-12 A displays f_a (for all simulations) categorised by effective permeability, whereas P_{eff} is divided into two categories. A P_{eff} value in the critical range of 0.5E-04 to 1.5E-04 cm/s can be responsible for incomplete absorption. Exceeding a P_{eff} of 1.5E-04 cm/s, usually enables the substance to be completely absorbed [36]. For the low effective permeability ($P_{eff} \leq$ 1.5E-04 cm/s) compounds, 33.3 % of the predictions were within 2-fold error of the *in vivo* data, whereas for the high permeability compounds (P_{eff} >1.5E-04 cm/s), 86.2 % of the predictions were within the acceptable deviation.

In Fig. 3-12 B f_a is categorised for compound solubility. Three categories for solubility were formed. The highest solubility category was > 0.1 mg/mL and the lowest solubility category was ≤ 0.01 mg/mL.

Compounds that feature a relatively good solubility (> 0.01 mg/mL), but poor permeability ($P_{eff} \leq$ 1.5E-04), exhibited low to moderate *in vivo* fraction absorbed (< 70 %) in the performed simulations.

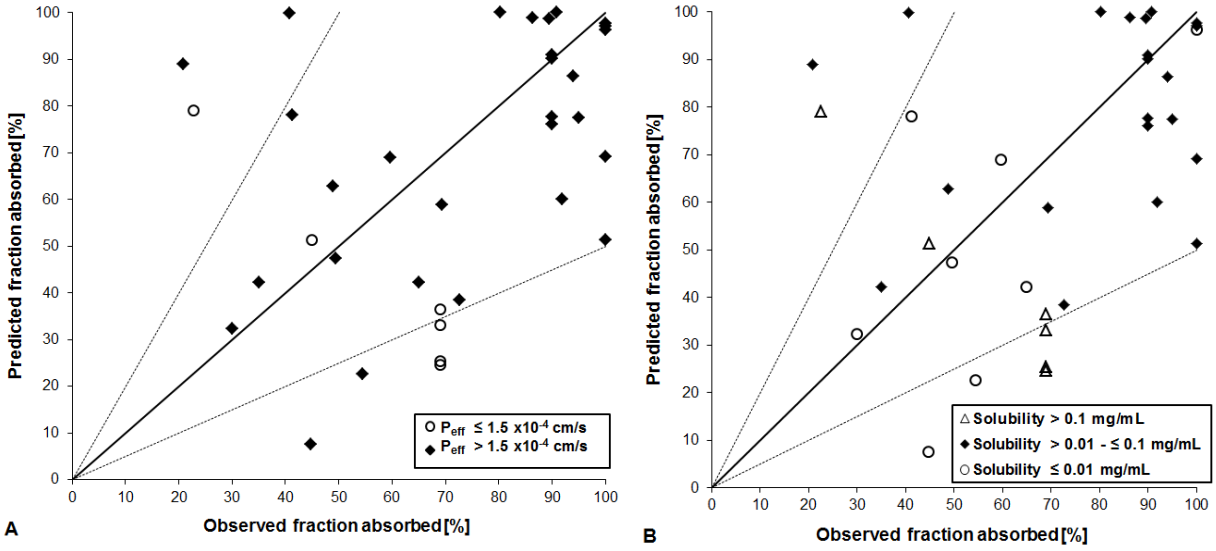

Fig. 3-12: Fraction absorbed categorised by effective permeability (**A**) and solubility (**B**). Predicted fraction absorbed using GastroPlus™ versus observed fraction absorbed determined in *in vivo* studies in percent (data points comprise all compounds, species, formulations and doses). Line of unity (**—**) and 2-fold error (- - -) n= 35.

For eight data points that were plotted outside the 2-fold error limit, six showed evidence of either restricted permeability (P_{eff} ≤ 1.5 cm/s) or low solubility (≤ 0.01 mg/mL). For the two remaining simulations, fraction absorbed was highly overpredicted despite displaying high effective permeability (> 1.5E-04 cm/s) and reasonable solubility (> 0.01 mg/mL). When combining all available information for these particular simulations, it could be concluded, that those data points belonged to a single compound (C_5) and were simulated in the species dog with the same formulation (suspension) at two different dose of 20 mg/kg and 200 mg/kg, respectively (Tab. 7-20). As the physicochemical properties of C_5 theoretically permit complete absorption, further evaluations (via parameter sensitivity analysis) were conducted, in order to elucidate the poor *in vivo – in silico* correlation (Chapter 3.3.1.3).

Tab. 3-13 and Tab. 3-14 display the quality parameter for the fraction absorbed predictions categorised for P_{eff} and solubility. Predictions were best for compounds with a high effective permeability (> 1.5E-04 cm/s) and low solubility (≤ 0.01 mg/mL) indicated by the lowest rmse of 26.1 and 23.4, respectively. Predictions with lower accuracy were observed for compounds with a low permeability or a high solubility with the highest rmse of 39.6 for both categories. As mentioned before, the difference of number of observations / predictions (n) per category should be considered when interpreting the data.

Tab. 3-13: Quality parameters for *in silico* prediction of *in vivo* fraction absorbed categorised by effective permeability.

Permeability category	rmse	% within 2-fold error	% within 2.5-fold error	% within 3-fold error
f_a for P_{eff} ≤ 1.5E-04 cm/s (n= 6)	39.6	33.3	50.0	83.3
f_a for P_{eff} > 1.5E-04 cm/s (n= 29)	26.1	86.2	93.1	93.1
All compounds (n= 35)	28.9	77.1	85.7	91.4

N.A. = not applicable
rmse = root mean square error

Tab. 3-14: Quality parameters for *in silico* prediction of *in vivo* fraction absorbed categorised by solubility.

Solubility category	rmse	% within 2-fold error	% within 2.5-fold error	% within 3-fold error
f_a for solubility ≤ 0.01 mg/mL (n= 8)	23.4	75.0	87.5	87.5
f_a for solubility > 0.01 - ≤ 0.1 mg/mL (n= 21)	27.1	90.5	95.2	95.2
f_a for solubility > 0.1 mg/mL (n= 6)	39.6	33.3	50.0	83.3
All compounds (n= 35)	28.9	77.1	85.7	91.4

N.A. = not applicable
rmse = root mean square error

In the course of analysing simulation results for f_a, further categorisation parameters have been investigate, e.g. molecular weight, Log $P_{o/w}$ and formulation (Fig. 7-1 to Fig. 7-4), with the limitation that data points for some categories with a parameter referred to only one compound. Based on this finding, no further calculation of quality parameters was performed.

3.3.1.3 Parameter sensitivity analysis

To further evaluate the findings described in Chapter 3.3.1.2, a parameter sensitivity analysis (PSA) of f_a was performed for all physicochemical properties of the compound C_5 as well as for the dog specific anatomical and physiological features. A detailed process description of this particular simulation type is given in Chapter 2.3.5.3. Tab. 3-15 lists the parameters that were tested using the parameter sensitivity analysis. The most noticeable parameter influencing the fraction absorbed in this PSA simulation was identified as the stomach pH of the dog.

Tab. 3-15: List of parameters that were investigated by running a parameter sensitivity analysis using GastroPlus™.

Physiological parameter	Physicochemical parameter	Formulation parameter
Gastrointestinal residence / transit time [h]	P_{eff} [cm/s]	Dose [mg]
Gastrointestinal pH	Solubility [mg/mL]	Particle radius [µm]
Intestinal length [cm]	Log $P_{o/w}$	Particle density [g/mL]
Intestinal radius [cm]		

In Fig. 3-13, the change of fraction absorbed for various gastrointestinal pH values is shown. In order to display stomach, small and large intestinal pH versus f_a in one chart, an illustration that displays the change from the default pH value of the physiological input parameter was chosen. Briefly, the x-axis displays the ratio of the changed pH value and the respective default value. The default pH (e.g. 1.5) of a particular part of the gastrointestinal tract (GIT) leads therefore to a ratio of 1. According to this, a ratio of 2 means that a 2-fold higher pH value (i.e. 3) was used as input parameter for this simulation compared to the default value of pH 1.5. The particular f_a for this pH can then be read off the y-axis. This illustration allows displaying all parts of the GIT with different pH value in one chart. The default values in GastroPlus™ for dog stomach, duodenum, jejunum, and colon were pH 3.0, 6.2, 6.2 and 6.5, respectively. The investigated pH range within the parameter sensitivity analysis was pH 0.5 to pH 8.0 or all parts of the gastrointestinal tract.

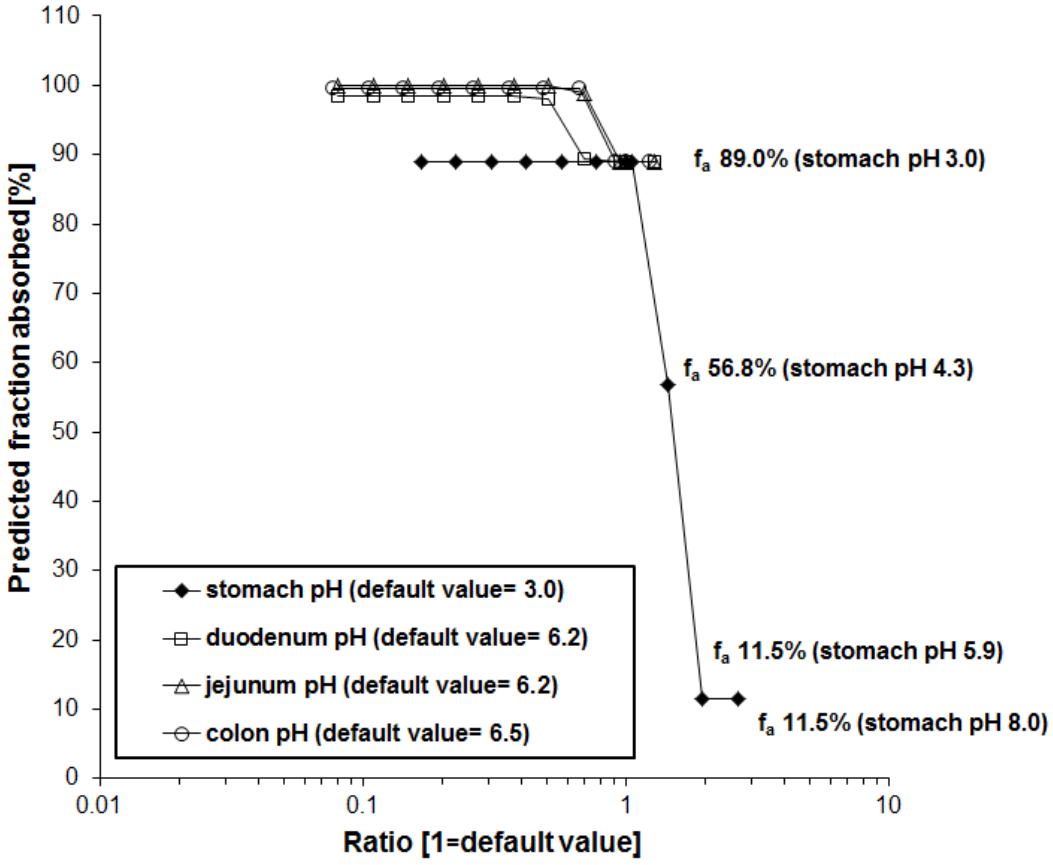

Fig. 3-13: Parameter sensitivity analysis for compound C_5. Effect of gastrointestinal pH value on the predicted fraction absorbed in dog (dose of 200 mg/kg). Gastrointestinal tract is divided into: stomach (-♦-), duodenum (-□-), jejunum (-Δ-) and colon (-○-).

Predicted fraction absorbed showed a high dependence on the stomach pH of the dog (Fig. 3-13). A slight shift from the default value (pH 3.0) to a less acidic pH (4.3) markedly decreased f_a from 89.0 % to only 56.8 %. In case the stomach pH reaches 5.9, the absorbed fraction would exhibit only 11.5 %. The outcome of this PSA suggests that with a stomach pH > 3.0, f_a can be as low as seen in the *in vivo* experiments, with a fraction absorbed of 20.8 % (Tab. 7-20). For the intestinal segments duodenum, jejunum and colon, a shift from the default pH to a less acidic pH showed no effect on fraction absorbed. Only a slight decrease of f_a could be observed for a change from a non-physiologically low pH of 0.5 to a less acidic pH of 4.3 in those parts of the GIT. Fraction absorbed in the segments duodenum (98 %), jejunum (100 %) and colon (100 %) at pH 0.5 decreased to a f_a of 89 % at their respective default pH values.

3.3.2 Absorption rate constant

Based on the available *in vivo* studies (Tab. 7-16 to Tab. 7-23), 105 simulations of plasma concentration-time profiles for the orally administered compounds C_1 to C_8 could be performed as described in Chapter 2.3.5.2. Of the performed simulation only 89 simulations were included into the evaluation. Reasons for exclusion were unavailable plasma concentration-time profiles after intravenous dosing (n= 10), which are mandatory to obtain the pharmacokinetic parameters clearance and volume of distribution to enable the software to simulate oral plasma concentration-time profiles (Fig. 2-4). Moreover, six simulations were excluded with insufficient number of data points to perform a successful compartmental analysis for the observed or predicted oral plasma concentration-time profiles. The absorption rate constants from the observed (range: 0.07 - 7.73 1/h) and predicted (range: 0.03 - 5.08 1/h) oral plasma concentration-time profiles are displayed in Fig. 3-14. The data is displayed as described in Chapter 3.3.1. As before, a deviation factor of two was the acceptance boundary. Fig. 3-14 illustrates the deviation of the predicted k_a from the *in vivo* k_a. The evaluated data exhibited a broad distribution based on the line of unity, with the majority of data points (61%) falling outside of the accepted range. The coefficient of determination (R^2) was very low, with 0.0004. For a better description of the deviation, the mean prediction error (mpe) was calculated and suggested an underprediction of k_a with a negative mpe of -0.52. A mean prediction error can be artificially small, as individual data points that have very large positive and negative errors can cancel each other out. In order to prevent that, the absolute value of error (mae) can be calculated. For the data shown in Fig. 3-14, the average absolute prediction error is 1.17. Hence, on average the k_a from the predicted oral plasma concentration-time profile differed from the *in vivo* plasma concentration-time profile derived k_a by 1.17 1/h.

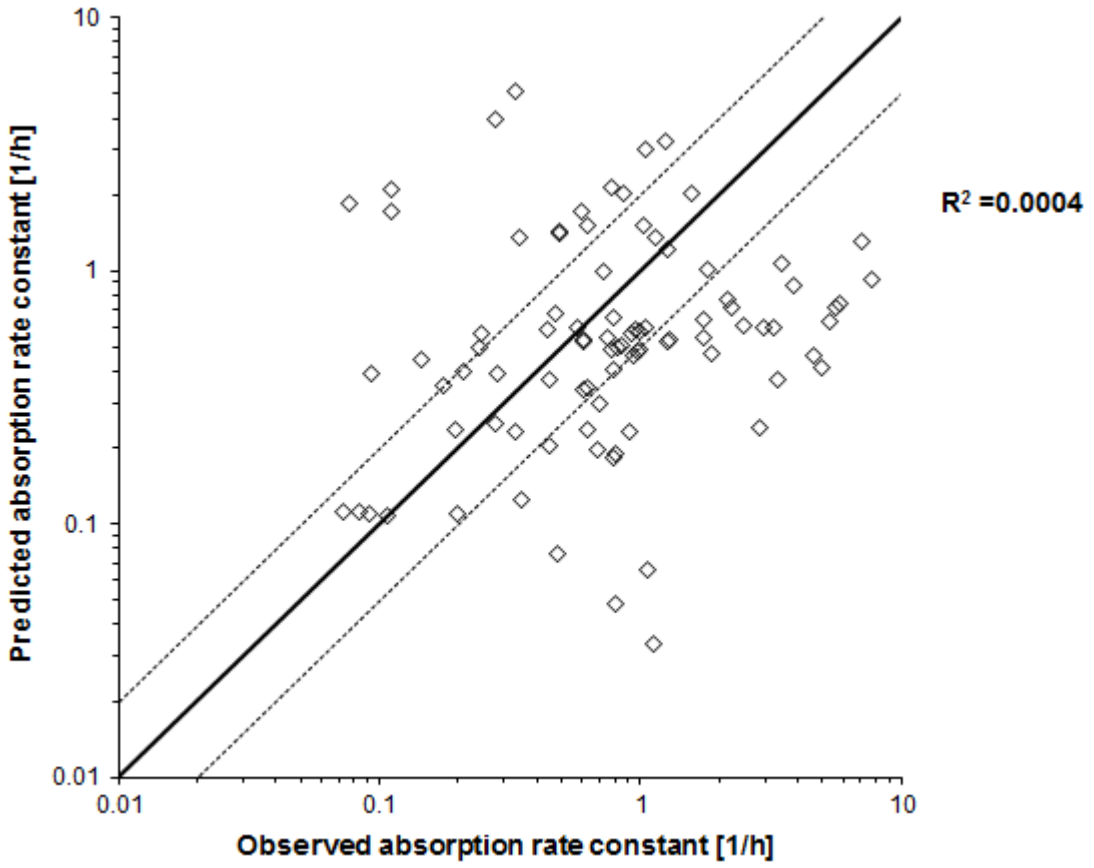

Fig. 3-14: Absorption rate constant derived from *in vivo* data (observed) versus absorption rate constant deriving from *in silico* simulations (predicted) using GastroPlus™ (data points comprise all compounds, species, formulations and doses) expressed as inverse time. Absorption rate constant (◊), line of unity (—), 2-fold error (- - -), n= 89. In addition the coefficient of determination (R^2) is shown.

In consideration of the underprediction of k_a (mpe= -0.52), further evaluations were performed to understand the reason for these findings. Therefore, the *in vivo* k_a was categorised for its respective time point of maximum concentration (T_{max}), in order to identify if the goodness of the prediction varies between rapidly and slowly absorbed compounds. Fig. 3-15 displays the residuals for the simulated absorption rate constants (the value for predicted k_a is subtracted from the actual *in vivo* k_a). The residuals are plotted in four categories: rapidly absorbed compounds with a T_{max} < 2 h, moderately and slowly absorbed compounds with a T_{max} of ≥ 2 - < 4 h and ≥ 4 - < 8 h, respectively. A fourth category was added due to the simulations for extended release formulations that exhibited a late time point of maximum plasma concentration (≥ 8 h). Residuals on the positive side of the y-axis imply a higher k_a for the predicted oral plasma profile compared to the k_a from the *in vivo* plasma concentration-time profile. The residuals on the negative side entail a lower predicted rate constant of absorption compared to that seen in the observed *in vivo* data.

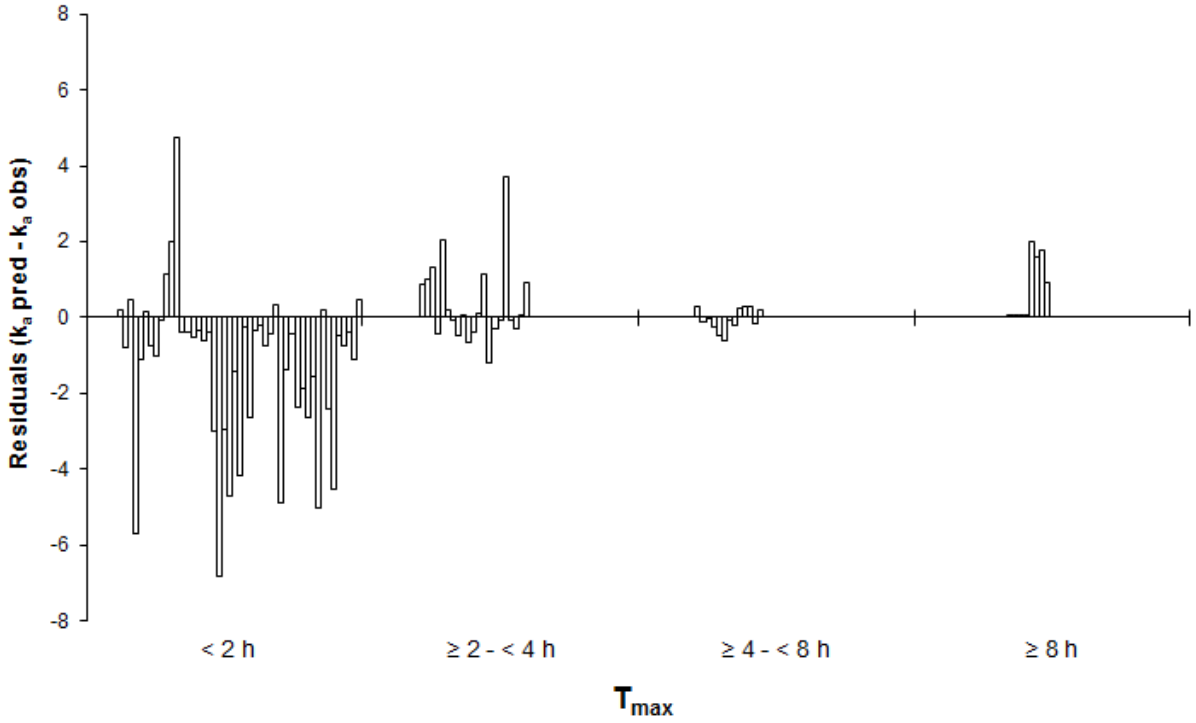

Fig. 3-15: Residuals of the absorption rate constant derived from *in silico* simulations ($(k_a)_{pred}$) using GastroPlus™ and absorption rate constant deriving from *in vivo* data ($(k_a)_{obs}$) categorised by the *in vivo* time point of maximum plasma concentration; n= 89.

The category for rapidly absorbed compounds (T_{max} < 2 h) contains simulations from all eight compounds including the species rat, dog, mouse, monkey and human. This category also includes predictions for several formulations namely solutions, micro-crystalline suspensions, immediate as well as modified release tablets (Appendix 7.2). In this category, k_a is underpredicted with a negative mean prediction error of -1.27, indicating that absorption occurs slower than predicted. In contrast, the categories T_{max} ≥ 2 - < 4 h (7 compounds), T_{max} ≥ 4 - < 8 h (5 compounds) and T_{max} ≥ 8 h (2 compounds) exhibit smaller deviations for the predicted k_a, with an mpe of 0.35, -0.05 and 0.80, respectively (Tab. 3-16).

Tab. 3-16: Residual values (resid) of the absorption rate constant derived from *in silico* simulations (pred) using GastroPlus™ and absorption rate constant deriving from *in vivo* data (obs) categorised by the *in vivo* time point of maximum plasma concentration, n= 89.

k_a at T_{max} <2 h			k_a at T_{max} ≥ 2-< 4 h			k_a at T_{max} ≥ 4-< 8 h			k_a at T_{max} ≥ 8 h		
obs	pred	resid	obs	pred	resid	obs	pre	resid	obs	pred	resid
1.14	1.36	0.22	0.62	1.50	0.88	0.72	0.99	0.27	0.08	0.11	0.03
1.81	1.02	-0.79	0.35	1.36	1.01	0.33	0.23	-0.10	0.07	0.11	0.04
1.57	2.02	0.45	0.78	2.12	1.34	0.28	0.25	-0.03	0.09	0.11	0.02
7.02	1.31	-5.71	0.48	0.08	-0.41	0.45	0.20	-0.24	0.11	0.11	0.00
1.13	0.03	-1.10	1.24	3.27	2.03	0.68	0.20	-0.48	0.11	2.11	1.99
0.44	0.59	0.15	0.21	0.40	0.19	0.81	0.19	-0.62	0.11	1.71	1.59
0.80	0.05	-0.75	0.45	0.37	-0.08	0.20	0.11	-0.09	0.08	1.86	1.79
1.07	0.07	-1.00	0.94	0.46	-0.48	0.35	0.13	-0.23	0.49	1.40	0.91
1.27	1.22	-0.05	0.20	0.24	0.04	0.24	0.50	0.26	-	-	-
0.87	2.02	1.15	0.90	0.23	-0.67	0.14	0.45	0.30	-	-	-
1.04	3.04	2.00	0.63	0.23	-0.39	0.09	0.39	0.30	-	-	-
0.33	5.08	4.75	0.28	0.39	0.11	0.79	0.65	-0.14	-	-	-
0.96	0.59	-0.37	0.59	1.72	1.13	0.17	0.35	0.18	-	-	-
0.79	0.41	-0.38	1.75	0.54	-1.20	-	-	-	-	-	-
1.00	0.49	-0.50	0.78	0.49	-0.29	-	-	-	-	-	-
0.82	0.49	-0.33	0.60	0.53	-0.08	-	-	-	-	-	-
0.78	0.18	-0.60	0.28	3.98	3.70	-	-	-	-	-	-
0.70	0.30	-0.40	0.61	0.54	-0.07	-	-	-	-	-	-
3.38	0.37	-3.01	0.63	0.35	-0.28	-	-	-	-	-	-
7.73	0.92	-6.81	0.58	0.60	0.02	-	-	-	-	-	-
3.85	0.88	-2.97	0.49	1.43	0.94	-	-	-	-	-	-
5.33	0.63	-4.70	-	-	-	-	-	-	-	-	-
1.87	0.47	-1.40	-	-	-	-	-	-	-	-	-
4.65	0.47	-4.18	-	-	-	-	-	-	-	-	-
0.60	0.34	-0.26	-	-	-	-	-	-	-	-	-
2.86	0.24	-2.62	-	-	-	-	-	-	-	-	-
0.85	0.51	-0.34	-	-	-	-	-	-	-	-	-
0.74	0.54	-0.20	-	-	-	-	-	-	-	-	-
1.28	0.53	-0.76	-	-	-	-	-	-	-	-	-
0.99	0.58	-0.42	-	-	-	-	-	-	-	-	-
0.24	0.57	0.32	-	-	-	-	-	-	-	-	-
5.60	0.72	-4.88	-	-	-	-	-	-	-	-	-
2.15	0.77	-1.39	-	-	-	-	-	-	-	-	-
1.04	0.60	-0.44	-	-	-	-	-	-	-	-	-
2.96	0.60	-2.37	-	-	-	-	-	-	-	-	-
2.48	0.60	-1.87	-	-	-	-	-	-	-	-	-
3.23	0.60	-2.63	-	-	-	-	-	-	-	-	-
2.25	0.71	-1.54	-	-	-	-	-	-	-	-	-
5.78	0.74	-5.04	-	-	-	-	-	-	-	-	-
0.48	0.68	0.20	-	-	-	-	-	-	-	-	-
3.49	1.06	-2.43	-	-	-	-	-	-	-	-	-
4.93	0.41	-4.52	-	-	-	-	-	-	-	-	-
0.98	0.48	-0.49	-	-	-	-	-	-	-	-	-
1.30	0.54	-0.76	-	-	-	-	-	-	-	-	-
0.93	0.56	-0.37	-	-	-	-	-	-	-	-	-
1.76	0.65	-1.11	-	-	-	-	-	-	-	-	-
1.04	1.51	0.47	-	-	-	-	-	-	-	-	-

T_{max} = time point of maximum plasma concentration

The goodness of prediction was also assessed by calculating the rmse (Tab. 3-17). The best agreement was observed for experiments with an *in vivo* T_{max} of ≥ 4 - < 8 h demonstrated by the lowest rmse of 0.29. Experiments with an *in vivo* T_{max} of < 2 h showed the highest rmse of 2.43 of the performed simulations, which indicates a less accurate prediction. Overall, only 39.3% of the simulations for the absorption rate constant were within the accepted 2-fold error (Tab. 3-17).

Tab. 3-17: Quality parameter for *in silico* prediction of *in vivo* absorption rate constant categorised by the *in vivo* time point of maximum plasma concentration.

T_{max} category	**rmse**	**% within 2-fold error**	**% within 2.5-fold error**	**% within 3-fold error**
T_{max} < 2 h (n= 47)	2.43	36.2	48.9	59.6
T_{max} ≥ 2 - < 4 h (n= 21)	1.12	42.9	52.4	81.0
T_{max} ≥ 4 - < 8 h (n= 13)	0.29	38.5	61.5	69.2
T_{max} ≥ 8 h (n= 8)	1.15	50.0	50.0	62.5
All compounds (n= 89)	1.88	39.3	51.7	66.3

rmse = route mean square error

T_{max} = time point of maximum plasma concentration

Regarding predictability of k_a in different species, the quality parameter for the *in silico* predictions showed that the highest accuracy was observed for the species dog (rmse= 0.90 for n= 10) and the lowest accuracy for the species mouse, with a route mean square error of 4.31 (0 % of the simulation results were within 2-fold error; n=4) (Tab. 3-18). Interestingly, the species human showed the second best accuracy of k_a prediction with an rmse of 1.26 for a markedly higher number of simulations (n=50).

Tab. 3-18: Quality parameter for *in silico* prediction of *in vivo* absorption rate constant categorised by species.

Species Category	**rmse**	**% within 2-fold error**	**% within 2.5-fold error**	**% within 3-fold error**
k_a in rat (n=12)	3.08	33.3	41.6	41.6
k_a in dog (n=10)	0.90	40.0	60.0	80.0
k_a in human (n=50)	1.26	48.0	64.0	70.0
k_a in monkey (n=8)	1.30	12.5	12.5	50.0
k_a in mouse (n=4)	4.31	0.00	0.00	25.0
k_a in rabbit (n=5)	2.30	40.0	40.0	40.0
All compounds (n=89)	1.88	39.3	51.7	66.3

rmse = root mean square error

4 Discussion

4.1 Permeability investigations using the Ussing chamber

Within the setting of early drug development, the vertical Ussing chamber system using rat jejunum tissue was successfully established in this thesis, in order to assess the intestinal permeability of drug development compounds. The system was validated using the five reference compounds mannitol, terbutaline, propranolol, verapamil and fexofenadine which are well described in the literature and cover all routes of absorption (passive paracellular, active and passive transcellular) (Tab. 2-5). For each reference compound, bidirectional permeability studies were performed using the stripped and full-thickness tissue preparation technique. The results of the permeability investigations are discussed within this chapter.

4.1.1 Experimental set-up: influential factors

The endeavour to simplify complex physiological processes using an *in vitro* method naturally contains disadvantages. When searching the literature for rat jejunal apparent permeability using the Ussing chamber, it strikes that for certain compounds (e.g. verapamil, terbutaline) results are highly variable when different sources are consulted (Tab. 4-1). Investigating and understanding those deviations is key to use the Ussing chamber as a powerful *in vitro* method to determine intestinal absorption.

Tab. 4-1: Rat jejunal experimental apparent permeability from several literature sources for the compounds terbutaline and verapamil.

Literature source	**Rat jejunal P_{app} [cm/s] mucosal to serosal direction**	
	Terbutaline	Verapamil
Ungell 1998 [68]	3.40E-06	-
Lennernas 1997 [128]	7.00E-06	-
Watanabe 2004 [65]	11.8E-06	-
Gotoh 2005 [64]	3.80E-06	16.0E-06
Annaert 2000 [63]	-	7.40E-06

One possible reason for variability is non-specific binding (NSB). As with most *in vitro* methods, the Ussing chamber has challenges with possible non-specific binding to the material of the experimental equipment, if very lipophilic compounds are to be tested. It is therefore advisable to conduct some unspecific binding studies prior to the actual experiments or use solutions containing 1 % bovine serum albumin (BSA) to reduce non-specific binding of compound to the plastic surface of the Ussing chamber [135]. As

presented in Fig. 3-3 the subject of non-specific binding can be crucial. For the highly lipophilic compound verapamil (log $P_{o/w}$ value 4.7), the NSB amounted to over 70 % within the first 5 minutes of the experiment (Fig. 3-1). This leads to a bias of the actual apparent permeability, by a factor of 6 for the stripped tissue preparation technique group (Tab. 3-8). To guarantee uniform treatment of permeability data for all compounds, the amount of substance reaching the receiver side was corrected for non-specific binding, even if binding was low or not detectable. Correcting for unspecific binding on the donor side was neglected, as bound compound is not available anymore for transport over the membrane and the actual concentration on the donor side by the end of the experiment was used to calculate the apparent permeability. The drawback of non-specific binding can therefore be overcome to a certain degree. Nevertheless, it should be kept in mind that especially with high NSB compounds; variability in the experiments is higher and may therefore bias the data (e.g. verapamil).

The Ussing chamber is a method that uses the excised tissue technique. Besides the obvious challenges of working with living tissue that naturally contains variability and when excised undergoes degradation processes, it can also be treated differently before mounting onto the chambers. One strategy is to leave the isolated intestinal fragment intact with all its stratums from the luminal mucosa to the outer serous membrane. This approach adds artificial layers to the absorption pathway, as the absorbed compound has to not only cross the mucosa but also the underlying submucosa, the circular and longitudinal muscle layer and subsequently the serosa. Consequently, the term full-thickness tissue is used. The other strategy is to remove additional layers unnecessary for the process of absorption. This procedure is called stripping. Two stripping approaches are known and practiced. Either the mucosa is stripped off from all underlying layers [67] [136] or only the serous membrane is removed, leaving the muscularis externa intact [60] [68]. In this thesis, the second technique was used when stripping was performed. The idea of removing layers not involved in intestinal absorption when using the Ussing chambers seems like the clear way forward, but every further manipulation of excised living tissue exposes the organic material to additional stress which reduces its viability. Eventually, this can lead to an increase of variability when considering permeability. Hence, it is important to evaluate the assets and drawbacks of using stripped or full-thickness tissue. Chapter 3.2.2 discussed the apparent permeability for verapamil, propranolol, fexofenadine, terbutaline and mannitol comparing the fluxes for stripped and full-thickness tissue either for the mucosal to serosal direction (Fig. 3-6) or the serosal to mucosal direction (Fig. 3-7). The additional layer of the serosa not involved in the *in vivo* absorption process (compound that exits the enterocytes on the basolateral immediately enters the blood vessels) seemed to have no influence on the transepithelial permeability for mannitol, terbutaline, fexofenadine and verapamil when considering the

mucosal to serosal fluxes. The P_{app} for the only passively transcellular diffusing propranolol was slightly higher when the excised tissue was stripped. The main purpose of the serosa is to secret fluids via transudation to reduce friction caused by muscle movement and to isolate the organ in the abdominal cavity [6]. The anatomy of the serosa is very different from the mucosa and not designed for absorptive processes. Therefore, the permeability of a compound undergoing only passive diffusion through the intestinal mucosa tissue can be reduced when encountering a less permeable tissue layer like the serosa. When comparing stripped and full-thickness tissue for the serosal to mucosal permeability experiments, the serosa had a marked influence on the apparent permeability for propranolol, as well as for verapamil. Verapamil seemed to enter the intestinal cells from the serosal side with difficulty when the serosa was present (Fig. 3-7). When the tissue was stripped, lipophilic compounds like propranolol and verapamil passed the remaining stratums of the jejunum effortlessly and exhibited a higher P_{app} compared to the full-thickness experiments (Fig. 3-7). When considering the mucosal to serosal flux, the same was true for the compound propranolol, where the stripped tissue experiments showed a higher permeability compared to the full-thickness experiments (Fig. 3-6). Surprisingly, these findings have not been seen in the mucosal to serosal verapamil experiments. Here, the P_{app} for stripped and full-thickness tissue was about equal for the stripped tissue experiments. A possible difference between the stripped and full-thickness study groups could be disguised by the high variability with a coefficient of variation of 37 % and 42 %, respectively (Tab. 3-7). For the hydrophilic and paracellular diffusing compounds terbutaline and mannitol, the presence of the serosa had no proven significant influence on the permeability. This might be due to their absorption mechanism. Small, hydrophilic compounds can permeate the intestinal barrier by bypassing the enterocytes as they are absorbed through the extracellular tight junctions present in epithelial cells in vertebrates [41]. Tight junctions laterally connect single cells of the epithelium and form a “tight” cell junction which is impermeable for most substances. Only water and small hydrophilic substances can use this pathway to cross the membrane. Tight junctions are present in all epithelial tissues which include the simple columnar epithelium of the gastrointestinal tract as well as the simple squamous epithelium found in the serosa. Therefore, it is highly likely that compounds that pass the intestinal mucosa by paracellular diffusion are also able to pass the serosal tissue layer in the same manner. All in all, the preparation technique of the intestinal tissue and the presence of the serous membrane can vary the permeability results for compounds that cross the intestinal epithelium via the transcellular pathway. In order to ensure equal experimental conditions and comparable permeability data for all kinds of compounds with different physicochemical and transepithelial transport properties, stripping of the epithelial tissue should be considered when performing Ussing chamber absorption studies.

To assess the quality of the Ussing chamber experiments and the validity of the ascertained data it is important to determine the experimental variability within the same compound. A simple but convincing way is to perform a mass balance evaluation. This approach was used for all compounds and the amount of radiolabeled compound on the donor and receiver side was determined as well as the amount of compound found in the tissue. Subsequently, the amount of substance non-specifically bound to the Ussing chamber equipment determined in the NSB studies was added. A good total recovery (> 84 %) for all compounds was observed with low variability within the compound, with a coefficient of variation ranging from 0.1 to 7.9 % for the mucosal to serosal study groups (Tab. 3-9). The low variability indicates that the Ussing chamber experiments were consistent within each investigated compound.
In consideration of varying results from Ussing chamber absorption studies for rat jejunum reported in literature, it would be desirable to have additional information to judge the validity of this data. First of all, potential non-specific binding should be evaluated and if applicable results should be corrected for it. Secondly, the tissue preparation technique should be mentioned to give an insight if permeability data from compounds with different physicochemical properties can be assessed in the same way. In addition to these two approaches, calculated total recovery and the determined experimental variability within each compound can give further information to assess the reliability of the permeability data ascertained with the Ussing chamber technique.

4.1.2 Permeability studies

To establish and validate the Ussing chamber as a model to predict intestinal absorption in the laboratory, bidirectional permeability studies for a variety of reference compounds were carried out using stripped rat jejunum. For the majority of compounds (propranolol, fexofenadine and mannitol; stripped) the m-s flux was slightly higher than the s-m flux (Fig. 3-4). The surface structure (villi, microvilli) on the apical side of the intestine offers a larger absorptive surface area compared to the basolateral side and could contribute to a higher m-s flux. For terbutaline, the P_{app} was slightly lower in the m-s direction but could not be proven statistically significant. For verapamil the lower m-s flux compared to the s-m flux was also not statistically significant but is consistent with the fact that the compound verapamil is substrate to the intestinal P-glycoprotein (Pgp) efflux transporter [137]. Drug compound that was diffusing through the enterocytes to the receiver side is actively transported back to the donor side by the Pgp transporter when entering the intestinal cells. While the gross-flux (compound entering the enterocytes) might still be higher compared to the s-m studies, the efflux reduces the net-flux (compound appearing on the receiver side). The same

phenomenon would be expected for the compound fexofenadine, as it is also substrate to the Pgp transporter. But in addition to the active efflux, this compound is also substrate to the active OATP influx transporter (Tab. 2-5), which is located on the apical side of the intestinal cells and also present in rat intestine [73]. Depending on the gene expression levels and possible saturation processes the active influx could potentially cancel out the effect of the Pgp efflux transporter and would result in a higher net-flux from the mucosal to the serosal side. One way of exploring the influence of these transporters would be to individually inhibit the active transporter of interest via known inhibitor compounds.

4.1.3 Absorption mechanisms

Predicting the extent of intestinal absorption is one aspect of using an absorption model. Another aspect is to learn and understand what the underlying mechanism of absorption for a compound is. As described in Chapter 1.3.3, three main mechanisms of absorption exist. In order to see if the known mechanism for the reference compounds could be confirmed, the extracellular and intracellular concentration of compound was calculated. The concentration of compound in the enterocytes was determined by weighing, measuring and subsequently calculating the concentration in the excised tissue. The calculated concentration was then compared to the concentration on the donor side by the end of the experiment. The ratio of the intra- and extracellular concentration gives information if the compound is transported transcellularly or paracellularly. Studying this ratio for m-s and s-m studies can also give information if the compound is actively transported into the cells. As the substance mannitol was used as an extracellular marker, ratios are only displayed for terbutaline, fexofenadine, verapamil and propranolol (Fig. 3-8 and Fig. 3-9). As expected, more terbutaline was found extracellularly than intracellularly, as it is a paracellularly transported drug. This was the case for stripped as well as for full-thickness tissue. Propranolol and verapamil were found predominantly in the enterocytes in correspondence to their known transcellular absorption mechanism. For both compounds the ratio was higher for the m-s fluxes compared to the s-m fluxes. This indicates that less compound entered the enterocytes when the serosal side was the donor side which could be explained by the contribution of the previously mentioned smaller absorptive surface area. For the actively transcellular transported fexofenadine, the mechanism of absorption could be clearly shown, as the m-s ratio indicated more compound in the enterocytes than located extracellularly. To the contrary, a higher concentration of drug was found extracellularly, when considering the s-m direction. This clearly shows that an active influx transporter is involved in the absorption, that is only located on the apical side of the membrane which enables fexofenadine to enter the enterocytes. Again, this result was

found for stripped as well as for full-thickness tissue. The OATP transporter involved in the active transcellular uptake of fexofenadine can be inhibited by esterone-3-sulfate and the Pgp transporter by its well-known inhibitor ketoconazole [62]. This would allow studying the individual influence of the active transporters on the overall permeability. As an alternative, experiments with tissue from knock-out animals could be performed in order to assess the involvement of specific transporters to the overall permeability [138].

Based on the findings described above, the Ussing chamber can be a valuable method to elucidate the actual mechanism of absorption.

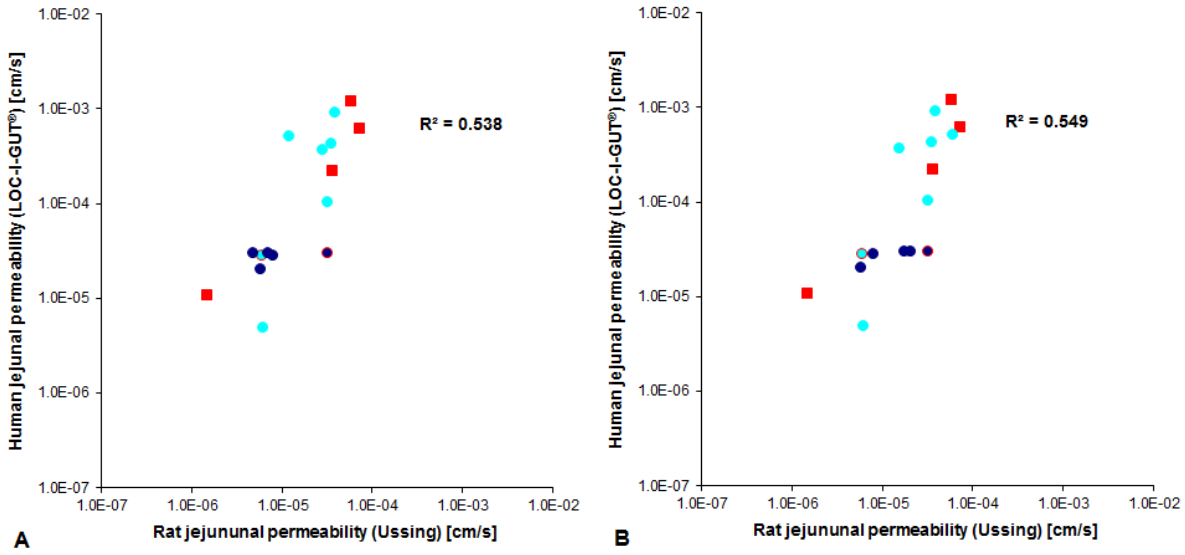

Fig. 4-1: Correlation of human jejunal permeability determined using the Loc-I-Gut® technique and rat jejunal permeability from Ussing chamber experiments expressed in centimetre per second for 16 compounds (for data see Tab. 7-1). **A:** displays data solely from literature, whereas **B:** shows literature data and integrated data of the five compounds from own Ussing experiments (Tab. 3-7). In addition the coefficient of determination (R^2) is shown for both data sets. Data itemize by their corresponding absorption mechanism: passive transcellular (●), active (■), passive paracellular through tight junctions (●), other data points combine routes of transport according to colour, whereas the outline symbolizes the less dominant pathway.

In order to assess if this *in vitro* method has been successfully established and can be used to predict human intestinal absorption; a correlation of rat jejunum P_{app} values from Ussing chamber experiments to human permeability data determined by the Loc-I-Gut® perfusion technique (Chapter 3.1.3.2) was performed to validate the system. Fig. 4-1 A shows the correlation of human and rat permeability for 16 compounds with different physiochemical properties and absorption mechanisms found in literature (Tab. 7-1). When more than one source of literature was found, the mean permeability was calculated. Fig. 4-1 B shows the

integrated data from the permeability experiments conducted within this thesis (Tab. 7-1 and Tab. 3-7). Rat Ussing chamber P_{app} values from literature were replaced by own data for mannitol, terbutaline, propranolol, verapamil and fexofenadine for stripped tissue from m-s direction. The coefficient of determination (R^2) for solely literature data and for the correlation with integrated own data was 0.538 and 0.549, respectively. This finding suggests that the ascertained rat jejunal permeability data within this thesis is comparable to that previously determined, in various literature sources. This finding indicates a successful establishment and validation of the Ussing chamber absorption model. It can therefore be used in the pharmaceutical development process to assess the permeability of new compounds with unknown permeability properties.

4.2 Simulation of intestinal absorption using GastroPlus™

Physiologically based *in silico* absorption models can be used as a tool to predict the rate and extent of absorption for orally administered drugs. The objective of this study was to perform a retrospective data evaluation to assess the ability of GastroPlus™ to predict fraction absorbed and the absorption rate constant for eight selected compounds (Tab. 2-10). Simulation results from the *in silico* predictions were compared to the respective *in vivo* PK-parameters characterising intestinal absorption (i.e. f_a and k_a). The aim was to investigate the basic predictability of the software tool, therefore only the default settings were used for all simulations. The option to optimise input parameter, species physiology or validating the system with data from animal studies in order to improve the prediction of human absorption, was omitted.

4.2.1 Fraction absorbed

Performed simulaitons included compounds with low, moderated and high *in vivo* fraction absorbed (range: 20.8 % to complete absorption) (Tab. 7-16 to Tab. 7-23). The accuracy of predicting f_a was generally successful (77.1 % within a 2-fold error), although for simulations with low *in vivo* absorption, prediction were not within a 3-fold error (Tab. 3-11). Nevertheless, only 6 % of all simulations classed among the low absorption group. Surprisingly, one compound in this class exhibited good *in vitro* permeability values and acceptable solubility (Fig. 3-12). Oral administration for this compound was performed in the species dog for two doses. It is well known that *in vivo*, dogs show a highly variable stomach pH when fasted, ranging from pH 3 to pH 5 [139]. GastroPlus™ offers the feature of a parameter sensitivity analysis (PSA) as described in Chapter 2.3.5.3. The performed PSA for the property stomach pH in the dog revealed that a slight change of pH from the default value (3.0) into a more basic pH (4.3) would decrease local solubility and therefore markedly the fraction absorbed by 64 %. Performing this parameter sensitivity analysis prior to the *in vivo* experiments purely from *in vitro* data could have raised awareness of encountering this problem. A possible solutions to avoid this effect would be to adjust the stomach pH of the dog by orally administering 0.1 mol/L HCl-KCl buffer in combination with an intravenous dose of omeprazole or pretreatment of the dogs with pentagastrin [140] [139]. Also classical conditioning of the dogs according to Pavlov, on the expectance of food and therefore secretion of gastrin, could be considered in order to lower the pH of the stomach before the start of the *in vivo* experiment. Simulation of the fraction absorbed also revealed species dependent differences in the accuracy of the *in silico* simulations. Whereas f_a for the species rat was by trend underpredicted, the species dog was generally overpredicted. The reason

for this finding could be related to the input parameter of effective permeability (P_{eff}). GastroPlus™ requires this permeability value as input in order to perform a simulation. As described before, this parameter is the *in vivo* derived human jejunal permeability coefficient. As this data is usually not available for compounds in the development process, the software offers a converter tool for different sources of permeability data. Data sets from in-house *in vitro* permeability tests (in this case Caco-2 cell assay) were entered for a given selection of compounds and GastroPlus™ calculated a regression function from implemented measured human P_{eff} values from literature. The best fitting calculated regression (linear, non-linear or power equations) were then used to convert the measured *in vitro* P_{app} into an estimated human P_{eff}. This value was entered into the input tab. As a next step, the human P_{eff} has to be converted to a rat P_{eff} by a second inbuilt converter where a converting factor is applied. For the species rat, the converting factor is taken from a publication by Kim et. al and is derived from rat single-pass perfusion experiments. The factor is described with 0.25 x human P_{eff} [49]. Consequently, the permeability in the species rat is rated to be four times lower than in human. For the species dog on the other hand, a higher permeability compared to man is assumed. The converting factor in GastroPlus™ was deduced from unpublished data that Gordon L. Amidon provided to Simulations Plus, Inc. (Tab. 4-2) [141]. Intestinal permeability for four compounds was measured using the Loc-I-Gut® technique in the dog and compared to human permeability measured with the same method. From that data, a converting factor of 3.3 was formed for dog intestinal permeability and implemented into the software.

Tab. 4-2: Effective intestinal permeability in human and dog determined by the Loc-I-Gut® technique for four compounds, expressed in centimetre per second used to establish the permeability conversion factor for the species dog used in GastroPlus™.

Compound	Human P_{eff} [cm/s]	Dog P_{eff} [cm/s]
Propranolol	2.7E-04	6.7E-04
Atenolol	0.2E-04	0.8E-04
Ranitidine	0.4E-04	2.0E-04
L-Phenylalanine	5.1E-04	18.5E-04

For some compounds, better absorption in dogs compared to man has previously been reported by Chiou et. al in a study comparing fraction of oral dose absorbed in dog and humans [142]. In 44 % of the 43 drugs evaluated, dog exhibited a higher fraction absorbed compared to man. In the remaining 56 %, f_a was the same in both species (19 %), or lower in dog (37 %). As a possible explanation for a higher f_a, a reported longer villi length in the small intestine was mentioned; this may result in a greater absorptive surface area. In addition, the

same source reported higher bile salt concentrations in dog than in human, which could potentially modify the intestinal membrane structure and make it more permeable for drug transport [23, 142]. Also, a study examining possible species differences in paracellular absorption came to the conclusion that dogs might possess a higher number, and overall, larger tight junctions and the intestine would therefore be more leaky [44]. In contrast to that, intestinal villi lengths of 645-971 µm [16, 143] for dogs, opposed to 500-800 µm in man [45], are reported. It seems difficult to believe that marginally longer villi can outweigh a significantly shorter small intestinal transit time and therefore a shorter absorption window in the species dog [144]. Another argument against better absorption in dogs would be the absence of circular folds in the small intestine of the dog, which is again decreasing the absorptive surface area compared to that in man. While the higher absorption for paracellularly absorbed compounds like atenolol [145] and ranitidine [146] might be true, caution should be applied translating that effect to compounds with other transport mechanisms as the factor of surface area or expression levels of intestinal transporters also play a crucial role in the absorption process. Based on the results from the fraction absorbed prediction performed within this thesis, an adjustment of the converting factor for the species dog to about 2 might improve the predicted f_a. For other species like monkey, mouse, rabbit etc. no converting factor is stored in GastroPlus™ mainly due to the lack of available and reliable data.

To sum up, it should be kept in mind that several converting steps can introduce uncertainties in the input parameter required for simulations, as the obtained results are highly dependent on the quality of the input parameters. As the P_{eff} value comprises all mechanisms of absorption including paracellular, transcellular and active influx and efflux transport, this input parameter could be optimised by using the Ussing chamber technique to determine the permeability of new compounds. In contrast to the Caco-2 cell model (Chapter 3.1.1.2.2.) in which permeability of paracellularly and actively transported substances can be distorted due to the origin of the cell line (i.e. colon carcinoma), the Ussing chamber using rat jejunum shows a better correlation of *in vitro* P_{app} and human P_{eff} for all intestinal absorption mechanisms (Fig. 4-2).

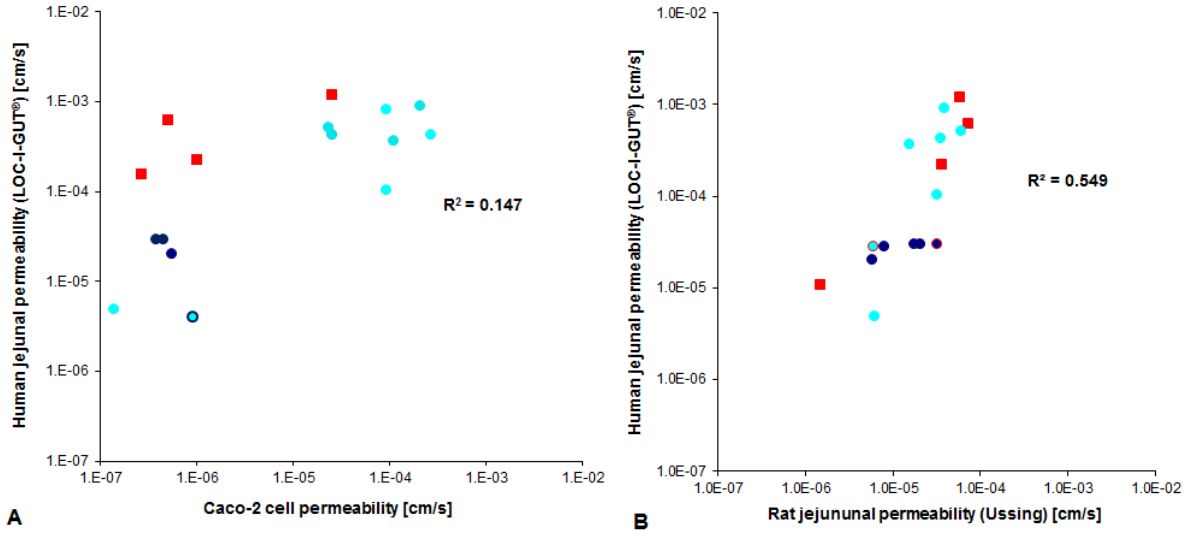

Fig. 4-2: Correlation of human jejunal permeability determined using the Loc-I-Gut® technique with permeability data from Caco-2 cells (**A**) or Ussing chamber experiments using rat jejunal tissue (**B**) expressed in centimetre per second (data: Tab. 7-1 and Tab. 3-7). Data itemize by their corresponding absorption mechanism: passive transcellular (●), active (■), passive paracellular through tight junctions (●), other data points combine routes of transport according to colour, whereas the outline symbolizes the less dominant pathway. In addition the coefficient of determination (R^2) is shown for both data sets.

4.2.2 Absorption rate constant

Equally as important as the extent, is the rate of absorption. The PK parameter k_a gives information on how fast an orally administered compound can reach the systemic circulation. Therefore, the predictability of k_a with GastroPlus™ was assessed in 105 cases. In a first evaluation, the predicted and observed absorption rate constant was compared resulting in a poor predictability with only 39 % within a 2-fold error (Fig. 3-14 and Tab. 3-18). When visually evaluating the plot, a general underprediction of k_a for the majority of simulations could be detected, meaning that the prediction suggest slower absorption than observed in the *in vivo* studies. After consulting all available information for the simulations, these findings could not be traced back to a specific compound, species or dosage form. As k_a is directly influencing the time point for the compound to reach maximum concentration (T_{max}) in the systemic circulation, k_a was categorised by T_{max} in order to further evaluate the predictability of the absorption rate constant. Four categories were formed, from fast absorbed cases (T_{max} < 2h) to very slowly absorbed cases (T_{max} ≥ 8h). Fig. 3-15 and Tab. 3-16 display the outcome of this categorisation. It could be concluded that the prediction of k_a was very poor for cases were the compound was rapidly absorbed, with a T_{max} shorter than 2 hours,

resulting in a major underprediction. Only 36 % of the predictions were within a 2-fold error. The best predictions were found for cases with slow absorption with a time point of maximum concentration between 4 and 8 hours. (Tab. 3-17).

A possible explanation for the poor fit of k_a for rapidly absorbed compounds could be the rate limiting step of solubility of the compound. Only solubilized drug can enter the enterocytes and eventually the systemic circulation of the body. Apart from one compound, the other compounds used for the simulations exhibited low solubility. In terms of biopharmaceutical classification, seven of eight compounds were BCS class II, while only one compound was BCS class I. BCS class II compounds are characterised by good permeability but poor solubility. The input parameter of solubility for GastroPlus™ was derived from *in vitro* pH depending buffer solubility experiments. *In vivo*, the solubility of a compound is supported by other factors aiding the solubilisation that are not present *in vitro*. In order to improve the predictability of k_a, the input parameter solubility should be optimised. One way could be to determine the solubility of a drug in a different buffer system closer mimicking the situation *in vivo* using biorelevant media. Input parameters concluded from solubility experiments using FaSSIF (fasted state simulated small intestinal fluid) or FeSSIF (fed state simulated small intestinal fluid) could improve predictability of the absorption rate constant for rapidly absorbed compounds [147].

4.3 Perspective

The need to gain better understanding of the processes involved in the rate and extent of absorption of orally administered drugs is omnipresent. One clear indication is that the Innovative Medicines Initiative (IMI) as Europe's largest public-private initiative in the life science sector is governing a key initiative named OrBiTo (Oral Biopharmaceutics Tools) [148, 149]. This project will address crucial gaps in the knowledge of the gastrointestinal drug absorption and aims to deliver predictive biopharmaceutics tools for oral drug delivery. Four work packages (WP) investigating physicochemical (WP1), *in vitro* (WP2), *in vivo* (WP3) and *in silico* tools (WP4) will be applied to streamline and optimise the development of orally administered drug products. The goal is to transform the ability to predict the *in vivo* performance of oral drug products from a mostly empirical to a rational, model based approach using novel and validated *in vitro*, *in silico* and *in vivo* tools. This tellingly shows the complexity and the importance of investigating suitable models to predict intestinal absorption throughout the pharmaceutical drug development process.

5 Summary

5.1 Abstract

As oral administration of pharmaceutical drugs in patients is the preferred route, special interest is given to predict the ability of a new compound to be absorbed in man. During the last 60 years, a vast number of *in vitro*, *in vivo* and *in silico* absorption models have been developed in order to estimate human intestinal permeability and eventually the fraction of dose absorbed of a compound administered. These were comprehensively characterised and discussed with regards to their strengths and limitations in this thesis. Depending on the stage of the pharmaceutical development process different models can be suitable. Furthermore, two common absorption models were challenged on their ability to investigate the extent of drug absorption.

Firstly, the *in vitro* Ussing chamber technique using rat jejunal tissue was experimentally established and successfully validated using the reference compounds ^{14}C-mannitol, ^{3}H-terbutaline, ^{3}H-propranolol, ^{3}H-verapamil and ^{14}C-fexofenadine. Bidirectional permeability studies were conducted, determining the apparent permeability (P_{app}) of the compounds and the ability to display absorption mechanisms was investigated. Furthermore, reasons for variability found when comparing several reported permeability values in literature was examined, focusing on studying non-specific binding (NSB) of the compound to the experimental equipment. Also, the influence of two tissue preparation techniques (“stripped” or full-thickness tissue) was investigated.
Results from the Ussing chamber experiments revealed that NSB can have a crucial influence on the P_{app} especially for lipophilic compounds. The tissue preparation technique showed a greater influence on the transcellularly absorbed compounds rather than the paracelullarly permeating ones. The route of absorption for each compound could be identified, showing paracellular absorption for mannitol and terbutaline, transcellular absorption for propranolol and verapamil and active uptake of fexofenadine. To ensure comparable results for all compounds, determination of NSB prior to permeability experiments should be mandatory and “stripping” of the rat jejunum is recommended.

Secondly, the *in silico* physiologically based absorption software GastroPlus™ was challenged, on the ability to predict fraction absorbed (f_a) and the absorption rate constant (k_a) for eight compounds under development at Bayer Pharma AG, in a retrospective analysis with preclinical and clinical data, using the basic default settings of the software. The influence of the input parameters (physicochemical, physiological and formulation properties)

were investigated via parameter sensitivity analysis and predictability for different species was compared.

Results from GastroPlus™ simulations showed good predictability of f_a with 77 % within a 2-fold error. The tendential overprediction of f_a for the species dog, suggested lowering the species-specific P_{eff} converting factor from 3.3 to about 2. The parameter sensitivity analysis for one compound (C_5) suggested that an increase of stomach pH in the dog from 3.0 to 4.3 could lead to a distinct decrease (by 64 %) in fraction absorbed. Adjusting the stomach pH prior to *in vivo* pharmacokinetic studies in the dogs should be considered for compounds with pH-dependent solubility to reduce variability.

The general underprediction of k_a for simulations with a fast absorption phase *in vivo*, recommends improvement of the solubility input data. The parameters permeability and solubility were identified as critical input properties. It was suggested, to use the Ussing chamber absorption model to generate a reliable permeability input parameter (P_{eff}). Furthermore, the use of biorelevant buffer systems that mimic the *in vivo* situation should be used for solubility tests to improve predictability of the *in silico* tool.

5.2 Zusammenfassung

Die orale Administration ist die präferierte Applikationsroute für die Versorgung von Patienten mit pharmazeutischen Arzneimitteln. In der Arzneimittelentwicklung ist es von großem Interesse die intestinale Absorption von neuen Entwicklungssubstanzen im Menschen vorherzusagen. Während der vergangenen 60 Jahre wurden zahlreiche *in vitro*, *in vivo* und *in silico* Absorptionsmodelle entwickelt um die intestinal Absorption im Menschen abzuschätzen und die absorbierte Fraktion der Dosis im Menschen vorherzusagen. Die wichtigsten Absorptionsmodelle wurden ausführlich in dieser Dissertation charakterisiert und evaluiert und ihre Stärken und Limitationen diskutiert. Die Eignung der einzelnen Absorptionsmodelle ist stark abhängig von der Fragestellung und dem Zeitpunkt der Untersuchungen in der Arzneimittelentwicklung. Desweitern wurden zwei Absorptionsmodelle genauer untersucht um ihre Vorhersagbarkeit der intestinalen Absorption zu bewerten.

Zunächst wurde die Ussingkammer Methode unter Einsatz von Rattenjejunum experimentell etabliert und unter Verwendung von bekannten Referenzsubstanzen für die Bestimmung der apparenten Permeabilität (P_{app}) in bidirektionalen Permeabilitätsexperimenten erfolgreich validiert. Die unterschiedlichen Absorptionsmechanismen der Referenzsubstanzen konnten klar dargestellt werden.

Zwei wichtige Einflüsse auf die Permeabilitätsexperimente wurden identifiziert: Zum einen die unspezifische Bindung an das Ussigkammer Material und die Präparationstechnik des Darmgewebes. Die unspezifische Bindung (NSB) kann im Falle von lipophilen Substanzen erheblich sein und sollte vor dem Durchführen von Permeabilitätsexperimenten für jede Substanz bestimmt werden. Dieser Wert kann dann als Korrekturfaktor für die Berechnung er Permeabilität mit einfließen. Desweitern ist es speziell für transzellulär absorbierte Substanzen empfehlenswert das Jejunum zu „strippen“ d.h. von zusätzliche Gewebeschichten wie der *Tunica serosa* zu befreien.

Als zweites Absorptionsmodell wurde das Physiologie-basierte *in silico* Absorptionsmodel GastroPlus™ in einer retrospektiven Analyse eingesetzt, um die intestinale Absorption für acht Entwicklungssubstanzen der Bayer Pharma AG vorherzusagen. Die Parameter, absorbierte Fraktion der Dosis (f_a) und Resorptionsgeschwindigkeitskonstante (k_a), wurden zur Beurteilung der Vorhersagbarkeit genutzt. Die mit den Standardeinstellungen vorhergesagten Parameter wurden anschließend mit den *in vivo* Parametern aus den präklinischen und klinischen Studien verglichen. Wichtige Faktoren die f_a und k_a beeinflussen, wurden mittels Parametersensitivitätsanalyse untersucht.

Die Vorhersagbarkeit für f_a war gut mit 77 % innerhalb der vorgegebenen Akzeptanzkriterien (d.h. zweifache Abweichung vom *in vivo* Wert). Es gab eine tendenzielle Überschätzung für die Spezies Hund, die suggeriert, dass der Spezieskonvertierungsfaktor abgepasst werden sollte. Die Parametersensitivitätsanalyse für Substanz C_5 zeigte eine starke Abnahme der absorbierte Fraktion um 64 %, wenn der Magen pH von 3.0 auf 4.3 steigt. Eine einfache Methode um solche Einflussgrößen zu reduzieren ist z.B. die Vorbehandlung der Hunde vor der Administration der oralen Formulierung in PK Studien um den Magen pH zu stabilisieren.
Der Parameter k_a wurde für Substanzen mit einer niedrigen *in vivo* Absorptionsrate vornehmlich unterschätzt. Die Einflussgrößen Permeabilität und Löslichkeit wurden als sensitive Parameter identifiziert. Die Nutzung von biorelevante Medien zur Bestimmung der Löslichkeit, und mit der Ussingkammer Methode generierten Permeabilitätswerte, könnten besseres Inputparametern bieten, die die Vorhersagbarkeit der *in silico* Methode verbessern könnte.

6 Bibliography

[1] Silva, C.O., B. Sarmento, and C.P. Reis, *Oral delivery of biopharmaceuticals*, in *Mucosal Delivery of Biopharmaceuticals: Biology, Challenges and Strategies*. 2014. p. 125-147.

[2] Fasano, A., *Novel approaches for oral delivery of macromolecules.* J Pharm Sci, 87(11): p. 1351-6 (1998).

[3] Tyle, P., *Controlled drug delivery: Fundamentals and applications.* J Pharma Sci, 77(1): p. 94-94 (1988).

[4] Magee, D.F. and A.F. Dalley, *Digestion and the structure and function of the gut*. 1986, Basel, Switzerland: Karger.

[5] Lippert, H., *Lehrbuch Anatomie.* (2012).

[6] Huch, R., G. Raichle, and M. Augustin, *Mensch, Körper, Krankheit* 2003, München; Jena: Urban und Fischer.

[7] Kirsten, R., et al., *Clinical pharmacokinetics of vasodilators. Part II.* Clin Pharmacokinet, 35(1): p. 9-36 (1998).

[8] Chen, L.L., D.J. Chetty, and Y.W. Chien, *A mechanistic analysis to characterize oramucosal permeation properties.* Int J Pharm, 184(1): p. 63-72 (1999).

[9] Singh, S.G., et al., *Buccal mucosa as a route for drug delivery: Mechanism, design and evaluation.* Research Journal of Pharmaceutical, Biological and Chemical Sciences, 2(3): p. 358-372 (2011).

[10] Manning, A.S. and D.F. Evered, *The absorption of sugars from the human buccal cavity.* Clin Sci Mol Med, 51(2): p. 127-32 (1976).

[11] Nicolazzo, J.A. and B.C. Finnin, *In Vivo and In Vitro Models for Assessing Drug Absorption Across the Buccal Mucosa*, in *Drug Absorption Studies: In Situ, In Vitro and In Silico Models*, C. Ehrhardt and K.-J. Kim, Editors. 2008, Springer US: Boston, MA. p. 89-111.

[12] Harris, D. and J.R. Robinson, *Drug delivery via the mucous membranes of the oral cavity.* J Pharm Sci, 81(1): p. 1-10 (1992).

[13] Patel, V.F., F. Liu, and M.B. Brown, *Advances in oral transmucosal drug delivery.* J Control Release, 153(2): p. 106-16 (2011).

[14] Gyawali, C.P., et al., *Evaluation of esophageal motor function in clinical practice.* Neurogastroenterol Motil, 25(2): p. 99-133 (2013).

[15] Devereux, J.E., J.M. Newton, and M.B. Short, *The influence of density on the gastrointestinal transit of pellets.* J Pharm Pharmacol, 42(7): p. 500-1 (1990).

[16] Martinez, M., et al., *Applying the biopharmaceutics classification system to veterinary pharmaceutical products. Part II. Physiological considerations.* Adv Drug Deliv Rev, 54(6): p. 825-50 (2002).

[17] Avdeef, A., *Absorption and drug development : solubility, permeability, and charge state*. 2. ed. 2012, Hoboken, N.J.: John Wiley & Sons. 698 s.

[18] Davis, S.S., J.G. Hardy, and J.W. Fara, *Transit of pharmaceutical dosage forms through the small intestine.* Gut, 27(8): p. 886-92 (1986).

[19] Intestine. Available from: [http://www.arthursclipart.org/medical/digestive/page_03.htm].

[20] Mucosa. Available from: [http://www.arthursclipart.org/medical/digestive/page_03.htm].

[21] Hume, I.D., *Optimal Digestive Strategies in Mammalian Herbivores.* Physiological Zoology, 62(6): p. 1145-1163 (1989).

[22] Schiller, C., et al., *Intestinal fluid volumes and transit of dosage forms as assessed by magnetic resonance imaging.* Alimentary Pharmacology & Therapeutics, 22(10): p. 971-979 (2005).

[23] Kararli, T.T., *Comparison of the gastrointestinal anatomy, physiology, and biochemistry of humans and commonly used laboratory animals.* Biopharm Drug Dispos, 16(5): p. 351-80 (1995).

[24] Stenberg, P., K. Luthman, and P. Artursson, *Prediction of membrane permeability to peptides from calculated dynamic molecular surface properties.* Pharm Res, 16(2): p. 205-12 (1999).

[25] Vermeulen, N.P.E., *Handbook of Chemical Property Estimation Methods. W. J. Lyman, W. F. Reehl and D. H. Rosenblatt. American Chemical Society, Washington DC, 1990. 960 pp., US $49.95. ISBN 0-8412-1761-0.* Recueil des Travaux Chimiques des Pays-Bas, 110(2): p. 61-61 (1991).

[26] Schmiedel, R., *Deutsches und Europäisches Arzneibuch Deutsches Arzneibuch DAB 2015 + Europäisches Arzneibuch 8.0 - 8.5 Amtliche deutsche Ausgabe*. 2016: Deutscher Apotheker-Verlag.

[27] Barthe, L., J. Woodley, and G. Houin, *Gastrointestinal absorption of drugs: methods and studies.* Fundam Clin Pharmacol, 13(2): p. 154-68 (1999).

[28] Martinez, M.N. and G.L. Amidon, *A mechanistic approach to understanding the factors affecting drug absorption: a review of fundamentals.* J Clin Pharmacol, 42(6): p. 620-43 (2002).

[29] Nigsch, F., W. Klaffke, and S. Miret, *In vitro models for processes involved in intestinal absorption.* Expert Opin Drug Metab Toxicol, 3(4): p. 545-56 (2007).

[30] Galia, E., et al., *Evaluation of various dissolution media for predicting in vivo performance of class I and II drugs.* Pharm Res, 15(5): p. 698-705 (1998).

[31] Dressman, J.B. and C. Reppas, *In vitro-in vivo correlations for lipophilic, poorly water-soluble drugs.* Eur J Pharm Sci, 11 Suppl 2: p. S73-80 (2000).

[32] Do, T.T., et al., *The conflict between in vitro release studies in human biorelevant media and the in vivo exposure in rats of the lipophilic compound fenofibrate.* Int J Pharm, 414(1-2): p. 118-24 (2011).

[33] Martinez, M., et al., *Applying the biopharmaceutics classification system to veterinary pharmaceutical products. Part I: biopharmaceutics and formulation considerations.* Adv Drug Deliv Rev, 54(6): p. 805-24 (2002).

[34] Stenberg, P., K. Luthman, and P. Artursson, *Virtual screening of intestinal drug permeability.* J Control Release, 65(1-2): p. 231-43 (2000).

[35] Lipinski, C.A., et al., *Experimental and computational approaches to estimate solubility and permeability in drug discovery and development settings.* Adv Drug Deliv Rev, 46(1-3): p. 3-26 (2001).

[36] Lennernas, H., *Human jejunal effective permeability and its correlation with preclinical drug absorption models.* J Pharm Pharmacol, 49(7): p. 627-38 (1997).

[37] Shargel, L., *Applied biopharmaceutics & pharmacokinetics*. 2016, New York: McGraw-Hill Education.

[38] Rang, H.P. and M.M. Dale, *Rang and Dale's pharmacology*. 2012, Edinburgh; New York: Elsevier/Churchill Livingstone.

[39] Gonen, T. and T. Walz, *The structure of aquaporins.* Q Rev Biophys, 39(4): p. 361-96 (2006).

[40] Terada, T. and K.-i. Inui, *Impact of Drug Transport Proteins.* (2008).

[41] Plattner, H., et al., *Zellbiologie*. 2011, Stuttgart: Georg Thieme Verlag.

[42] Mitragotri, S., P.A. Burke, and R. Langer, *Overcoming the challenges in administering biopharmaceuticals: Formulation and delivery strategies.* Nature Reviews Drug Discovery, 13(9): p. 655-672 (2014).

[43] Lennernas, H., *Does fluid flow across the intestinal mucosa affect quantitative oral drug absorption? Is it time for a reevaluation?* Pharm Res, 12(11): p. 1573-82 (1995).

[44] He, Y.L., et al., *Species differences in size discrimination in the paracellular pathway reflected by oral bioavailability of poly(ethylene glycol) and D-peptides.* J Pharm Sci, 87(5): p. 626-33 (1998).

[45] Madara, J.L., *Functional Morphology of Epithelium of the Small Intestine*, in *Comprehensive Physiology*. 2010, John Wiley & Sons, Inc.

[46] Pappenheimer, J.R. and K.Z. Reiss, *Contribution of solvent drag through intercellular junctions to absorption of nutrients by the small intestine of the rat.* J Membr Biol, 100(2): p. 123-36 (1987).

[47] Le Ferrec, E.C., C.; Artusson, P., et al., *In vitro models of the intestinal barrier: The report and recommendations of ECVAM workshop 461,2.* ATLA Alternatives to Laboratory Animals, 29(6): p. 649-668 (2001).

[48] Cao, X., et al., *Why is it challenging to predict intestinal drug absorption and oral bioavailability in human using rat model.* Pharm Res, 23(8): p. 1675-86 (2006).

[49] Kim, J.S., et al., *The suitability of an in situ perfusion model for permeability determinations: utility for BCS class I biowaiver requests.* Mol Pharm, 3(6): p. 686-94 (2006).

[50] Sun, D., et al., *Comparison of human duodenum and Caco-2 gene expression profiles for 12,000 gene sequences tags and correlation with permeability of 26 drugs.* Pharm Res, 19(10): p. 1400-16 (2002).

[51] Salphati, L., et al., *Evaluation of a single-pass intestinal-perfusion method in rat for the prediction of absorption in man.* J Pharm Pharmacol, 53(7): p. 1007-13 (2001).

[52] Lennernas, H., *Animal data: the contributions of the Ussing Chamber and perfusion systems to predicting human oral drug delivery in vivo.* Adv Drug Deliv Rev, 59(11): p. 1103-20 (2007).

[53] Berggren, S., et al., *Characterization of jejunal absorption and apical efflux of ropivacaine, lidocaine and bupivacaine in the rat using in situ and in vitro absorption models.* Eur J Pharm Sci, 21(4): p. 553-60 (2004).

[54] Hidalgo, I.J., *Assessing the absorption of new pharmaceuticals.* Curr Top Med Chem, 1(5): p. 385-401 (2001).

[55] Briske-Anderson, M.J., J.W. Finley, and S.M. Newman, *The influence of culture time and passage number on the morphological and physiological development of Caco-2 cells.* Proc Soc Exp Biol Med, 214(3): p. 248-57 (1997).

[56] Walter, E. and T. Kissel, *Heterogeneity in the human intestinal cell line Caco-2 leads to differences in transepithelial transport.* European journal of pharmaceutical sciences., 3(4): p. 215 (1995).

[57] Theil, F.P., et al., *Utility of physiologically based pharmacokinetic models to drug development and rational drug discovery candidate selection.* Toxicol Lett, 138(1-2): p. 29-49 (2003).

[58] Van de Waterbeemd, H. and E. Gifford, *ADMET in silico modelling: towards prediction paradise?* Nat Rev Drug Discov, 2(3): p. 192-204 (2003).

[59] Grass, G.M. and S.A. Sweetana, *In vitro measurement of gastrointestinal tissue permeability using a new diffusion cell.* Pharm Res, 5(6): p. 372-6 (1988).

[60] Polentarutti, B.I., et al., *Evaluation of viability of excised rat intestinal segments in the Ussing chamber: investigation of morphology, electrical parameters, and permeability characteristics.* Pharm Res, 16(3): p. 446-54 (1999).

[61] Zakelj, S., et al., *The influence of buffer composition on tissue integrity during permeability experiments "in vitro".* Int J Pharm, 272(1-2): p. 173-80 (2004).

[62] Kikuchi, A., et al., *Transporter-mediated intestinal absorption of fexofenadine in rats.* Drug Metab Pharmacokinet, 21(4): p. 308-14 (2006).

[63] Annaert, P., et al., *In vitro, ex vivo, and in situ intestinal absorption characteristics of the antiviral ester prodrug adefovir dipivoxil.* J Pharm Sci, 89(8): p. 1054-62 (2000).

[64] Gotoh, Y., N. Kamada, and D. Momose, *The advantages of the Ussing chamber in drug absorption studies.* J Biomol Screen, 10(5): p. 517-23 (2005).

[65] Watanabe, E., M. Takahashi, and M. Hayashi, *A possibility to predict the absorbability of poorly water-soluble drugs in humans based on rat intestinal permeability assessed by an in vitro chamber method.* Eur J Pharm Biopharm, 58(3): p. 659-65 (2004).

[66] Pantzar, N., et al., *Bidirectional small-intestinal permeability in the rat to some common marker molecules in vitro.* Scand J Gastroenterol, 29(8): p. 703-9 (1994).

[67] Nejdfors, P., et al., *Mucosal in vitro permeability in the intestinal tract of the pig, the rat, and man: species- and region-related differences.* Scand J Gastroenterol, 35(5): p. 501-7 (2000).

[68] Ungell, A.L., et al., *Membrane transport of drugs in different regions of the intestinal tract of the rat.* J Pharm Sci, 87(3): p. 360-6 (1998).

[69] Menon, R.M. and W.H. Barr, *Comparison of ceftibuten transport across Caco-2 cells and rat jejunum mounted on modified Ussing chambers.* Biopharm Drug Dispos, 24(7): p. 299-308 (2003).

[70] Sandstrom, R., et al., *Jejunal absorption and metabolism of R/S-verapamil in humans.* Pharm Res, 15(6): p. 856-62 (1998).

[71] Sandstrom, R., A. Karlsson, and H. Lennernas, *The absence of stereoselective P-glycoprotein-mediated transport of R/S-verapamil across the rat jejunum.* J Pharm Pharmacol, 50(7): p. 729-35 (1998).

[72] Pauli-Magnus, C., et al., *Characterization of the Major Metabolites of Verapamil as Substrates and Inhibitors of P-glycoprotein.* Journal of Pharmacology and Experimental Therapeutics, 293(2): p. 376-382 (2000).

[73] Cvetkovic, M., et al., *OATP and P-glycoprotein transporters mediate the cellular uptake and excretion of fexofenadine.* Drug Metab Dispos, 27(8): p. 866-71 (1999).

[74] Dresser, G.K., et al., *Fruit juices inhibit organic anion transporting polypeptide-mediated drug uptake to decrease the oral availability of fexofenadine.* Clin Pharmacol Ther, 71(1): p. 11-20 (2002).

[75] Walters, H.C., et al., *Expression, transport properties, and chromosomal location of organic anion transporter subtype 3.* Am J Physiol Gastrointest Liver Physiol, 279(6): p. G1188-200 (2000).

[76] L'Annunziata, M. and M. Kessler, *Chapter 7 - Liquid Scintillation Analysis: Principles and Practice*, in *Handbook of Radioactivity Analysis (Third Edition)*. 2012, Academic Press: Amsterdam. p. 423-573.

[77] Loo, D.D., E.M. Wright, and T. Zeuthen, *Water pumps.* J Physiol, 542(Pt 1): p. 53-60 (2002).

[78] Schultz, S.G., *Epithelial water absorption: osmosis or cotransport?* Proc Natl Acad Sci U S A, 98(7): p. 3628-30 (2001).

[79] Shapiro, S.S. and M.B. Wilk, *An analysis of variance test for normality (complete samples).* Biometrika, 52(3-4): p. 591-611 (1965).

[80] SimulationsPlus, *User manual for GastroPlus*.

[81] Yu, L.X., et al., *Transport approaches to the biopharmaceutical design of oral drug delivery systems: prediction of intestinal absorption.* Adv Drug Deliv Rev, 19(3): p. 359-76 (1996).

[82] Yu, L.X. and G.L. Amidon, *A compartmental absorption and transit model for estimating oral drug absorption.* Int J Pharm, 186(2): p. 119-25 (1999).

[83] Hogben, C.A., et al., *Absorption of drugs from the stomach. II. The human.* J Pharmacol Exp Ther, 120(4): p. 540-5 (1957).

[84] Agoram, B., W.S. Woltosz, and M.B. Bolger, *Predicting the impact of physiological and biochemical processes on oral drug bioavailability.* Adv Drug Deliv Rev, 50 Suppl 1: p. S41-67 (2001).

[85] Lennernas, H., et al., *Regional jejunal perfusion, a new in vivo approach to study oral drug absorption in man.* Pharm Res, 9(10): p. 1243-51 (1992).

[86] Ludden, T.M., S.L. Beal, and L.B. Sheiner, *Comparison of the Akaike Information Criterion, the Schwarz criterion and the F test as guides to model selection.* Journal of Pharmacokinetics and Biopharmaceutics, 22(5): p. 431-445 (1994).

[87] Yamaoka, K., T. Nakagawa, and T. Uno, *Application of Akaike's information criterion (AIC) in the evaluation of linear pharmacokinetic equations.* Journal of Pharmacokinetics and Biopharmaceutics, 6(2): p. 165-175 (1978).

[88] Gottfried, B.S., *Introduction to optimization theory*. Prentice-Hall international series in industrial and systems engineering, ed. J. Weisman. 1973, Englewood Cliffs, N.J: Prentice-Hall.

[89] De Buck, S.S., et al., *The prediction of drug metabolism, tissue distribution, and bioavailability of 50 structurally diverse compounds in rat using mechanism-based absorption, distribution, and metabolism prediction tools.* Drug Metab Dispos, 35(4): p. 649-59 (2007).

[90] Poulin, P. and F.P. Theil, *Prediction of pharmacokinetics prior to in vivo studies. II. Generic physiologically based pharmacokinetic models of drug disposition.* J Pharm Sci, 91(5): p. 1358-70 (2002).

[91] Van de Waterbeemd, H., *Which in vitro Screens Guide the Prediction of Oral Absorption and Volume of Distribution?* Basic & Clinical Pharmacology & Toxicology, 96(3): p. 162-166 (2005).

[92] Loidl-Stahlhofen, A., et al., *Multilamellar liposomes and solid-supported lipid membranes (TRANSIL): screening of lipid-water partitioning toward a high-throughput scale.* Pharm Res, 18(12): p. 1782-8 (2001).

[93] Kansy, M., F. Senner, and K. Gubernator, *Physicochemical high throughput screening: parallel artificial membrane permeation assay in the description of passive absorption processes.* J Med Chem, 41(7): p. 1007-10 (1998).

[94] Zhu, C., et al., *A comparative study of artificial membrane permeability assay for high throughput profiling of drug absorption potential.* Eur J Med Chem, 37(5): p. 399-407 (2002).

[95] Sugano, K., et al., *High throughput prediction of oral absorption: improvement of the composition of the lipid solution used in parallel artificial membrane permeation assay.* J Biomol Screen, 6(3): p. 189-96 (2001).

[96] Schmitz, J., et al., *Purification of the human intestinal brush border membrane.* Biochim Biophys Acta, 323(1): p. 98-112 (1973).

[97] Hopfer, U., et al., *Glucose transport in isolated brush border membrane from rat small intestine.* J Biol Chem, 248(1): p. 25-32 (1973).

[98] Moyer, M.P., *Culture of human gastrointestinal epithelial cells.* Proc Soc Exp Biol Med, 174(1): p. 12-5 (1983).

[99] Bermejo, M. and A. Ruiz-Garcia, *Oral Permeability predictions - from in silico to in vivo models.* Business Briefing Pharma Tech p. 175-180 (2002).

[100] Stern, B.K. and W.E. Jensen, *Active transport of glucose by suspensions of isolated rat intestinal epithelial cells.* Nature, 209(5025): p. 789-90 (1966).

[101] Gall, D.G., et al., *Sodium ion transport in isolated intestinal epithelial cells. The effect of actively transported sugars on sodium ion efflux.* Biochim Biophys Acta, 339(3): p. 291-302 (1974).

[102] Raul, F., et al., *Intestinal enzymes activities in isolated villus and crypt cells during postnatal development of the rat.* Cell Tissue Res, 176(2): p. 167-78 (1977).

[103] Carter, J.H., R.D. Poretz, and A. Eichholz, *Separation of isolated hamster intestinal epithelial cells by velocity sedimentation on Ficoll Gradients.* J Cell Physiol, 111(1): p. 68-76 (1982).

[104] Ricci, V. and G. Rindi, *Thiamin uptake by rat isolated enterocytes: relationship between transport and phosphorylation.* Arch Int Physiol Biochim Biophys, 100(3): p. 275-9 (1992).

[105] Cartwright, I.J. and J.A. Higgins, *Isolated rabbit enterocytes as a model cell system for investigations of chylomicron assembly and secretion.* J Lipid Res, 40(7): p. 1357-65 (1999).

[106] Fogh, J., W.C. Wright, and J.D. Loveless, *Absence of HeLa cell contamination in 169 cell lines derived from human tumors.* J Natl Cancer Inst, 58(2): p. 209-14 (1977).

[107] Artursson, P., K. Palm, and K. Luthman, *Caco-2 monolayers in experimental and theoretical predictions of drug transport.* Adv Drug Deliv Rev, 46(1-3): p. 27-43 (2001).

[108] Artursson, P. and J. Karlsson, *Correlation between oral drug absorption in humans and apparent drug permeability coefficients in human intestinal epithelial (Caco-2) cells.* Biochem Biophys Res Commun, 175(3): p. 880-5 (1991).

[109] Lennernas, H., et al., *Comparison between active and passive drug transport in human intestinal epithelial (caco-2) cells in vitro and human jejunum in vivo.* International Journal of Pharmaceutics, 127(1): p. 103-107 (1996).

[110] Watson, C.J., M. Rowland, and G. Warhurst, *Functional modeling of tight junctions in intestinal cell monolayers using polyethylene glycol oligomers.* Am J Physiol Cell Physiol, 281(2): p. C388-97 (2001).

[111] Arrieta, M.C., L. Bistritz, and J.B. Meddings, *Alterations in intestinal permeability.* Gut, 55(10): p. 1512-20 (2006).

[112] Bohets, H., et al., *Strategies for absorption screening in drug discovery and development.* Curr Top Med Chem, 1(5): p. 367-83 (2001).

[113] Saha, P. and J.H. Kou, *Effect of bovine serum albumin on drug permeability estimation across Caco-2 monolayers.* Eur J Pharm Biopharm, 54(3): p. 319-24 (2002).

[114] Wilson, T.H. and G. Wiseman, *The use of sacs of everted small intestine for the study of the transference of substances from the mucosal to the serosal surface.* J Physiol, 123(1): p. 116-25 (1954).

[115] Le Ferrec, c., Artusson, Brayden, Fabre, Gires, Guillou, Rousset, Rubas, Scarino, *In vitro models of the interstinal barrier.* ATLA, 29: p. 649-668 (2001).

[116] Ussing, H.H. and K. Zerahn, *Active transport of sodium as the source of electric current in the short-circuited isolated frog skin.* Acta Physiol Scand, 23(2-3): p. 110-27 (1951).

[117] Luo, Z.L., Y.; Zhao, B.; Tang, M.;, et al., *Ex vivo and in situ approaches used to study intestinal absorption.* Journal of Pharmacological and Toxicological Methods, 68(2): p. 208-216 (2013).

[118] FDA, *Guidance for Industry: Waiver of in vivo bioavaiability and bioequivalence studies for immediate-release solid oral dosage forms base on a biopharmaceutics classification system / DRAFT.* (2000).

[119] Fagerholm, U., M. Johansson, and H. Lennernas, *Comparison between permeability coefficients in rat and human jejunum.* Pharm Res, 13(9): p. 1336-42 (1996).

[120] Fihn, B.M., A. Sjoqvist, and M. Jodal, *Permeability of the rat small intestinal epithelium along the villus-crypt axis: effects of glucose transport.* Gastroenterology, 119(4): p. 1029-36 (2000).

[121] Yuasa, H., K. Matsuda, and J. Watanabe, *Influence of anesthetic regimens on intestinal absorption in rats.* Pharm Res, 10(6): p. 884-8 (1993).

[122] Stewart, B.H., et al., *Comparison of intestinal permeabilities determined in multiple in vitro and in situ models: relationship to absorption in humans.* Pharm Res, 12(5): p. 693-9 (1995).

[123] Savina, P.M., et al., *Optimal perfusion rate determined for in situ intestinal absorption studies in rats.* J Pharm Sci, 70(3): p. 239-43 (1981).

[124] Lewis, L.D. and J.S. Fordtran, *Effect of perfusion rate on absorption, surface area, unstirred water layer thickness, permeability, and intraluminal pressure in the rat ileum in vivo.* Gastroenterology, 68(6): p. 1509-16 (1975).

[125] Yuasa, H., et al., *Comparative assessment of the resistance of the unstirred water layer to solute transport between two different intestinal perfusion systems.* Biochim Biophys Acta, 938(2): p. 189-98 (1988).

[126] Knutson, L., B. Odlind, and R. Hallgren, *A new technique for segmental jejunal perfusion in man.* Am J Gastroenterol, 84(10): p. 1278-84 (1989).

[127] Isin, E.M., et al., *Use of radiolabeled compounds in drug metabolism and pharmacokinetic studies.* Chem Res Toxicol, 25(3): p. 532-42 (2012).

[128] Lennernas, H., S. Nylander, and A.L. Ungell, *Jejunal permeability: a comparison between the ussing chamber technique and the single-pass perfusion in humans.* Pharm Res, 14(5): p. 667-71 (1997).

[129] Johnson, K.C., *Dissolution and absorption modeling: model expansion to simulate the effects of precipitation, water absorption, longitudinally changing intestinal permeability, and controlled release on drug absorption.* Drug Dev Ind Pharm, 29(8): p. 833-42 (2003).

[130] Dressman, J.B. and D. Fleisher, *Mixing-tank model for predicting dissolution rate control or oral absorption.* J Pharm Sci, 75(2): p. 109-16 (1986).

[131] Willmann, S., et al., *A physiological model for the estimation of the fraction dose absorbed in humans.* J Med Chem, 47(16): p. 4022-31 (2004).

[132] Parrott, N. and T. Lavé, *Prediction of intestinal absorption: comparative assessment of Gastroplus™ and IDEA™.* European Journal of Pharmaceutical Sciences, 17(1–2): p. 51-61 (2002).

[133] Hendriksen, B.A., M.V. Felix, and M.B. Bolger, *The composite solubility versus pH profile and its role in intestinal absorption prediction.* AAPS PharmSci, 5(1): p. E4 (2003).

[134] Huang, W., S.L. Lee, and L.X. Yu, *Mechanistic approaches to predicting oral drug absorption.* AAPS Journal, 11(2): p. 217-224 (2009).

[135] Rozehnal, V., et al., *Human small intestinal and colonic tissue mounted in the Ussing chamber as a tool for characterizing the intestinal absorption of drugs.* European Journal of Pharmaceutical Sciences, 46(5): p. 367-373 (2012).

[136] Bijlsma, P.B., et al., *Differential in vivo and in vitro intestinal permeability to lactulose and mannitol in animals and humans: a hypothesis.* Gastroenterology, 108(3): p. 687-96 (1995).

[137] Amidon, G.L. and W. Sadée, *Membrane transporters as drug targets.* (2004).

[138] Giacomini, K.M., et al., *Membrane transporters in drug development.* Nat Rev Drug Discov, 9(3): p. 215-36 (2010).

[139] Akimoto, M., et al., *Gastric pH profiles of beagle dogs and their use as an alternative to human testing.* Eur J Pharm Biopharm, 49(2): p. 99-102 (2000).

[140] Polentarutti, B., et al., *Modification of gastric pH in the fasted dog.* J Pharm Pharmacol, 62(4): p. 462-9 (2010).

[141] Bolger, M.B., *personal communication*. 2007.

[142] Chiou, W.L., et al., *Evaluation of using dog as an animal model to study the fraction of oral dose absorbed of 43 drugs in humans.* Pharm Res, 17(2): p. 135-40 (2000).

[143] Robinson, J.W., et al., *Functional and structural characteristics of the jejunum and ileum in the dog and the rat.* Digestion, 15(3): p. 188-99 (1977).

[144] Dressman, J.B., *Comparison of canine and human gastrointestinal physiology.* Pharm Res, 3(3): p. 123-31 (1986).

[145] Hilgendorf, C., et al., *Caco-2 versus Caco-2/HT29-MTX co-cultured cell lines: permeabilities via diffusion, inside- and outside-directed carrier-mediated transport.* J Pharm Sci, 89(1): p. 63-75 (2000).

[146] Collett, A., et al., *Modulation of the permeability of H2 receptor antagonists cimetidine and ranitidine by P-glycoprotein in rat intestine and the human colonic cell line Caco-2.* J Pharmacol Exp Ther, 288(1): p. 171-8 (1999).

[147] Klein, S., *The use of biorelevant dissolution media to forecast the in vivo performance of a drug.* AAPS J, 12(3): p. 397-406 (2010).

[148] Lennernas, H., et al., *Oral biopharmaceutics tools - time for a new initiative - an introduction to the IMI project OrBiTo.* Eur J Pharm Sci, 57: p. 292-9 (2014).

[149] Hunter, A.J., *The Innovative Medicines Initiative: a pre-competitive initiative to enhance the biomedical science base of Europe to expedite the development of new medicines for patients.* Drug Discov Today, 13(9-10): p. 371-3 (2008).

[150] DrugBank. Available from: [http://www.drugbank.ca].

[151] PubChem. Available from: [http://pubchem.ncbi.nlm.nih.gov].

[152] Nilsson, D., U. Fagerholm, and H. Lennernas, *The influence of net water absorption on the permeability of antipyrine and levodopa in the human jejunum.* Pharm Res, 11(11): p. 1540-7 (1994).

[153] Lennernas, H., *Gastrointestinal absorption mechanisms: a comparison between animal and human models.* European Journal of Pharmaceutical Sciences, 2(1): p. 39-43 (1994).

[154] Lindahl, A., et al., *Jejunal permeability and hepatic extraction of fluvastatin in humans.* Clin Pharmacol Ther, 60(5): p. 493-503 (1996).

[155] Lennernas, H., et al., *The effect of L-leucine on the absorption of levodopa, studied by regional jejunal perfusion in man.* Br J Clin Pharmacol, 35(3): p. 243-50 (1993).

[156] Fagerholm, U., et al., *The lack of effect of induced net fluid absorption on the in vivo permeability of terbutaline in the human jejunum.* J Drug Target, 3(3): p. 191-200 (1995).

[157] Winiwarter, S., et al., *Correlation of human jejunal permeability (in vivo) of drugs with experimentally and theoretically derived parameters. A multivariate data analysis approach.* J Med Chem, 41(25): p. 4939-49 (1998).

[158] Irvine, J.D., et al., *MDCK (Madin-Darby canine kidney) cells: A tool for membrane permeability screening.* J Pharm Sci, 88(1): p. 28-33 (1999).

[159] Takamatsu, N., et al., *Human jejunal permeability of two polar drugs: cimetidine and ranitidine.* Pharm Res, 18(6): p. 742-4 (2001).

[160] Fagerholm, U., et al., *Jejunal permeability in humans in vivo and rats in situ: investigation of molecular size selectivity and solvent drag.* Acta Physiol Scand, 165(3): p. 315-24 (1999).

[161] Lennernas, H., *Human intestinal permeability.* J Pharm Sci, 87(4): p. 403-10 (1998).

[162] Tannergren, C., et al., *The effect of ketoconazole on the in vivo intestinal permeability of fexofenadine using a regional perfusion technique.* Br J Clin Pharmacol, 55(2): p. 182-90 (2003).

[163] Takamatsu, N., et al., *Human intestinal permeability of piroxicam, propranolol, phenylalanine, and PEG 400 determined by jejunal perfusion.* Pharm Res, 14(9): p. 1127-32 (1997).

7 Appendix

7.1 Permeability investigations

Tab. 7-1: Physicochemical properties and results for effective or apparent permeability for compounds reported in literature for different absorption models. In addition own results from Ussing chamber studies are included (Chapter 3.2.2).

Compound	MW [g/mol]	Log $P_{o/w}$	Absorption mechanism*	Ussing chamber (rat)	Caco-2 cells	Human perfusion (LOC-I-GUT®)	Source
	[150, 151]	[150, 151]	[95]	P_{app} [cm/s]	P_{app} [cm/s]	P_{eff} [cm/s]	
Antipyrine	188	1.1	●	3.46E-05	2.67E-04	4.29E-04	[65, 68, 109, 128, 152-156]
Atenolol	266	1.3	●	5.65E-06	5.50E-07	2.05E-05	[64, 65, 68, 109, 128, 153, 154]
Carbamazepine	236	2.7	●	-	2.53E-05	4.30E-04	in house data,[157]
Cephalexin	347	0.0	■	-	2.70E-07	1.57E-04	[48, 158]
Cimetidine	252	0.9	●	3.20E-05	-	2.99E-05	[64, 159]
Creatinine	113	-0.6	●	7.87E-06	-	2.90E-05	[68, 128, 160]
D-Glucose	180	-2.9	■	5.69E-05	2.50E-05	1.20E-03	[43, 68, 109, 128, 155, 160, 161]
Enalaprilate	348	-0.8	● / ■	6.00E-06	-	2.90E-05	[128, 153]
Fexofenadine	502	5.6	■	1.47E-06	-	1.10E-05	own results, [162]
Furosemide	331	1.5	●	6.06E-06	1.40E-07	5.00E-06	[65, 157, 158]
Hydrochlorthiazide	297	-0.3	● / ●	-	9.20E-07	4.00E-06	[157, 158]
Ketoprofen	254	3.6	●	-	9.30E-05	8.40E-04	[157, 158]
L-Dopa	197	-2.2	■	3.60E-05	1.00E-06	2.26E-04	[109, 128, 152, 155]
L-Leucine	131	-1.7	■	7.12E-05	5.10E-07	6.20E-04	[68, 109, 128, 155]
Mannitol	182	-3.5	●	1.73E-05	4.48E-07	3.00E-05	in house data, own results
Metoprolol	267	2.5	●	3.13E-05	9.20E-05	1.06E-04	[36, 65, 68, 109, 154, 161]
Naproxen	230	3.3	●	3.76E-05	2.06E-04	9.15E-04	[65, 109, 128, 157, 158, 161]
Propranolol	259	3.6	●	1.53E-05	1.10E-04	3.73E-04	[158], own results, [159, 163]
Terbutaline	225	1.6	●	2.03E-05	3.80E-07	3.00E-05	[109], own results, [156]
Verapamil	455	5.9	●	5.92E-05	2.32E-05	5.15E-04	in house data, own results, [70, 157]

*Absorption mechanism: passive transcellular (●), active (■), passive paracellular through tight junctions (●)

Tab. 7-2: Parameter used for calculation of apparent permeability for each chamber of the Ussing chamber studies using reference compound propranolol in mucosal to serosal and serosal to mucoal direction for stripped tissue.

Permeability direction m-s	Time [min]	Chamber 1	2	3	4	5	6
A_R*corrected* [µmol]	5	5.86E-10	1.47E-09	2.34E-09	0.00E+00	5.86E-10	8.79E-10
	10	0.00E+00	9.12E-10	1.52E-09	3.34E-09	1.22E-09	6.08E-10
	20	0.00E+00	1.92E-09	3.19E-10	2.87E-09	1.92E-09	3.83E-09
	40	2.38E-09	2.98E-09	1.49E-09	1.76E-08	9.84E-09	1.19E-08
	60	5.46E-09	5.76E-09	6.67E-09	3.49E-08	2.49E-08	2.12E-08
	90	1.11E-08	1.29E-08	1.47E-08	7.48E-08	4.74E-08	5.11E-08
	120	2.24E-08	2.54E-08	3.25E-08	1.30E-07	9.89E-08	9.04E-08
	150	3.59E-08	3.10E-08	4.99E-08	1.78E-07	1.52E-07	1.26E-07
C_D*end* [µmol/mL]		9.94E-07	1.06E-06	1.09E-06	1.05E-06	1.03E-06	1.09E-06
Flux [µmol/cm^2/s]		5.81E-12	5.81E-12	7.75E-12	3.88E-11	1.94E-11	1.94E-11
P_{app} [cm/s]		5.85E-06	5.48E-06	7.11E-06	3.69E-05	1.88E-05	1.78E-05

Permeability direction s-m	Time [min]	Chamber 7	8	9	10	11	12
A_R*corrected* [µmol]	5	0.00E+00	1.47E-09	2.05E-09	0.00E+00	5.86E-10	8.79E-10
	10	6.08E-10	0.00E+00	1.52E-09	5.17E-09	3.65E-09	5.17E-09
	20	2.24E-09	2.24E-09	9.58E-10	5.11E-09	2.24E-09	3.83E-09
	40	5.96E-09	4.17E-09	2.09E-09	1.40E-08	1.01E-08	5.37E-09
	60	2.43E-09	4.25E-09	6.37E-09	2.64E-08	2.06E-08	1.76E-08
	90	8.11E-09	1.23E-08	1.20E-08	6.82E-08	5.17E-08	3.99E-08
	120	1.46E-08	2.70E-08	3.03E-08	1.16E-07	1.00E-07	7.39E-08
	150	2.32E-08	3.72E-08	4.70E-08	1.73E-07	1.46E-07	9.56E-08
C_D*end* [µmol/mL]		1.08E-06	1.11E-06	1.10E-06	1.06E-06	1.07E-06	1.06E-06
Flux [µmol/cm^2/s]		3.88E-12	7.75E-12	7.75E-12	1.94E-11	1.94E-11	1.74E-11
P_{app} [cm/s]		3.60E-06	6.98E-06	7.06E-06	1.82E-05	1.80E-05	1.64E-05

Tab. 7-3: Parameter used for calculation of apparent permeability for each chamber of the Ussing chamber studies using reference compound propranolol in mucosal to serosal and serosal to mucoal direction for full-thickness tissue.

Permeability direction	Time	Chamber					
m-s	[min]	1	2	3	4	5	6
A_R*corrected* [µmol]	5	0.00E+00	0.00E+00	0.00E+00	0.00E+00	0.00E+00	-
	10	3.04E-10	0.00E+00	0.00E+00	0.00E+00	6.08E-10	-
	20	0.00E+00	0.00E+00	0.00E+00	0.00E+00	0.00E+00	-
	40	2.98E-10	1.49E-09	0.00E+00	0.00E+00	2.38E-09	-
	60	6.07E-10	0.00E+00	1.52E-09	2.12E-09	2.43E-09	-
	90	0.00E+00	2.40E-09	4.20E-09	5.11E-09	9.61E-09	-
	120	2.28E-09	6.83E-09	6.18E-09	1.27E-08	2.34E-08	-
	150	6.52E-09	1.04E-08	1.40E-08	1.66E-08	2.94E-08	-
C_D*end* [µmol/mL]		1.01E-06	9.79E-07	9.32E-07	9.44E-07	9.79E-07	-
Flux [µmol/cm^2/s]		5.81E-13	1.94E-12	1.55E-12	3.88E-12	5.81E-12	-
P_{app} [cm/s]		5.76E-07	1.98E-06	1.66E-06	4.11E-06	5.94E-06	-

Permeability direction	Time	Chamber					
s-m	[min]	7	8	9	10	11	12
A_R*corrected* [µmol]	5	0.0E+00	0.0E+00	5.9E-10	2.9E-10	0.0E+00	-
	10	0.0E+00	0.0E+00	3.0E-10	0.0E+00	6.1E-10	-
	20	0.0E+00	0.0E+00	3.2E-10	9.6E-10	0.0E+00	-
	40	0.0E+00	1.2E-09	0.0E+00	3.0E-10	-	-
	60	6.1E-10	1.2E-09	3.0E-10	1.2E-09	1.2E-09	-
	90	1.2E-09	1.2E-09	4.8E-09	6.0E-10	4.2E-09	-
	120	3.6E-09	2.6E-09	1.1E-08	6.8E-09	1.3E-08	-
	150	4.9E-09	5.9E-09	2.0E-08	8.2E-09	1.5E-08	-
C_D*end* [µmol/mL]		1.03E-06	9.20E-07	1.00E-06	1.02E-06	1.03E-06	-
Flux [µmol/cm^2/s]		9.69E-13	3.88E-13	3.88E-12	1.74E-12	3.88E-12	-
P_{app} [cm/s]		9.37E-07	4.21E-07	3.86E-06	1.72E-06	3.75E-06	-

Tab. 7-4: Parameter used for calculation of apparent permeability for each chamber of the Ussing chamber studies using reference compound verapamil in mucosal to serosal and serosal to mucoal direction for stripped tissue.

Permeability direction m-s	Time [min]	Chamber 1	2	3	4	5	6
A_R*corrected* [µmol]	5	-	0.00E+00	0.00E+00	0.00E+00	3.57E-09	0.00E+00
	10	0.00E+00	0.00E+00	0.00E+00	0.00E+00	0.00E+00	0.00E+00
	20	0.00E+00	4.65E-10	0.00E+00	0.00E+00	4.65E-10	3.72E-09
	40	0.00E+00	3.11E-09	0.00E+00	2.59E-09	6.75E-09	4.15E-09
	60	2.79E-09	5.58E-09	4.19E-09	2.33E-09	6.51E-09	1.02E-08
	90	-	1.32E-08	1.16E-08	1.21E-08	1.82E-08	2.15E-08
	120	1.76E-08	1.70E-08	2.70E-08	1.99E-08	2.99E-08	2.35E-08
	150	2.45E-08	2.95E-08	3.51E-08	4.52E-08	3.26E-08	3.83E-08
C_D*end* [µmol/mL]		9.73E-08	9.41E-08	9.11E-08	9.48E-08	8.97E-08	9.35E-08
Flux [µmol/cm^2/s]		3.88E-12	3.88E-12	7.75E-12	5.81E-12	7.75E-12	3.88E-12
P_{app} [cm/s]		3.98E-05	4.12E-05	8.51E-05	6.13E-05	8.64E-05	4.14E-05

Permeability direction s-m	Time [min]	Chamber 7	8	9	10	11	12
A_R*corrected* [µmol]	5	7.94E-10	0.00E+00	0.00E+00	0.00E+00	0.00E+00	0.00E+00
	10	3.43E-09	0.00E+00	1.96E-09	0.00E+00	0.00E+00	0.00E+00
	20	9.31E-10	3.26E-09	3.26E-09	4.65E-09	0.00E+00	0.00E+00
	40	5.19E-10	7.27E-09	3.11E-09	0.00E+00	5.19E-10	1.56E-09
	60	3.72E-09	7.44E-09	5.12E-09	4.65E-09	5.12E-09	9.31E-10
	90	9.91E-09	1.54E-08	1.43E-08	1.65E-08	2.04E-08	1.49E-08
	120	2.11E-08	1.88E-08	2.41E-08	2.46E-08	2.82E-08	1.88E-08
	150	2.76E-08	2.51E-08	2.95E-08	3.83E-08	4.02E-08	3.01E-08
C_D*end* [µmol/mL]		8.04E-08	8.95E-08	8.59E-08	8.16E-08	8.99E-08	9.02E-08
Flux [µmol/cm^2/s]		5.81E-12	3.88E-12	5.81E-12	5.81E-12	7.75E-12	5.81E-12
P_{app} [cm/s]		7.23E-05	4.33E-05	6.77E-05	7.13E-05	8.62E-05	6.44E-05

Tab. 7-5: Parameter used for calculation of apparent permeability for each chamber of the Ussing chamber studies using reference compound verapamil in mucosal to serosal and serosal to mucoal direction for full-thickness tissue.

Permeability direction m-s	Time [min]	Chamber 1	2	3	4	5	6
A_R*corrected* [µmol]	5	0.00E+00	0.00E+00	0.00E+00	0.00E+00	0.00E+00	0.00E+00
	10	0.00E+00	0.00E+00	2.94E-09	0.00E+00	0.00E+00	0.00E+00
	20	0.00E+00	0.00E+00	0.00E+00	0.00E+00	0.00E+00	0.00E+00
	40	1.56E-09	3.63E-09	5.19E-10	2.59E-09	1.56E-09	5.19E-10
	60	4.65E-09	9.31E-09	3.72E-09	5.12E-09	5.58E-09	5.12E-09
	90	1.49E-08	1.54E-08	9.91E-09	9.36E-09	1.65E-08	9.36E-09
	120		2.05E-08	1.94E-08	2.23E-08	3.11E-08	1.47E-08
	150	2.01E-08	2.89E-08	2.26E-08	2.70E-08	3.20E-08	2.51E-08
C_D*end* [µmol/mL]		9.62E-08	9.93E-08	9.92E-08	9.74E-08	7.03E-08	9.46E-08
Flux [µmol/cm^2/s]		5.81E-12	3.88E-12	5.81E-12	5.81E-12	7.75E-12	3.88E-12
P_{app} [cm/s]		6.04E-05	3.90E-05	5.86E-05	5.97E-05	1.10E-04	4.10E-05

Permeability direction s-m	Time [min]	Chamber 7	8	9	10	11	12
A_R*corrected* [µmol]	5	0.00E+00	0.00E+00	-	0.00E+00	0.00E+00	-
	10	0.00E+00	0.00E+00	-	0.00E+00	0.00E+00	-
	20	0.00E+00	0.00E+00	-	0.00E+00	0.00E+00	-
	40	0.00E+00	2.08E-09	-	0.00E+00	0.00E+00	-
	60	9.31E-10	4.65E-09	-	1.40E-09	4.65E-09	-
	90	3.30E-09	8.26E-09	-	8.26E-09	1.10E-08	-
	120	6.45E-09	9.39E-09	-	9.39E-09	1.82E-08	-
	150	1.32E-08	2.07E-08	-	1.88E-08	2.32E-08	-
C_D*end* [µmol/mL]		9.10E-08	9.57E-08	-	9.46E-08	9.34E-08	-
Flux [µmol/cm^2/s]		1.74E-12	1.55E-12	-	1.94E-12	3.88E-12	-
P_{app} [cm/s]		1.92E-05	1.62E-05	-	2.05E-05	4.15E-05	-

Tab. 7-6: Parameter used for calculation of apparent permeability for each chamber of the Ussing chamber studies using reference compound fexofenadine in mucosal to serosal and serosal to mucoal direction for stripped tissue.

Permeability direction m-s	Time [min]	Chamber 1	2	3	4	5	6
A_R*corrected* [µmol]	5	0.00E+00	0.00E+00	0.00E+00	0.00E+00	-	0.00E+00
	10	0.00E+00	0.00E+00	4.12E-07	-	-	1.37E-07
	20	3.88E-06	0.00E+00	8.31E-07	4.16E-07	-	6.93E-07
	40	4.04E-06	1.21E-06	4.30E-06	2.42E-06	-	3.23E-06
	60	5.29E-06	1.67E-06	4.17E-06	5.56E-06	-	8.48E-06
	90	8.50E-06	6.27E-06	1.03E-05	1.52E-05	-	1.66E-05
	120		8.79E-06	1.49E-05	3.09E-05	-	2.58E-05
	150	2.49E-05	1.80E-05	2.23E-05	5.74E-05	-	4.33E-05
C_D*end* [µmol/mL]		2.94E-03	3.00E-03	2.91E-03	2.94E-03	-	2.82E-03
Flux [µmol/cm^2/s]		1.94E-09	1.94E-09	3.88E-09	7.75E-09	-	5.81E-09
P_{app} [cm/s]		6.60E-07	6.45E-07	1.33E-06	2.64E-06	-	2.06E-06

Permeability direction s-m	Time [min]	Chamber 7	8	9	10	11	12
A_R*corrected* [µmol]	5	0.00E+00	0.00E+00	-	-	0.00E+00	0.00E+00
	10	0.00E+00	0.00E+00	-	-	0.00E+00	0.00E+00
	20	0.00E+00	6.93E-07	-	-	0.00E+00	0.00E+00
	40	4.04E-07	9.42E-07	-	-	9.42E-07	1.35E-07
	60	1.95E-06	2.36E-06	-	-	2.23E-06	1.81E-06
	90	5.44E-06	3.48E-06	-	-	1.10E-05	7.67E-06
	120	9.92E-06	9.35E-06	-	-	2.11E-05	1.35E-05
	150	1.59E-05	1.83E-05	-	-	3.41E-05	2.38E-05
C_D*end* [µmol/mL]		2.97E-03	2.99E-03	-	-	2.91E-03	2.86E-03
Flux [µmol/cm^2/s]		1.94E-09	1.94E-09	-	-	5.81E-09	3.88E-09
P_{app} [cm/s]		6.53E-07	6.49E-07	-	-	1.99E-06	1.35E-06

Tab. 7-7: Parameter used for calculation of apparent permeability for each chamber of the Ussing chamber studies using reference compound fexofenadine in mucosal to serosal and serosal to mucoal direction for full-thickness tissue.

Permeability direction m-s	Time [min]	Chamber 1	2	3	4	5	6
A_R*corrected* [µmol]	5	0.00E+00	0.00E+00	0.00E+00	0.00E+00	-	0.00E+00
	10	7.14E-06	0.00E+00	1.37E-07	0.00E+00	-	0.00E+00
	20	0.00E+00	0.00E+00	0.00E+00	2.77E-07	-	0.00E+00
	40	2.69E-07	8.07E-07	0.00E+00	8.07E-07	-	2.69E-07
	60	2.78E-07	1.25E-06	9.74E-07	3.62E-06	-	2.09E-06
	90	1.25E-06	5.02E-06	3.35E-06	1.00E-05	-	6.13E-06
	120	3.83E-06	1.20E-05	5.53E-06	2.32E-05	-	1.56E-05
	150	7.80E-06	2.05E-05	1.10E-05	3.90E-05	-	2.91E-05
C_D*end* [µmol/mL]		2.96E-03	2.96E-03	3.09E-03	3.00E-03	-	3.01E-03
Flux [µmol/cm^2/s]		1.16E-09	3.88E-09	1.55E-09	5.81E-09	-	3.88E-09
P_{app} [cm/s]		3.92E-07	1.31E-06	5.02E-07	1.94E-06	-	1.29E-06

Permeability direction s-m	Time [min]	Chamber 7	8	9	10	11	12
A_R*corrected* [µmol]	5	2.3E-06	0.0E+00	0.0E+00	0.0E+00	9.6E-07	0.0E+00
	10	8.8E-06	0.0E+00	0.0E+00	0.0E+00	4.1E-07	0.0E+00
	20	8.5E-06	0.0E+00	0.0E+00	0.0E+00	6.9E-07	0.0E+00
	40	1.0E-05	0.0E+00	2.7E-07	6.7E-07	1.3E-06	5.4E-07
	60	1.0E-05	5.6E-07	4.2E-07	3.6E-06	1.8E-06	3.1E-06
	90	1.4E-05	1.5E-06	4.6E-06	8.9E-06	5.4E-06	1.4E-05
	120	1.8E-05	4.1E-06	7.8E-06	2.3E-05	1.3E-05	2.9E-05
	150	2.7E-05	8.9E-06	1.8E-05	4.2E-05	2.3E-05	4.8E-05
C_D*end* [µmol/mL]		2.97E-03	3.05E-03	3.10E-03	3.05E-03	3.06E-03	3.00E-03
Flux [µmol/cm^2/s]		1.94E-09	1.16E-09	1.94E-09	5.81E-09	3.88E-09	7.75E-09
P_{app} [cm/s]		6.52E-07	3.81E-07	6.26E-07	1.91E-06	1.27E-06	2.58E-06

Tab. 7-8: Parameter used for calculation of apparent permeability for each chamber of the Ussing chamber studies using reference compound terbutaline in mucosal to serosal and serosal to mucoal direction for stripped tissue.

Permeability direction	Time	Chamber					
m-s	[min]	1	2	3	4	5	6
A_R*corrected* [µmol]	5	5.54E-09	8.46E-09	7.59E-09	9.05E-09	-	7.88E-09
	10	1.10E-08	1.27E-08	1.27E-08	1.39E-08	-	1.30E-08
	20	2.20E-08	2.48E-08	2.68E-08	2.43E-08	-	2.29E-08
	40	5.07E-08	5.02E-08	5.48E-08	6.11E-08	-	4.58E-08
	60	7.88E-08	8.26E-08	8.86E-08	8.89E-08	-	7.60E-08
	90	1.24E-07	1.19E-07	1.24E-07	1.35E-07	-	1.13E-07
	120	1.52E-07	1.49E-07	1.67E-07	1.70E-07	-	1.59E-07
	150	1.95E-07	1.90E-07	2.13E-07	2.08E-07	-	1.97E-07
C_D*end* [µmol/mL]		9.43E-07	9.71E-07	9.44E-07	9.53E-07	-	9.55E-07
Flux [µmol/cm^2/s]		1.94E-11	1.94E-11	1.94E-11	1.94E-11	-	1.94E-11
P_{app} [cm/s]		2.05E-05	2.00E-05	2.05E-05	2.03E-05	-	2.03E-05

Permeability direction	Time	Chamber					
s-m	[min]	7	8	9	10	11	12
A_R*corrected* [µmol]	5	2.92E-09	5.54E-09	2.04E-09	2.04E-09	2.92E-09	1.75E-09
	10	5.09E-09	7.91E-09	3.67E-09	3.67E-09	2.54E-09	5.65E-09
	20	1.31E-08	1.09E-08	1.14E-08	8.37E-09	9.48E-09	1.12E-08
	40	3.32E-08	4.06E-08	4.01E-08	2.59E-08	2.59E-08	4.27E-08
	60	5.47E-08	6.82E-08	7.22E-08	4.55E-08	4.86E-08	7.25E-08
	90	9.50E-08	1.07E-07	1.29E-07	7.83E-08	8.65E-08	1.29E-07
	120	1.24E-07	1.44E-07	1.65E-07	1.11E-07	1.14E-07	1.60E-07
	150	1.62E-07	1.73E-07	-	1.40E-07	1.52E-07	2.08E-07
C_D*end* [µmol/mL]		9.74E-07	9.64E-07	9.50E-07	9.81E-07	9.03E-07	9.47E-07
Flux [µmol/cm^2/s]		1.94E-11	1.94E-11	3.88E-11	1.94E-11	1.94E-11	1.94E-11
P_{app} [cm/s]		1.99E-05	2.01E-05	4.08E-05	1.98E-05	2.15E-05	2.05E-05

Tab. 7-9: Parameter used for calculation of apparent permeability for each chamber of the Ussing chamber studies using reference compound terbutaline in mucosal to serosal and serosal to mucoal direction for full-thickness tissue.

Permeability direction m-s	Time [min]	Chamber 1	2	3	4	5	6
A_R*corrected* [µmol]	5	6.13E-09	6.71E-09	2.63E-09	8.75E-09	7.59E-09	2.92E-09
	10	1.47E-08	1.61E-08	1.30E-08	1.67E-08	2.60E-08	1.47E-08
	20	2.29E-08	2.93E-08	2.40E-08	3.37E-08	3.90E-08	2.20E-08
	40	4.87E-08	5.39E-08	5.30E-08	6.49E-08	8.82E-08	5.74E-08
	60	8.06E-08	8.92E-08	8.69E-08	9.72E-08	1.20E-07	7.80E-08
	90	1.19E-07	1.34E-07	1.31E-07	1.43E-07	1.71E-07	1.32E-07
	120	1.51E-07	1.71E-07	1.62E-07	1.68E-07	2.11E-07	1.73E-07
	150	1.81E-07	2.06E-07	2.01E-07	2.18E-07	2.72E-07	2.12E-07
C_D*end* [µmol/mL]		9.55E-07	9.47E-07	9.63E-07	9.64E-07	9.49E-07	9.65E-07
Flux [µmol/cm^2/s]		1.94E-11	1.94E-11	1.94E-11	1.94E-11	3.88E-11	3.88E-11
P_{app} [cm/s]		2.03E-05	2.05E-05	2.01E-05	2.01E-05	4.08E-05	4.02E-05

Permeability direction s-m	Time [min]	Chamber 7	8	9	10	11	12
A_R*corrected* [µmol]	5	6.42E-09	4.67E-09	3.21E-09	1.46E-09	3.50E-09	4.08E-09
	10	5.09E-09	5.09E-09	7.07E-09	5.65E-09	5.94E-09	6.50E-09
	20	1.78E-08	1.51E-08	2.01E-08	1.62E-08	1.62E-08	1.76E-08
	40	3.92E-08	4.70E-08	5.39E-08	5.19E-08	5.45E-08	6.52E-08
	60	7.48E-08	7.22E-08	8.23E-08	8.57E-08	8.43E-08	9.78E-08
	90	1.07E-07	1.18E-07	1.26E-07	1.32E-07	1.34E-07	1.52E-07
	120	1.45E-07	1.60E-07	1.62E-07	1.74E-07	1.71E-07	1.93E-07
	150	1.75E-07	1.84E-07	1.92E-07	2.12E-07	2.10E-07	2.33E-07
C_D*end* [µmol/mL]		9.68E-07	9.86E-07	8.66E-07	9.59E-07	9.88E-07	1.00E-06
Flux [µmol/cm^2/s]		1.94E-11	1.94E-11	1.94E-11	1.94E-11	1.94E-11	3.88E-11
P_{app} [cm/s]		2.00E-05	1.97E-05	2.24E-05	2.02E-05	1.96E-05	3.86E-05

Tab. 7-10: Parameter used for calculation of apparent permeability for each chamber of the Ussing chamber studies using reference compound mannitol in mucosal to serosal and serosal to mucoal direction for stripped tissue from verapamil permeability studies.

Permeability direction m-s	Time [min]	Chamber 1	2	3	4	5	6
A_R*corrected* [µmol]	5	-	0.00E+00	0.00E+00	0.00E+00	0.00E+00	0.00E+00
	10	0.00E+00	0.00E+00	0.00E+00	0.00E+00	0.00E+00	0.00E+00
	20	0.00E+00	0.00E+00	0.00E+00	0.00E+00	0.00E+00	0.00E+00
	40	0.00E+00	0.00E+00	0.00E+00	0.00E+00	0.00E+00	3.87E-03
	60	0.00E+00	0.00E+00	0.00E+00	2.58E-03	1.29E-03	2.58E-03
	90	4.04E-03	1.08E-02	1.21E-02	8.08E-03	1.35E-02	1.89E-02
	120	8.45E-03	1.13E-02	1.13E-02	1.55E-02	2.68E-02	2.82E-02
	150	1.76E-02	1.24E-02	2.17E-02	1.14E-02	3.10E-02	2.89E-02
C_D*end* [µmol/mL]		4.01E-01	3.79E-01	4.00E-01	4.18E-01	4.07E-01	4.03E-01
Flux [µmol/cm^2/s]		1.94E-06	3.88E-06	3.88E-06	3.88E-06	7.75E-06	7.75E-06
P_{app} [cm/s]		4.83E-06	1.02E-05	9.70E-06	9.27E-06	1.90E-05	1.92E-05

Permeability direction s-m	Time [min]	Chamber 7	8	9	10	11	12
A_R*corrected* [µmol]	5	0.00E+00	0.00E+00	0.00E+00	0.00E+00	0.00E+00	0.00E+00
	10	0.00E+00	0.00E+00	0.00E+00	0.00E+00	0.00E+00	0.00E+00
	20	0.00E+00	0.00E+00	0.00E+00	0.00E+00	0.00E+00	0.00E+00
	40	0.00E+00	0.00E+00	0.00E+00	0.00E+00	0.00E+00	0.00E+00
	60	0.00E+00	0.00E+00	0.00E+00	5.12E-07	3.42E-07	0.00E+00
	90	3.56E-07	8.91E-07	1.43E-06	-	1.60E-06	5.35E-07
	120	1.30E-06	1.68E-06	1.86E-06	-	2.24E-06	1.49E-06
	150	1.37E-06	1.91E-06	1.78E-06	-	2.32E-06	1.23E-06
C_D*end* [µmol/mL]		5.36E-05	6.12E-05	5.18E-05	4.98E-05	5.77E-05	5.63E-05
Flux [µmol/cm^2/s]		3.88E-10	5.81E-10	5.81E-10	-	5.81E-10	3.88E-10
P_{app} [cm/s]		7.23E-06	9.51E-06	1.12E-05	-	1.01E-05	6.88E-06

Tab. 7-11: Parameter used for calculation of apparent permeability for each chamber of the Ussing chamber studies using reference compound mannitol in mucosal to serosal and serosal to mucoal direction for stripped tissue from propranolol permeability studies.

Permeability direction	Time	Chamber					
m-s	[min]	1	2	3	4	5	6
A_R*corrected* [µmol]	5	2.58E-03	0.00E+00	1.29E-03	0.00E+00	0.00E+00	1.29E-03
	10	0.00E+00	1.82E-03	0.00E+00	3.64E-03	1.82E-03	1.82E-03
	20	1.35E-03	0.00E+00	2.69E-03	4.04E-03	1.35E-03	4.04E-03
	40	1.16E-02	6.45E-03	1.29E-02	1.03E-02	9.04E-03	9.04E-03
	60	1.16E-02	1.55E-02	1.68E-02	1.68E-02	2.19E-02	2.19E-02
	90	2.83E-02	3.50E-02	2.96E-02	4.45E-02	5.12E-02	3.77E-02
	120	4.93E-02	4.08E-02	4.22E-02	6.48E-02	6.34E-02	7.32E-02
	150	4.75E-02	4.65E-02	4.85E-02	6.40E-02	5.78E-02	6.30E-02
C_D*end* [µmol/mL]		5.45E-01	5.55E-01	5.49E-01	5.64E-01	5.37E-01	5.38E-01
Flux [µmol/cm^2/s]		1.16E-05	7.75E-06	7.75E-06	1.55E-05	1.36E-05	1.74E-05
P_{app} [cm/s]		2.13E-05	1.40E-05	1.41E-05	2.75E-05	2.53E-05	3.24E-05

Permeability direction	Time	Chamber					
s-m	[min]	7	8	9	10	11	12
A_R*corrected* [µmol]	5	0.00E+00	0.00E+00	0.00E+00	0.00E+00	1.71E-07	0.00E+00
	10	0.00E+00	0.00E+00	0.00E+00	7.23E-07	0.00E+00	0.00E+00
	20	0.00E+00	0.00E+00	0.00E+00	3.56E-07	5.35E-07	1.78E-07
	40	1.71E-07	3.42E-07	1.02E-06	1.37E-06	8.54E-07	1.71E-06
	60	1.02E-06	2.22E-06	2.39E-06	3.93E-06	2.39E-06	1.54E-06
	90	2.14E-06	2.85E-06	2.32E-06	5.35E-06	6.06E-06	3.56E-06
	120	2.79E-06	5.22E-06	5.59E-06	1.04E-05	8.38E-06	6.15E-06
	150	2.73E-06	5.33E-06	5.33E-06	9.56E-06	8.20E-06	6.28E-06
C_D*end* [µmol/mL]		7.11E-05	7.39E-05	7.03E-05	7.27E-05	7.38E-05	7.20E-05
Flux [µmol/cm^2/s]		3.88E-10	9.69E-10	9.69E-10	1.94E-10	1.94E-10	1.55E-09
P_{app} [cm/s]		5.45E-06	1.31E-05	1.38E-05	2.67E-06	2.62E-06	2.15E-05

Tab. 7-12: Parameter used for calculation of apparent permeability for each chamber of the Ussing chamber studies using reference compound mannitol in mucosal to serosal and serosal to mucoal direction for stripped tissue from terbutaline permeability studies.

Permeability direction m-s	Time [min]	Chamber 1	2	3	4	5	6
A_R*corrected* [µmol]	5	0.00E+00	1.29E-03	0.00E+00	0.00E+00	-	0.00E+00
	10	0.00E+00	3.64E-03	0.00E+00	0.00E+00	-	1.82E-03
	20	4.04E-03	5.39E-03	0.00E+00	5.39E-03	-	5.39E-03
	40	1.16E-02	1.03E-02	9.04E-03	9.04E-03	-	3.87E-03
	60	1.55E-02	1.42E-02	1.55E-02	1.94E-02	-	1.29E-02
	90	2.96E-02	2.96E-02	3.50E-02	3.23E-02	-	3.23E-02
	120	3.66E-02	4.08E-02	4.51E-02	3.94E-02	-	4.37E-02
	150	3.82E-02	2.89E-02	3.20E-02	3.72E-02	-	4.03E-02
C_D*end* [µmol/mL]		4.78E-01	4.55E-01	4.55E-01	4.98E-01	4.81E-01	4.69E-01
Flux [µmol/cm^2/s]		7.75E-06	7.75E-06	9.69E-06	5.81E-06	-	9.69E-06
P_{app} [cm/s]		1.62E-05	1.70E-05	2.13E-05	1.17E-05	-	2.06E-05

Permeability direction s-m	Time [min]	Chamber 7	8	9	10	11	12
A_R*corrected* [µmol]	5	0.00E+00	0.00E+00	0.00E+00	3.42E-07	1.02E-06	8.54E-07
	10	0.00E+00	0.00E+00	0.00E+00	0.00E+00	2.41E-07	2.41E-07
	20	0.00E+00	1.78E-07	1.78E-07	7.13E-07	0.00E+00	0.00E+00
	40	5.12E-07	1.54E-06	8.54E-07	6.83E-07	0.00E+00	1.02E-06
	60	1.54E-06	2.22E-06	1.71E-06	1.02E-06	1.02E-06	1.71E-06
	90	3.56E-06	1.96E-06	4.63E-06	2.14E-06	1.78E-06	3.03E-06
	120		5.22E-06	5.59E-06	3.35E-06	4.28E-06	5.77E-06
	150	4.10E-06	3.14E-06	-	3.69E-06	2.87E-06	4.51E-06
C_D*end* [µmol/mL]		6.29E-05	6.37E-05	6.15E-05	6.25E-05	5.79E-05	6.19E-05
Flux [µmol/cm^2/s]		9.69E-10	7.75E-10	1.16E-09	9.69E-10	7.75E-10	9.69E-10
P_{app} [cm/s]		1.54E-05	1.22E-05	1.89E-05	1.55E-05	1.34E-05	1.57E-05

Tab. 7-13: Parameter used for calculation of apparent permeability for each chamber of the Ussing chamber studies using reference compound mannitol in mucosal to serosal and serosal to mucoal direction for full-thickness tissue from verapamil permeability studies.

Permeability direction	Time	Chamber					
m-s	[min]	1	2	3	4	5	6
A_R*corrected* [µmol]	5	-	1.29E-03	0.00E+00	0.00E+00	0.00E+00	1.29E-02
	10	1.82E-03	0.00E+00	2.92E-02	0.00E+00	0.00E+00	0.00E+00
	20	0.00E+00	0.00E+00	0.00E+00	0.00E+00	0.00E+00	0.00E+00
	40	2.58E-03	1.29E-03	0.00E+00	0.00E+00	0.00E+00	0.00E+00
	60	2.58E-03	1.29E-03	0.00E+00	1.29E-03	5.16E-03	5.16E-03
	90	1.35E-02	1.48E-02	1.08E-02	1.48E-02	0.00E+00	1.21E-02
	120	1.55E-02	2.39E-02	1.97E-02	1.69E-02	2.53E-02	2.25E-02
	150	1.86E-02	3.20E-02	2.07E-02	2.48E-02	1.86E-02	2.17E-02
C_D*end* [µmol/mL]		4.10E-01	4.39E-01	4.37E-01	4.42E-01	4.34E-01	3.64E-01
Flux [µmol/cm^2/s]		3.88E-06	7.75E-06	5.81E-06	5.81E-06	5.81E-06	5.81E-06
P_{app} [cm/s]		9.45E-06	1.77E-05	1.33E-05	1.31E-05	1.34E-05	1.60E-05

Permeability direction	Time	Chamber					
s-m	[min]	7	8	9	10	11	12
A_R*corrected* [µmol]	5	0.00E+00	0.00E+00	-	0.00E+00	0.00E+00	-
	10	0.00E+00	0.00E+00	-	0.00E+00	0.00E+00	-
	20	0.00E+00	0.00E+00	-	0.00E+00	0.00E+00	-
	40	0.00E+00	0.00E+00	-	0.00E+00	3.42E-07	-
	60	0.00E+00	3.42E-07	-	0.00E+00	8.54E-07	-
	90	5.35E-07	1.25E-06	-	7.13E-07	8.91E-07	-
	120	1.68E-06	-	-	1.30E-06	1.30E-06	-
	150	1.23E-06	9.56E-07	-	1.64E-06	2.32E-06	-
C_D*end* [µmol/mL]		5.36E-05	5.79E-05	-	5.38E-05	6.03E-05	-
Flux [µmol/cm^2/s]		5.81E-10	5.81E-10	-	3.88E-10	1.55E-10	-
P_{app} [cm/s]		1.08E-05	1.00E-05	-	7.20E-06	2.57E-06	-

Tab. 7-14: Parameter used for calculation of apparent permeability for each chamber of the Ussing chamber studies using reference compound mannitol in mucosal to serosal and serosal to mucoal direction for full-thickness tissue from propranolol permeability studies.

Permeability direction	Time	Chamber					
m-s	[min]	1	2	3	4	5	6
A_R*corrected* [µmol]	5	0.00E+00	0.00E+00	0.00E+00	0.00E+00	0.00E+00	-
	10	0.00E+00	0.00E+00	0.00E+00	0.00E+00	0.00E+00	-
	20	0.00E+00	0.00E+00	0.00E+00	0.00E+00	0.00E+00	-
	40	0.00E+00	0.00E+00	0.00E+00	0.00E+00	0.00E+00	-
	60	1.29E-03	6.45E-03	2.58E-03	3.87E-03	0.00E+00	-
	90	8.08E-03	8.08E-03	6.74E-03	9.43E-03	1.35E-02	-
	120	1.41E-02	2.25E-02	2.11E-02	1.55E-02	1.69E-02	-
	150	1.34E-02	2.38E-02	1.45E-02	1.55E-02	1.65E-02	-
C_D*end* [µmol/mL]		5.46E-01	5.39E-01	5.39E-01	5.38E-01	5.37E-01	-
Flux [µmol/cm^2/s]		3.88E-06	5.81E-06	5.81E-06	3.88E-06	5.81E-06	-
P_{app} [cm/s]		7.10E-06	1.08E-05	1.08E-05	7.21E-06	1.08E-05	-

Permeability direction	Time	Chamber					
s-m	[min]	7	8	9	10	11	12
A_R*corrected* [µmol]	5	0.00E+00	0.00E+00	0.00E+00	0.00E+00	0.00E+00	-
	10	0.00E+00	0.00E+00	0.00E+00	0.00E+00	0.00E+00	-
	20	0.00E+00	1.78E-07	0.00E+00	0.00E+00	0.00E+00	-
	40	0.00E+00	0.00E+00	0.00E+00	0.00E+00		-
	60	1.71E-07	3.42E-07	5.12E-07	3.42E-07	8.54E-07	-
	90	1.07E-06	5.35E-07	1.25E-06	1.07E-06	8.91E-07	-
	120	1.49E-06	1.30E-06	1.12E-06	2.05E-06	2.24E-06	-
	150	0.00E+00	1.23E-06	1.50E-06	1.91E-06	2.19E-06	-
C_D*end* [µmol/mL]		7.31E-05	7.00E-05	7.14E-05	7.08E-05	7.20E-05	-
Flux [µmol/cm^2/s]		3.88E-10	3.88E-10	1.94E-10	5.81E-10	3.88E-10	-
P_{app} [cm/s]		5.30E-06	5.54E-06	2.71E-06	8.22E-06	5.39E-06	-

Tab. 7-15: Parameter used for calculation of apparent permeability for each chamber of the Ussing chamber studies using reference compound mannitol in mucosal to serosal and serosal to mucoal direction for full-thickness tissue from terbutaline permeability studies.

Permeability direction m-s	Time [min]	Chamber 1	2	3	4	5	6
A_R*corrected* [µmol]	5	6.45E-03	1.29E-03	0.00E+00	0.00E+00	0.00E+00	0.00E+00
	10	1.82E-03	0.00E+00	0.00E+00	0.00E+00	1.82E-03	0.00E+00
	20	5.39E-03	6.74E-03	0.00E+00	2.69E-03	0.00E+00	0.00E+00
	40	9.04E-03	2.58E-03	9.04E-03	7.75E-03	6.45E-03	9.04E-03
	60	1.42E-02	1.42E-02	7.75E-03	1.03E-02	1.16E-02	2.07E-02
	90	2.69E-02	3.50E-02	1.75E-02	2.02E-02	2.29E-02	3.10E-02
	120	4.37E-02	4.22E-02	2.82E-02	3.94E-02	5.35E-02	3.52E-02
	150	3.10E-02	3.61E-02	3.51E-02	3.72E-02	3.61E-02	3.30E-02
C_D*end* [µmol/mL]		4.73E-01	4.68E-01	4.68E-01	4.80E-01	4.60E-01	4.83E-01
Flux [µmol/cm^2/s]		9.69E-06	9.69E-06	5.81E-06	9.69E-06	1.36E-05	3.88E-06
P_{app} [cm/s]		2.05E-05	2.07E-05	1.24E-05	2.02E-05	2.95E-05	8.03E-06

Permeability direction s-m	Time [min]	Chamber 7	8	9	10	11	12
A_R*corrected* [µmol]	5	0.00E+00	0.00E+00	0.00E+00	0.00E+00	0.00E+00	0.00E+00
	10	0.00E+00	0.00E+00	0.00E+00	0.00E+00	0.00E+00	0.00E+00
	20	0.00E+00	0.00E+00	5.35E-07	0.00E+00	0.00E+00	0.00E+00
	40	1.54E-06	3.42E-07	1.02E-06	1.02E-06	1.37E-06	5.12E-07
	60	6.83E-07	8.54E-07	1.02E-06	1.54E-06	1.88E-06	1.20E-06
	90	2.67E-06	3.92E-06	1.43E-06	3.03E-06	1.96E-06	2.85E-06
	120	3.91E-06	3.54E-06	2.79E-06	4.10E-06	4.84E-06	4.10E-06
	150	3.69E-06	4.51E-06	5.19E-06	4.23E-06	5.19E-06	6.28E-06
C_D*end* [µmol/mL]		6.37E-05	6.23E-05	5.68E-05	6.35E-05	6.53E-05	6.35E-05
Flux [µmol/cm^2/s]		9.69E-10	7.75E-10	5.81E-10	7.75E-10	9.69E-10	9.69E-10
P_{app} [cm/s]		1.52E-05	1.24E-05	1.02E-05	1.22E-05	1.48E-05	1.53E-05

7.2 Simulations of intestinal absorption using GastroPlus™

Tab. 7-16: Observed (obs) and predicted (pred) pharmacokinetic parameters and *in vivo* study details for compound $C_{1.}$

Species	Formulation	Dose [mg]‡	f_a in [%]		k_a in [1/h]		T_{max} in [h]		MRT in [h]		$t_{1/2\ eff.}$ in [h]	
			obs	pred	obs	pred	obs	pred	obs	pred	obs	pred
dog	solution	3	80.2	100	0.99	0.58	1.50	0.88	6.85	4.57	4.75	3.17
dog	solution	10	90.8	100	0.24	0.57	1.50	1.00	5.16	4.58	3.58	3.18
rat	MCS	16.5	69.4	58.8	5.60	0.72	0.75	0.80	24.9	4.12	17.3	2.85
rat	solution	20	91.9	60.1	2.15	0.77	1.00	0.75	3.02	3.86	2.09	2.68
rat	MCS	100	72.7	38.5	0.28	3.98	2.00	0.75	8.19	3.65	5.68	2.53
human	solution	1	-	99.9	1.04	0.60	0.50	0.83	2.13	3.57	1.47	2.47
human	solution	2.5	-	99.9	2.96	0.60	0.50	0.83	4.06	3.40	2.81	2.36
human	solution	5	-	99.9	2.48	0.60	0.50	0.83	2.50	3.46	1.74	2.40
human	solution	10	-	99.9	3.23	0.60	0.38	0.83	4.09	3.57	2.84	2.47
human	solution	20	-	99.9	2.25	0.71	0.50	0.88	2.54	3.43	1.76	2.37
human	solution	40	-	99.9	5.78	0.74	0.25	1.20	1.97	3.51	1.37	2.43
human	solution	80	-	99.7	0.48	0.68	1.25	1.84	2.65	4.02	1.84	2.78
human	solution	120	-	91.0	3.49	1.06	1.00	2.08	2.93	4.85	2.03	3.36
human	solution	160	-	78.8	4.93	0.41	0.75	0.40	2.68	6.50	1.86	4.50
human	MR tab.	100	-	76.6	0.98	0.48	1.13	2.60	18.2	10.0	12.6	6.94
human	MR tab.	200	-	61.9	0.61	0.54	2.00	2.50	13.0	11.7	9.04	8.13
human	MR tab.	300	-	53.4	1.30	0.54	1.75	2.50	15.8	11.7	11.0	8.13
human	MR tab.	400	-	48.0	0.93	0.56	1.50	2.70	37.3	12.5	25.8	8.66
human	MR tab.	500	-	53.7	0.63	0.35	2.50	3.10	15.6	11.9	10.8	8.27
human	MR tab.	600	-	41.5	0.58	0.60	2.50	3.10	22.0	13.7	15.3	9.51
human	MR tab.	900	-	36.3	1.76	0.65	1.75	3.10	11.8	16.1	8.16	11.1
human	MR tab.	1200	-	33.3	0.49	1.43	3.50	3.10	13.7	18.8	9.46	13.1
human	MR tab.	1500	-	31.4	1.04	1.51	1.75	3.10	9.54	21.0	6.61	14.6
human	EC MR tab.	300	-	57.7	0.79	0.65	6.01	2.10	12.9	9.59	8.91	6.65
human♦	EC MR tab.	300	-	71.5	0.17	0.35	6.01	2.93	9.13	8.44	6.33	5.85

MCS = micro-crystalline suspension

MR tab. = modified-release tablet

EC MR tab.= enteric coated modified-release tablet

‡ dose for animals in mg/kg

♦ non-fasting

Tab. 7-17: Observed (obs) and predicted (pred) pharmacokinetic parameters and *in vivo* study details for compound $C_{2.}$

Species	Formulation	Dose [mg]‡	f_a in [%]		k_a in [1/h]		T_{max} in [h]		MRT in [h]		$t_{1/2\ eff.}$ in [h]	
			obs	pred	obs	pred	obs	pred	obs	pred	obs	pred
mouse	MCS	3	-	99.4	7.73	0.92	0.50	1.23	2.30	5.21	1.6	3.61
mouse	MCS	5	86.3	98.9	-	0.74	-	1.36	-	9.24	-	6.40
mouse	MCS	10	-	96.6	-	0.57	-	1.76	-	5.91	-	4.10
mouse	MCS	30	-	79.9	-	1.01	-	1.84	-	6.84	-	4.74
rat	MCS	1	121	97.1	3.85	0.88	1.00	1.84	4.49	6.13	3.12	4.25
rat	MCS	4.8	153	69.1	-	0.96	-	2.08	-	7.51	-	5.20
rat	MCS	10	138	51.3	5.33	0.63	1.00	2.00	5.13	8.09	3.56	5.61
rabbit	MCS	0.5	-	66.2	1.87	0.47	1.50	2.10	6.75	5.46	4.68	3.79
rabbit	MCS	1	-	66.9	4.65	0.47	0.50	2.20	4.44	5.49	3.08	3.81
rabbit	MCS	5	95.0	77.4	0.60	0.34	1.50	4.36	7.11	6.39	4.93	4.43
rabbit	MCS	10	-	83.5	2.86	0.24	0.50	6.76	4.98	7.98	3.45	5.53
rabbit	MCS	100	-	50.8	0.20	0.11	4.00	12.5	11.4	15.8	7.91	10.9
dog	IR tab.	1	-	99.6	0.59	1.72	2.00	1.40	8.19	8.21	5.68	5.69
dog	EC tab.	1	-	99.8	1.75	0.54	2.00	1.74	37.2	8.43	25.8	5.84
monkey	MCS	1	89.6	98.8	0.85	0.51	1.50	1.92	9.97	22.0	6.91	15.2
monkey	MCS	10	-	77.8	0.35	0.13	6.00	2.88	14.0	18.3	9.69	12.7
human	EC tab.	1	-	99.7	0.24	0.50	5.00	2.16	27.1	46.7	18.8	32.3
human	EC tab.	2	-	99.7	0.78	0.49	2.00	2.24	16.8	46.7	11.7	32.4
human	IR tab.	2	-	94.1	0.74	0.54	1.00	2.16	20.9	44.3	14.5	30.7
human	IR tab.	3	-	94.2	0.60	0.53	2.00	2.16	69.9	44.4	48.4	30.8
human	MCS	3.13	100	97.8	1.28	0.53	1.00	2.08	101	46.2	69.8	32.0
human	EC tab.	5	-	99.7	0.14	0.45	4.00	2.48	27.3	47.0	18.9	32.6
human	EC tab.	10	-	99.6	0.09	0.39	5.00	2.80	29.9	47.6	20.8	33.0

MCS = micro-crystalline suspension

IR tab. = immediate-release Tablet

EC tab.= enteric coated Tablet

MR tab. = modified-release Tablet

‡ dose for animals in mg/kg

Tab. 7-18: Observed (obs) and predicted (pred) pharmacokinetic parameters and *in vivo* study details for compound $C_{3.}$

Species	Formulation	Dose [mg]‡	f_a in [%]		k_a in [h^{-1}]		T_{max} in [h]		MRT in [h]		$t_{1/2\ eff.}$ in [h]	
			obs	pred	obs	pred	obs	pred	obs	pred	obs	pred
rat	MCS	10	54.5	22.7	0.45	0.37	3.00	1.70	15.7	21.1	10.9	14.6
rat	MCS	30	-	19.5	3.38	0.37	0.75	1.40	21.5	20.2	14.9	14.0
dog	MCS	4	-	82.1	0.94	0.46	2.00	1.50	9.51	10.3	6.59	7.15
dog	MCS	5	41.3	78.0	-	-	-	-	-	-	-	-
monkey	solution	10	-	47.5	0.11	2.11	8.00	0.90	31.2	18.7	21.6	12.9
monkey	MCS	10	-	42.8	0.11	1.71	8.00	0.90	37.2	19.1	25.8	13.2
monkey	IR tab.	10	-	42.8	0.08	1.86	8.00	0.90	33.1	19.1	23.0	13.2
monkey	NCS	7	-	49.5	0.49	1.40	8.00	0.90	28.4	18.4	19.7	12.8
human	IR tab.	15	-	71.1	0.28	0.25	4.00	3.92	8.60	10.0	5.96	6.92
human	IR tab.	25	-	56.5	0.20	0.24	2.00	4.48	13.7	10.1	9.52	6.99
human	IR tab.	35	-	47.7	0.90	0.23	2.00	4.80	52.4	10.1	36.3	7.03
human	IR tab.	45	-	41.9	0.63	0.23	2.00	4.96	12.3	10.3	8.52	7.11
human	IR tab.	90	-	29.9	0.28	0.39	2.00	5.20	8.71	10.1	6.04	6.97
human	IR tab.	180	-	22.4	0.45	0.20	4.00	4.56	11.2	9.95	7.75	6.89
human	IR tab.	270	-	26.4	0.68	0.20	4.00	1.68	13.0	9.29	9.04	6.44
human	IR tab.	360	-	23.2	0.81	0.19	4.00	1.60	11.9	9.47	8.27	6.56

MCS = micro-crystalline suspension

IR tab. = immediate-release tablet

NCS = nano-crystalline suspension

‡ dose for animals in mg/kg

Tab. 7-19: Observed (obs) and predicted (pred) pharmacokinetic parameters and *in vivo* study details for compound $C_{4.}$

Species	Formulation	Dose [mg]‡	f_a in [%]		k_a in [h^{-1}]		T_{max} in [h]		MRT in [h]		$t_{1/2\ eff.}$ in [h]	
			obs	pred	obs	pred	obs	pred	obs	pred	obs	pred
dog	solution	10	112	96.4	0.96	0.59	1.00	3.20	8.68	12.07	6.01	8.37
rat	MCS	13	49.5	47.3	0.33	0.23	4.00	1.22	8.11	6.16	5.62	4.27
rat	MCS	86	-	14.5	0.21	0.40	3.00	1.40	8.65	6.29	5.99	4.36
human	solution	10	-	99.5	0.79	0.41	1.50	3.30	14.8	22.5	10.3	15.6
human	solution	25	-	92.2	1.00	0.49	1.00	4.00	23.5	23.6	16.3	16.4
human	solution	50	-	70.4	0.82	0.49	1.00	4.56	24.5	25.3	17.0	17.5
human	solution	70	-	60.0	0.78	0.18	1.50	4.80	20.5	25.9	14.2	17.9
human	solution	90	-	52.9	0.70	0.30	1.50	5.04	21.2	26.3	14.7	18.3

MCS = micro-crystalline suspension

‡ dose for animals in mg/kg

Tab. 7-20: Observed (obs) and predicted (pred) pharmacokinetic parameters and *in vivo* study details for compound $C_{5.}$

Species	Formulation	Dose [mg]‡	f_a in [%]		k_a in [h^{-1}]		T_{max} in [h]		MRT in [h]		$t_{1/2\ eff.}$ in [h]	
			obs	pred	obs	pred	obs	pred	obs	pred	obs	pred
dog	MCS	200	20.8	89.0	1.24	3.27	2.00	0.72	33.4	6.87	23.2	4.76
dog	MCS	20	40.7	99.8	1.27	1.22	0.75	0.72	2.56	4.49	1.78	3.11
rat	MCS	30	48.9	62.8	0.87	2.02	1.00	0.80	2.34	4.17	1.62	2.89
mouse	solution	30	-	99.9	1.04	3.04	0.75	0.32	2.03	1.22	1.40	0.85
mouse	solution	150	-	96.7	0.33	5.08	1.00	0.32	5.09	1.50	3.53	1.04
human	IR caps.	50	-	99.8	-	-	-	-	-	-	-	-
human	IR caps.	150	-	94.4	-	-	-	-	-	-	-	-
human	IR caps.	300	-	74.1	-	-	-	-	-	-	-	-
human	IR caps.	500	-	57.0	-	-	-	-	-	-	-	-
human	IR caps.	750	-	47.4	-	-	-	-	-	-	-	-
human	IR caps.	1000	35.0	42.3	-	-	.	-	-	-	-	
human	IR caps.	1200	-	39.6	-	-	-	-	-	-	-	-
human	IR caps.	1250	-	39.3	-	-	-	-	-	-	-	-
human	IR caps.	1500	-	36.8	-	-	-	-	-	-	-	-
human	IR caps.	2000	-	33.9	-	-	-	-	-	-	-	-

MCS = micro-crystalline suspension

IR caps. = immediate-release capsule

‡ dose for animals in mg/kg

Tab. 7-21: Observed (obs) and predicted (pred) pharmacokinetic parameters and *in vivo* study details for compound $C_{6.}$

Species	Formulation	Dose [mg]‡	f_a in [%]		k_a in [h^{-1}]		T_{max} in [h]		MRT in [h]		$t_{1/2\ eff.}$ in [h]	
			obs	pred	obs	pred	obs	pred	obs	pred	obs	pred
mouse	MCS	10	65.0	42.4	1.13	0.03	1.50	16.5	28.5	76.2	19.8	52.8
rat	MCS	100	44.8	7.67	0.44	0.59	1.50	3.46	50.1	59.2	34.8	41.1
dog	suspension	20	30.0	32.4	0.80	0.05	1.00	21.4	49.5	38.0	34.3	26.4
dog	suspension	100	-	9.07	0.72	0.99	7.00	1.44	158	12.0	109	8.32
human	solution	6.25	59.7	69.1	0.78	2.12	2.00	1.46	184	35.2	127	24.4
human	solution	50	-	43.4	1.07	0.07	1.12	0.42	16.6	21.6	11.5	15.0
human	IR tab.	50	-	32.5	0.48	0.08	3.04	2.76	37.2	21.6	25.8	15.0

MCS = micro-crystalline suspension

IR tab. = immediate-release tablet

‡ dose for animals in mg/kg

Tab. 7-22: Observed (obs) and predicted (pred) pharmacokinetic parameters and *in vivo* study details for compound $C_{7.}$

Species	Formulation	Dose [mg]‡	f_a in [%]		k_a in [h^{-1}]		T_{max} in [h]		MRT in [h]		$t_{1/2\ eff.}$ in [h]	
			obs	pred	obs	pred	obs	pred	obs	pred	obs	pred
human	IR tab.	500	69.0	25.5	1.14	1.36	1.50	0.72	6.05	3.18	4.20	2.21
human	MR tab.	500	69.0	24.7	0.62	1.50	2.00	1.20	6.89	7.68	4.78	5.32
human	IR tab.	250	69.0	36.4	1.81	1.02	1.50	0.72	5.46	8.02	3.78	5.56
human	solution	250	69.0	33.2	1.57	2.02	0.50	0.50	5.46	7.86	3.78	5.45
rat	solution	5	45.0	51.3	7.02	1.31	0.33	0.99	3.32	4.47	2.30	3.10
monkey	solution	30	22.7	79.0	0.35	1.36	3.01	1.07	8.42	3.18	5.83	2.21

IR tab. = immediate-release tablet

MR tab. = modified-release tablet

‡ dose for animals in mg/kg

Tab. 7-23: Observed (obs) and predicted (pred) pharmacokinetic parameters and *in vivo* study details for compound $C_{8.}$

Species	Formulation	Dose [mg]‡	f_a in [%]		k_a in [h^{-1}]		T_{max} in [h]		MRT in [h]		$t_{1/2\ eff.}$ in [h]	
			obs	pred	obs	pred	obs	pred	obs	pred	obs	pred
rat	solution	6	94.0	86.5	-	-	-	-	-	-	-	-
human	MR caps.	30	90.0	91.0	0.08	0.11	10.0	10.6	21.7	14.1	15.1	9.74
human♦	MR caps.	30	90.0	90.1	0.07	0.11	19.5	9.9	23.5	14.1	16.3	9.80
human	MR caps.	60	90.0	77.8	0.09	0.11	10.0	12.3	21.9	15.4	15.2	10.6
human♦	MR caps.	60	90.0	76.0	0.11	0.11	10.0	11.9	20.6	15.6	14.3	10.8

MR caps. = modified-release capsule

♦ non-fasting

‡ dose for animals in mg/kg

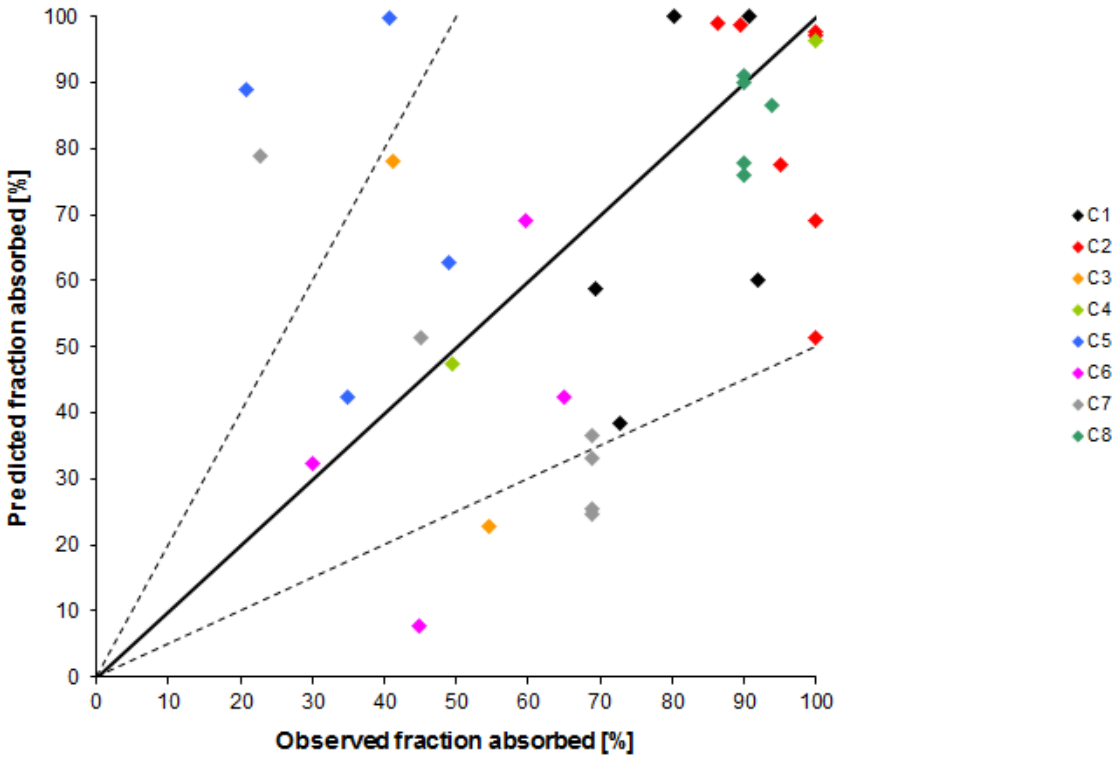

Fig. 7-1: Fraction absorbed categorised by compound C_1-C_8. Predicted fraction absorbed using GastroPlus™ versus observed fraction absorbed determined in *in vivo* studies in percent (data points comprise all species, formulations and doses). Line of unity (—) and 2-fold error (- - -) n= 35.

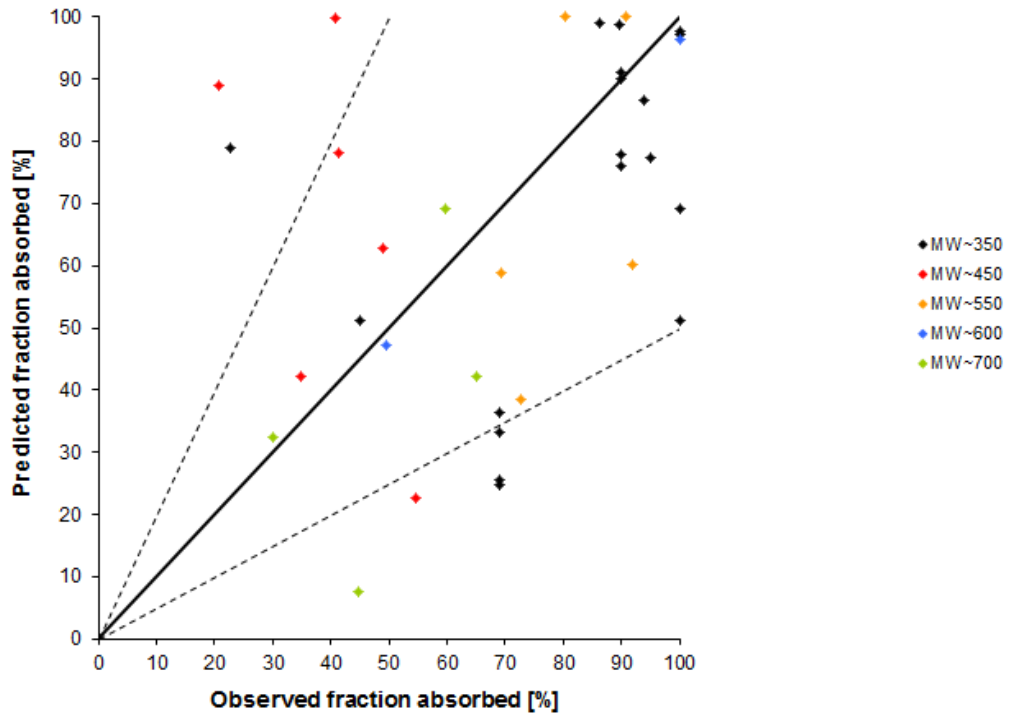

Fig. 7-2: Fraction absorbed categorised by molecular weight. Predicted fraction absorbed using GastroPlus™ versus observed fraction absorbed determined in *in vivo* studies in percent (data points comprise all compounds, species, formulations and doses). Line of unity (—) and 2-fold error (- - -) n= 35

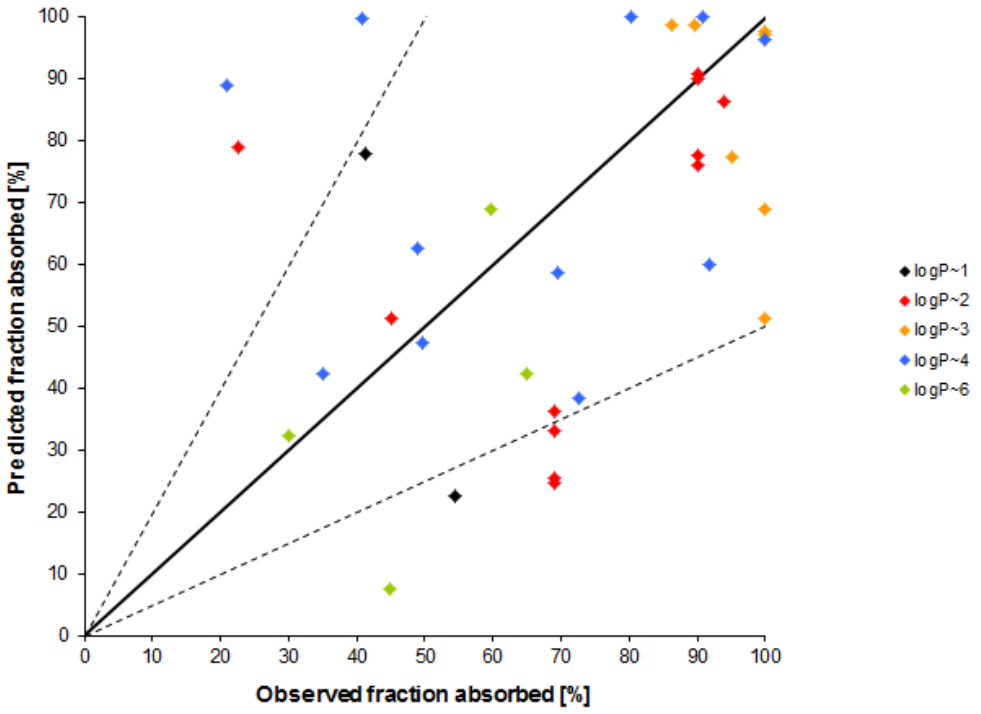

Fig. 7-3: Fraction absorbed categorised by log P. Predicted fraction absorbed using GastroPlus™ versus observed fraction absorbed determined in *in vivo* studies in percent (data points comprise all compounds, species, formulations and doses). Line of unity (—) and 2-fold error (- - -) n= 35

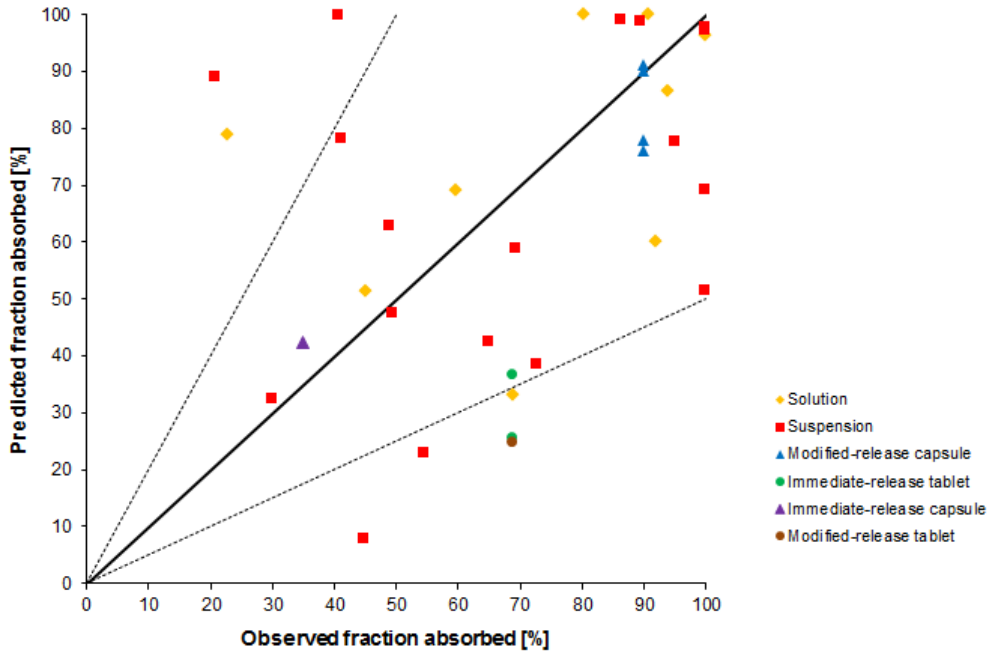

Fig. 7-4: Fraction absorbed categorised by formulation. Predicted fraction absorbed using GastroPlus™ versus observed fraction absorbed determined in *in vivo* studies in percent (data points comprise all compounds, species, formulations and doses). Line of unity (—) and 2-fold error (- - -) n= 35

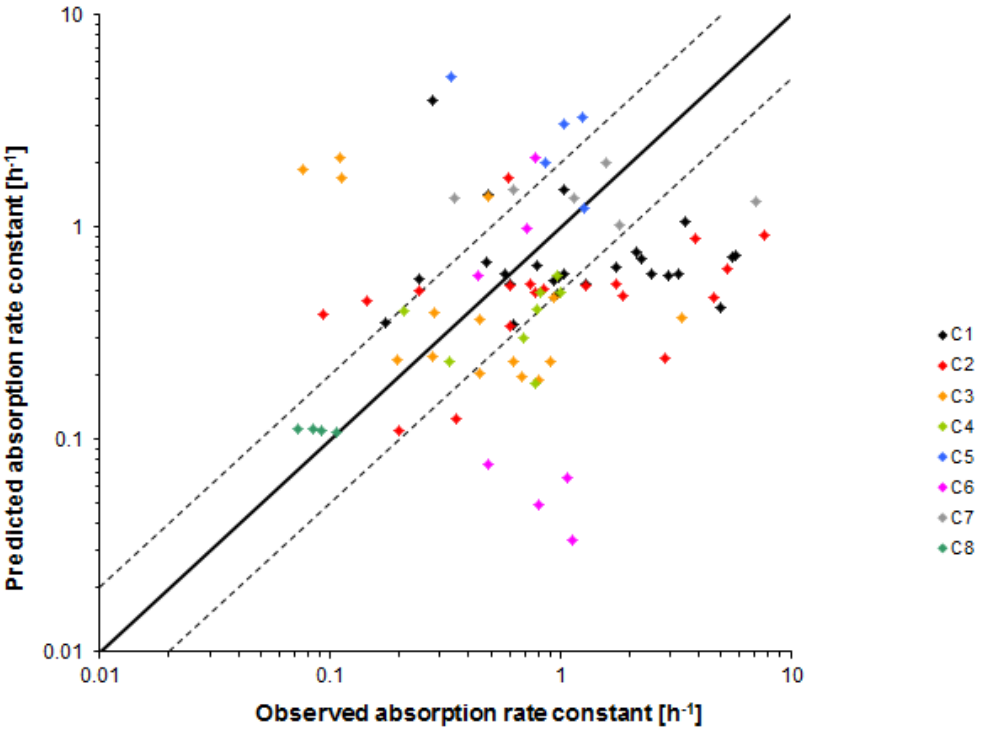

Fig. 7-5: Absorption rate constant derived from *in vivo* data (observed) versus absorption rate constant deriving from *in silico* simulations (predicted) using GastroPlus™ categorised by compound (data points comprise all species, formulations and doses) expressed as inverse time. Absorption rate constant (◊), line of unity (—), 2-fold error (- - -), n= 89.

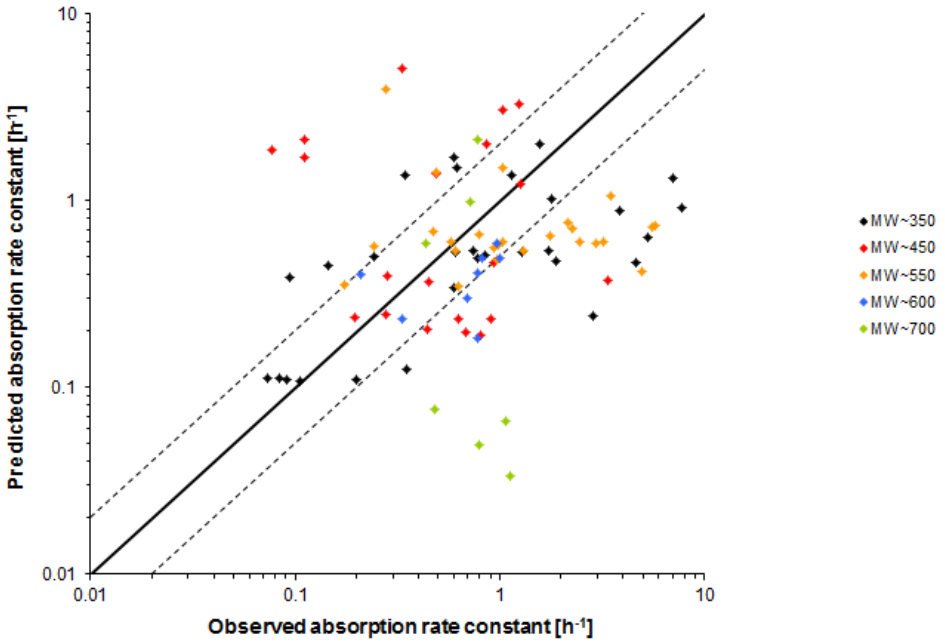

Fig. 7-6: Absorption rate constant derived from *in vivo* data (observed) versus absorption rate constant deriving from *in silico* simulations (predicted) using GastroPlus™ categorised by molecular weight (data points comprise all compounds, species, formulations and doses) expressed as inverse time. Absorption rate constant (◊), line of unity (—), 2-fold error (- - -), n= 89.

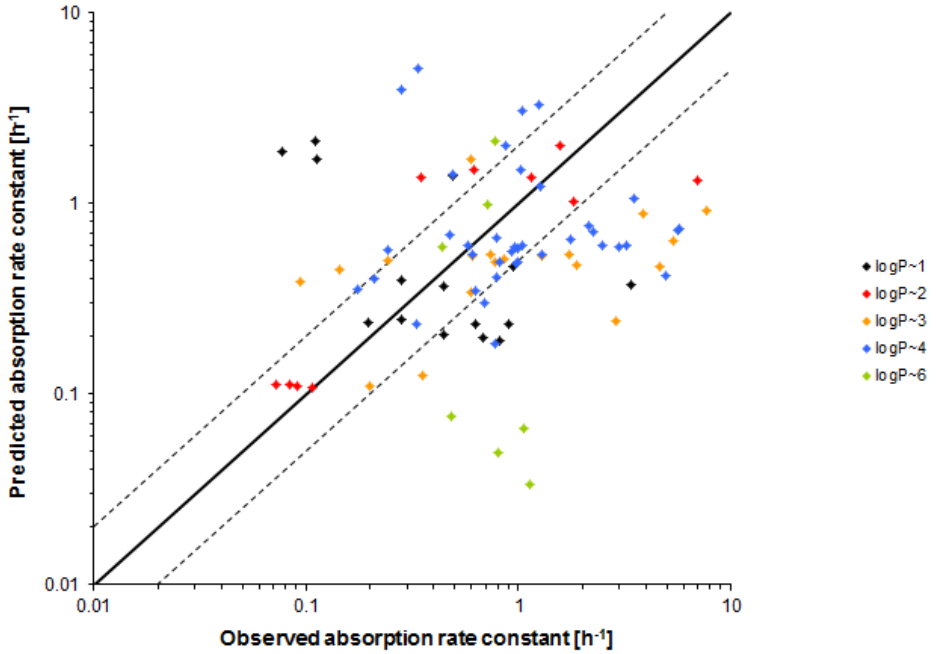

Fig. 7-7: Absorption rate constant derived from *in vivo* data (observed) versus absorption rate constant deriving from *in silico* simulations (predicted) using GastroPlus™ categorised by log P (data points comprise all compounds, species, formulations and doses) expressed as inverse time. Absorption rate constant (◊), line of unity (—), 2-fold error (- - -), n= 89.

List of Tables

List of Figures

Acknowledgements

An erster Stelle möchte ich seitens Bayer Pharma AG, *Dr. Dr. Cornelia Preusse* danken, ohne deren Ideen und Wissen, Unterstützung und Motivation diese Arbeit nicht möglich gewesen wäre.
Ebenfalls herzlichen Dank an *Dr. Hille Gieschen* für die Möglichkeit die Promotionstätigkeiten in der Gruppe Nonclinical Pharmacokinetics durchzuführen.

Prof. Dr. Charlotte Kloft vom Institut für Klinische Pharmazie und Biochemie der Freien Universität Berlin gilt mein Dank für die Betreuung der Arbeit von universitärer Seite und die wissenschaftlichen Diskussionen speziell im Rahmen des Graduate Research Training Program „PharMetrX“.

Für die praktische Einführung in die Ussingkammer Methode möchte ich *Prof. Dr. Martin Diener* und seiner Arbeitsgruppe vom Institut für Veterinär-Physiologie und -Biochemie der Justus-Liebig-Universität Gießen und *Prof. a.D. Dr. Holger Martens* und seiner Arbeitsgruppe vom Institut Veterinär-Physiologie der Freien Universität Berlin danken.

Danken möchte ich außerdem *Dr. Valerie Nock* für aufheiternde Worte und ihr Geschick im Umgang mit R, *Dr. Simone Blattner* für gewissenhaftes Korrekturlesen, *Christoph Geiger* für die Rettung wichtiger elektronischer Daten und *Alexandra Moll* für ihre Expertise im Bereich Textverarbeitung.

Die Zeit mit den Berliner Kollegen der Gruppe Nonclincal Pharmacokinetics der Bayer Pharma AG bleibt bei mir in außerordentlich guter Erinnerung. Vielen Dank für diese Erfahrung.

Besonderer Dank geht an meine Familie die mich immer auf meinem Weg unterstützt hat.

Last but by far not least, I would like to express my most sincere gratitude to my husband *Stephen W. James* for the relentless support. We achieved this together.

Erklärung

Hiermit erkläre ich, dass ich mich mit der vorliegenden Dissertation erstmals um die Erlangung eines Doktorgrades bewerbe. Ferner erkläre ich, dass ich die vorliegende Arbeit selbständig und ohne fremde Hilfe angefertigt, andere als die von mir angegebenen Quellen und Hilfsmittel nicht benutzt und die den verwendeten Werken wörtlich oder inhaltlich entnommenen Stellen als solche kenntlich gemacht habe.

Warthausen, 18. Oktober 2017

Jeannine Fleth-James